Institut für Medizinische Mikrobiologie und Hygiene

Universitätsklinikum Tübingen

# Characterization of phenotypical changes of *P. aeruginosa* according to the action of murein endopeptidases MepM

Inaugural-Dissertation
zur Erlangung des Doktorgrades
der Medizin

der Medizinischen Fakultät
der Eberhard Karls Universität
zu Tübingen

vorgelegt von

Aidoo, Stephanie Ampoma

2025

| | |
|---|---|
| Dekan: | Professor Dr. rer. nat. Bernd Pichler |
| 1. Berichterstatter: | PD Dr. rer. nat. Erwin Bohn |
| 2. Berichterstatter: | Professor Dr. rer. nat. Frank Stubenrauch |

Tag der Disputation: 18.08.2025

## Table of contents

## List of figures

## List of tables

## Abbreviations

| | |
|---|---|
| A | Ampere |
| AG | Research Group |
| Arb. Units | Arbitrary units |
| Approx. | Approximately |
| AZT | Azidothymidine |
| BME | ß-Mercaptoethanol |
| Bp | Base Pairs |
| CDS | Coding Sequence |
| CF | Cystic Fibrosis |
| CFU | Colony-Forming Units |
| CP | DD-carboxypeptidase |
| CtpA | Carboxy-Terminal Processing Protease |
| CV | Crystal Violet Solution |
| d | Days |
| DPBS | Dulbecco's Phosphate Buffered Saline |
| $ddH_2O$ | Double-Distilled Water |
| DI-water | Deionized Water |
| DNA | Deoxyribonucleic Acid |
| dNTP | Deoxyribonucleotide Triphosphate |
| dsDNA | Double-stranded DNA |
| *Ec.* | *Escherichia coli* |
| *E. coli* | *Escherichia coli* |
| EDTA | Ethylenediaminetetraacetic Acid |

| | |
|---|---|
| EP | Endopeptidase |
| EPS | Extracellular Polymeric Substance |
| FEP | Cefepime |
| gDNA | Genomic DNA |
| GlcNAc | N-acetyl-glucosamine |
| GlmS | Glucosamine-6-Phosphate Synthetase |
| GTF | Glycosyltransferase |
| HAP | Hospital-Acquired Pneumonia |
| HCAP | Healthcare-Associated Pneumonia |
| HCl | Hydrogen chloride |
| HMM-PBP | High Molecular Mass Penicillin-Binding Protein |
| ICU | Intensive Care Units |
| IM | Inner Membrane |
| IPTG | Isopropyl β-D-1-Thiogalactopyranoside |
| kb | Kilobase |
| kDa | Kilodalton |
| LB | Lysogeny Broth |
| $LD_{50}$ | Lethal Dose at 50% |
| LdcA | LD-carboxypeptidase |
| LMM-PBP | Low-Molecular-Mass-Penicillin-Binding Protein |
| LPS | Lipopolysaccharides |
| LT | Lytic Transglycosylase |
| MDR | Multidrug-Resistant |

| | |
|---|---|
| MEM | Meropenem |
| MEP | Murein Endopeptidase |
| *mepM* | Murein Endopeptidase M |
| MIC | Minimal Inhibitory Concentration |
| Min | minute(s) |
| MurNAc | N-Acetyl-Muramic Acid |
| NAG | N-acetylglucosamine |
| NagZ | β-N- acetylglucosaminidase |
| NAM | N-acetylmuramic Acid |
| OD | Optical Density |
| OM | Outer Membrane |
| *Pa.* | *Pseudomonas aeruginosa* |
| *P. aeruginosa* | *Pseudomonas aeruginosa* |
| PBS | Phosphate-Buffered Saline |
| PCH | Pyochelin |
| PCR | Polymerase Chain Reaction |
| PG | Peptidoglycan |
| PVD | Pyoverdine |
| PYO | Pyocyanin |
| Pyr/AcOH | Pyridine-Acetic Acid Buffer |
| rpm | Revolutions Per Minute |
| SD | Standard Deviation |
| SDS | Sodium Dodecyl Sulfate |
| SDS PAGE | Sodium Dodecyl Sulfate Polyacrylamide Gel |

| | |
|---|---|
| | Electrophoresis |
| SRGs | Secondary Resistance Genes |
| SOC | Super Optimal Broth with Catabolite Repression |
| TBE | TRIS-Borate-EDTA |
| TCP | Non-Treated 96-Welled Microplate, (Nunc$^{Tm}$) |
| Tn | Transposon |
| TP | Transpeptidase |
| TraDis | Transposon-Directed Insertion Sequencing |
| TRIS | Tris(hydroxymethyl)aminomethane |
| TSP lids | Transferable Solid Phase Lids |
| UDP | Uridine-Diphosphate |
| Und-P | Undercaprenyl Pyrophosphate |
| UTI | Urinary Tract Infection |
| V | Volt |
| VAP | Ventilator-Associated Pneumonia |
| WHO | World Health Organization |
| WT | Wild Type |

# 1 Introduction

## 1.1 *Pseudomonas aeruginosa*, a dreaded pathogen

*Pseudomonas aeruginosa (P. aeruginosa)* is the model organism with which this study was conducted. *P. aeruginosa* is an aerobic, non-fermenting, Gram-negative rod-shaped bacterium, first isolated by Gessard in 1882 and termed *Bacillus pyocyaneus,* due to its characteristic pyocyanin production, which gave infected pus a blue-greenish colour (Driscoll et al., 2007; Hof et al., 2019; Lyczak et al., 2000). As an opportunistic pathogen with low nutrient requirement, *P. aeruginosa* can be found ubiquitously, such as in soil, water, bath taps, surfaces, and even in eye drops, liquid soap or in disinfection products with insufficient strength (Hof et al., 2019). Thus, making this pathogen a notable threat for community-acquired infections and one of the most important causes of hospital-acquired infections (Driscoll et al., 2007). Community-acquired infections include ulcerative keratitis after the use of extensive-wear soft contact lenses, which can lead to an increased risk of vision loss or cornea perforation (Driscoll et al., 2007; Vazirani et al., 2015; Weissman et al., 1984). In patients with weakened immune system, infections such as otitis externa or 'swimmers' ear' can be attributed to *P. aeruginosa* due to its preference for colonisation of wet environments such as lakes or swimming pools (Schaefer & Baugh, 2012). Furthermore, skin and soft tissues as in diabetic foot infections can be co-infected with *P. aeruginosa* (Driscoll et al., 2007).

### *1.1.1 Nosocomial infections caused by P. aeruginosa*

In the case of infections acquired in the hospital setting (nosocomial infections), patients can be colonised prior to admission (Bonten et al., 1999), or contract an infection with *P. aeruginosa* at the hospital (Driscoll et al., 2007). As an opportunistic pathogen, infections in immune-non-compromised individuals can stay asymptomatic. Consequently, immunocompromised patients including such receiving chemotherapy, being neutropenic or immune suppressed with medication as well as AIDS patients are most vulnerable to infections caused by *P. aeruginosa* (Driscoll et al., 2007). Additionally, tissues with disrupted barriers, as can occur during insertion of catheters, in the case of wounds, burn injuries,

or in chronic lung infections such as cystic fibrosis (CF) are prone to offer these pathogens entry (Driscoll et al., 2007; Lyczak et al., 2000). Thereby making patients belonging to vulnerable groups such as immunocompromised patients or intensive care patients those most severely affected by *P. aeruginosa* derived infections. Thereby evolving their illnesses to life-threatening stages. Leading nosocomial infections, caused by *P. aeruginosa* are superinfections of burn injuries, urinary tract infection (UTI), (Lyczak et al., 2000) pneumonia or chronic lung infections in CF patients, with each posing risk of aggravation into septicaemia (Driscoll et al., 2007; Weiner-Lastinger et al., 2020).

In fact, *P. aeruginosa* is one of the most important pathogens causing nosocomial infections. Over 8% of all nosocomial infections can be accounted to this pathogen, exceeded in frequency only by selected *Klebsiella spp*. (8.8%), *Staphylococcus aureus* (11.8%) and *E. coli (Ec.)* (17,5%) (Driscoll et al., 2007; Weiner-Lastinger et al., 2020). In intensive care units (ICUs) even higher percentage of *P. aeruginosa* associated infections are reported. Up to 22.3 % of reported nosocomial infections were attributed to *P. aeruginosa* (Driscoll et al., 2007; Ibrahim et al., 2000). Furthermore, with account to varying patterns between healthcare centres, microbiological investigations have found *P. aeruginosa* to be the second most common pathogen causing healthcare-associated pneumonia (HCAP), hospital-acquired pneumonia (HAP) and ventilator-associated pneumonia (VAP), only been surpassed by *Staphylococcus aureus* at first place (Driscoll et al., 2007; Weiner-Lastinger et al., 2020). Moreover, VAPs occurring after 4 days of mechanical ventilation and around 16% of surgical site infections in paediatric ICU have been attributed to *P. aeruginosa*. (Driscoll et al., 2007). In burn units, *P. aeruginosa* has been identified as an important threat and a frequent infectious isolate, which is been held responsible for the significant increase of *P. aeruginosa* colonisation in burn wounds within the first weeks of hospitalization.

Altogether, considering the development of *P. aeruginosa* infections and the vulnerable groups affected by them, the immense danger posed by *P. aeruginosa* infections and the need to prevent and counteract these infections becomes more evident. It is therefore not surprising, that infections with *P. aeruginosa* have been

linked with comparatively higher morbidity and mortality than infections with other bacterial species (Driscoll et al., 2007; Osmon et al., 2004). This can on one hand be attributed to the fact that those most vulnerable to *P. aeruginosa* infections are patients with suppressed immunity or in critical health stages as in ICUs. On the other hand, *P. aeruginosa* employs a vast arsenal of aggressive virulence factors and antimicrobial resistance mechanisms, bestowing it with remarkable flexibility and adaptability (Dhar et al., 2018; Driscoll et al., 2007). Thus, conferring the pathogen easier colonisation skills and survival in difficult conditions during infection of host. Thereby making *P. aeruginosa* an utmost important threat in the healthcare systems. Hereby, the rationale to increase existing knowledge as to enable better and adequate treatment in targeting and eradicating this perilous pathogen is giving.

## 1.2 Virulence factors of *P. aeruginosa*

The virulence factors of *P. aeruginosa* include adhesion pili type 4, flagella, LPS-O-side chain of the outer membrane as well as protease, elastase, and biofilm production (Jurado-Martin et al., 2021). In addition, *P. aeruginosa* has been found to possess a type-III-secretion system (Lyczak et al., 2000). These virulence factors shall be described in more detail in the following sections.

### *1.2.1 Biofilm formation*

Microorganisms can primarily attach and grow on a variety of surfaces. The spectrum of possible surfaces ranges from hydrophobic (plastic, latex, silicone) over highly charged hydrophilic (metal or glass) to materials even containing antimicrobial properties (materials made from copper or antibiotic-impregnated catheters/threads). It is generally considered that the rougher and more hydrophobic the surface, the easier and more convenient it is for biofilm formation (Donlan, 2001).

Biofilms (Figure 1) are a manner of growth in which microorganisms develop or organise in microcolonies that are embedded in complex extracellular polymeric substance (EPS) ) (Donlan, 2001; Driscoll et al., 2007; Kostakioti et al., 2013). Such microcolonies offer many advantages compared to the planktonic (free- swimming) stage of the bacterium. These include survival in adverse

environments, protection against attacks from the immune system or reduced susceptibility against antimicrobial agents (Donlan, 2001; Kostakioti et al., 2013). The process of biofilm formation follows a series of stages beginning with a reversible attachment of a planktonic bacterium to the target surface. Microorganisms possessing flagellar motility can easily overcome various repulsive forces around the contact surface and stick to it (Donlan, 2001). Irreversible attachment is attained when bacteria deploy their adhesive organelles such as pili. *P. aeruginosa* has been described as an avid biofilm former, which makes use of its flagella and type IV pili to reach and adhere to surfaces irreversibly, attaching to it until more permanent adhesion mechanisms such as extracellular DNA (eDNA) or EPS are produced (Donlan, 2001; Kostakioti et al., 2013). In *Ec.* type I pili are common (Kostakioti et al., 2013).

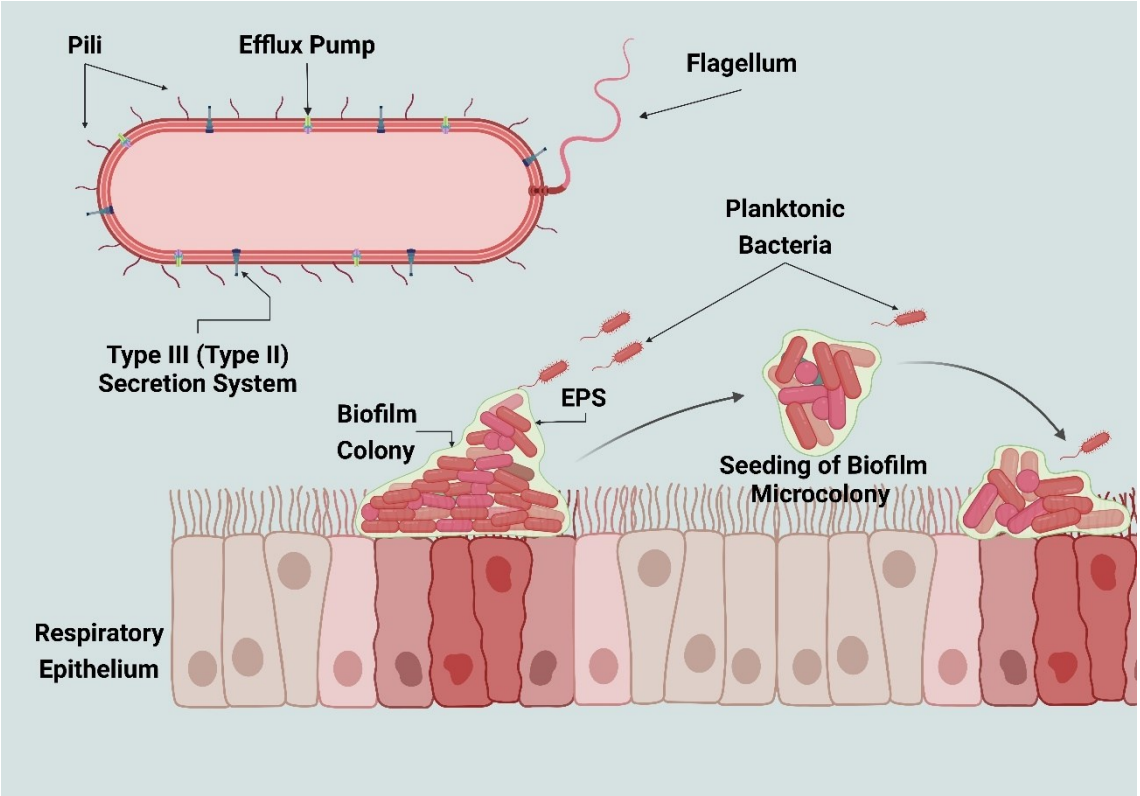


**Figure 1: Schematic depiction of a Gram-negative bacterium during biofilm formation**
*An infected respiratory epithelium due to biofilm formation is shown. Bacteria in a biofilm association are embedded in a complex extracellular polymeric substance (EPS). Cell dispersal can occur in the form of seeding of microcolonies or in planktonic bacteria state as an attempt to avoid external shear forces or increasing of stress conditions. Depicted is the cell wall of a Gram-negative bacterium with the embedded virulence mechanisms including pili, efflux pumps, flagellum, and Type III / Type II secretory system. Figure was created in BioRender. Aidoo, S. (2023) BioRender.com/h08u342*

Apart from the surface contact, intercellular signalling (quorum sensing via substances such as acyl homoserine lactones (acyl-HSLs)) triggers collective gene expression changes and regulations. Thus, resulting in effects on (toxin) secretion, metabolism, virulence, and up-regulation of exopolysaccharide production (Driscoll et al., 2007; Kostakioti et al., 2013). When multiple adhesive planktonic bacteria gather and adhere to a surface, they form microcolonies. This can also be achieved via multiple cell division of a single bacteria. Microcolonies are held together by a complex architecture of EPS, which provides some sort of "water channels" transporting nutrients and oxygen to the bacteria (Donlan, 2001). EPS consists primarily of water (98%) and polysaccharides such as alginate (Donlan, 2001; Driscoll et al., 2007; Kostakioti et al., 2013).

Cell dispersal from biofilm formation can be a result of external shear forces (blood flow), resumption of the planktonic lifestyle to evade diminishing nutrient or oxygen supply or to escape increasing toxic products and other stress-inducing conditions (Driscoll et al., 2007; Kostakioti et al., 2013) Microorganisms growing in biofilm associations have been observed to show comparatively slower growth than their planktonic counterparts, probably due to limited oxygen and nutrient availability as well as increase in toxin production (Donlan, 2001).

In the clinical setting, biofilm formation can be found in indwelling medical devices, including but not limited to catheters (urinal or central venous), heart valves (endocarditis), as well as in chronic osteomyelitis, on tooth enamel, in the middle ear (otitis media) and also in cases of lung infection (e.g. CF) (Donlan, 2001; Driscoll et al., 2007). Biofilms can also form in medically used ventilation devices, thus explaining the increased risk of *P. aeruginosa* colonisation in VAP patients.

In summary, bacteria capable of biofilm formation pose a serious threat to the healthcare. In biofilm associations, bacteria can weaken or even escape the attacks of the immune system and antimicrobial therapy by making themselves difficult to reach for endogenous attacks and antibiotic therapy. Finding ways to prevent biofilm formation, especially for the dreaded nosocomial pathogens, is invaluable as it deprives the pathogens of one of their most powerful weapons.

### *1.2.2 Type III Secretion System*

One important key factor determining the virulence of *P. aeruginosa* is its complex type III secretion system (T3SS, Figure 1). The T3SS is one of the supramolecular structures which enables the bacteria upon contact with cells such as epithelial cells of the lungs, to inject toxic effector proteins into the host. Thus, causing cell injury or cell death. Bacteraemia can occur as a result of penetration into pulmonary blood vessels (Berube et al., 2016; Driscoll et al., 2007; Hauser, 2009). Such toxic effector-proteins are exoenzymes ExoS, ExoT, ExoU and ExoY, of which ExoU is described to be the most virulent (Driscoll et al., 2007).

*In vivo* study models, in which mice, rabbits and rats were affected by pneumonia caused by *P. aeruginosa*, administration of specific antibodies, which targeted PcrV (a component of the integral element of the type III secretory system) showed a comparatively lower count of lung injuries, shock or even death compared to the control group (Driscoll et al., 2007). Thereby validating previous findings, which link the type III secretion system with higher morbidity or mortality in patients suffering from sepsis, pneumonia or in those who are been treated due to VAP (Driscoll et al., 2007).

### *1.2.3 Secreted proteases and elastases*

Major players involved in the pathogenesis of *P. aeruginosa* are secreted proteases such as alkaline protease, (AprA or aeruginolysin), elastase A (LasA or staphylolysin), elastase B (LasB or pseudolysin) and protease IV. These secreted enzymes are metalloproteases with the exception of protease IV, which is a serine protease. They disarm multiple immunoregulatory proteins of the host by degrading multiple immune-defence components, antibacterial peptides, immunoglobins and complement factors such as C1q, C3, as well as cytokines and chemokines (Driscoll et al., 2007; Kida et al., 2008; Suarez-Cuartin et al., 2017). Elastase B (LasB) is one of the most predominant proteases, which possesses a decisive virulent role in burn injuries and acute-stage lung infections. This zinc metalloprotease has a molecular mass of approx. 33 kDA (Kida et al., 2008) and is suspected to degrade several components of the extracellular matrix

of the host, including collagens type III and IV, fibronectin, elastin, vitronectin, and laminin, thus causing tissue injury and haemorrhage (Yang et al., 2015). Azghani et al. earlier attributed *P. aeruginosa's* elastase to disrupt cell-cell connection (tight junction) in host epithelial cells leading to increased permeability and subsequent adverse consequences (Azghani, 1996).

### *1.2.4 Further secretory virulence factors*

Further virulence factors of *P. aeruginosa* are mentioned here briefly. This comprises phenazines and Exotoxin A. Phenazines (e.g. pyocyanin) are secretory virulent metabolites typical for *P. aeruginosa*, which are capable of damaging host cells through proinflammatory and oxidative stress (Driscoll et al., 2007). In the respiratory tract, the effect of pyocyanin has been linked with ciliary dysfunction. Additionally, Exotoxin A is found to interfere with eukaryotic elongation factor 2, thus hampering protein synthesis and leading to cell death (Driscoll et al., 2007).

All these factors orchestrate *P. aeruginosa's* ability to resist treatment and establish persistent chronic infections as often seen in CF patients. In addition to possessing an arsenal of virulence factors, *P. aeruginosa* also has several resistance mechanisms that enable it to resist antibiotic therapy, thus rendering many of the commonly used antibiotics useless in the fight against *P. aeruginosa* infections.

## 1.3 Resistance Mechanisms:

### *1.3.1 Intrinsic Resistance Mechanisms*

1.3.1.1 Low permeability of the outer membrane

*P. aeruginosa* is a cunning pathogen with multiple intrinsic and acquired resistance mechanisms, which enable it to evade antimicrobial targeting and treatment. This pathogen shows outstanding ability by being resistant to many antimicrobial agents, despite their difference and being unrelated in their chemical structures (Mesaros et al., 2007; Strateva & Yordanov, 2009). This ability of *P. aeruginosa* can be accounted firstly to the low permeability of the outer membrane, (Strateva & Yordanov, 2009) which shows a 10 – 100 fold lower

permeability than that of *E. coli (Ec.)* strains (Livermore, 1984; Yoshimura & Nikaido, 1982). Thus, preventing agents from entering the cell in the first place. Additionally, OprD (also known as D2 porin) is an outer membrane porin, which enables entry of carbapenem into the cytosol (Driscoll et al., 2007). Deficiency of this porin resulting from mutation or inactivation is thought to result in reduced uptake of certain antimicrobial agents such as imipenem through the outer membrane (Strateva & Yordanov, 2009). Also, loss of OprD activity is thought to be responsible for carbapenem resistance in *P. aeruginosa* isolates (Driscoll et al., 2007). *P. aeruginosa* is also known for its ability to modify the targets of the antimicrobial agent which is the case in altered penicillin-binding proteins (PBP) (Strateva & Yordanov, 2009).

#### 1.3.1.2 Efflux Pumps

Furthermore, the expression of efflux pumps plays a pivotal role in bestowing intrinsic resistance to *P. aeruginosa*. The possession of multiple efflux pumps, having specifications for different antimicrobial substances of several antibiotic groups (Livermore, 1984; Strateva & Yordanov, 2009) confers almost universal resistance to this pathogen and makes its treatment difficult. *P. aeruginosa* is said to possess minimum 10 distinct efflux systems (Driscoll et al., 2007). Four of these belong to the resistance-nodulation-division (RND) family (Livermore, 2001, 2002) and are of utmost importance regarding the expulsion of antimicrobial agents. All four efflux systems are genetically different and are each made up of three components namely MexA-MexB-OprM, MexC-MexD-OprJ, MexX-MexY-OprM and MexE-MexF-OprN (Strateva & Yordanov, 2009). Of the three components of the efflux system, one subunit (precise MexB, MexD, MexY and MexF) is located in the cytoplasmic membrane and acts there as an energy-dependent pump. The components OprM, OprJ, and OprN act as an outer membrane pore and facilitate excretion while the third component (MexA, MexC, MexX and MexE) is located in the periplasmic space and acts as a linkage between the two other components (Livermore, 2002; Strateva & Yordanov, 2009). The efflux system MexE-MexF-OprN (MexEF-OprN), which plays an important role in this study and will be discussed further in later sections, has substrates including but not limited to (fluoro-)quinolones, chloramphenicol and

trimethoprim (Strateva & Yordanov, 2009) (see Table 1).Table 1 furthermore highlights some antibiotics, which are substrates of the four mentioned efflux pumps.

**Table 1: List of selected antibiotics classes, which are substrates of the efflux pumps.**
*Presented is a selective list of antibiotic classes and antimicrobial agents, which are substrates of the four efflux pumps described. Data compiled from(Driscoll et al., 2007; Lorusso et al., 2022; Strateva & Yordanov, 2009).*

| **MexA-MexB-OprM** | **MexC-MexD-OprJ** | **MexX-MexY.OprM** | **MexE-MexF-OprN** |
|---|---|---|---|
| (Fluoro-)quinolones | (Fluoro-)quinolones | (Fluoro-)quinolones | (Fluoro-)quinolones |
| Macrolides | Macrolides | Macrolides | Trimethoprim |
| Linocomycin | Linocomycin | Linocomycin | Clavulanic acid |
| Novobiocin | Novobiocin | Aminoglycosides | ß-Lactamase inhibitor |
| Chloramphenicol | Chloramphenicol | Chloramphenicol | Chloramphenicol |
| Tetracycline | Tetracycline | Tetracycline | |
| Trimethoprim | Chlorhexidine | | |
| ß-lactams (exceptions include Imipenem) | Penicillins (exceptions include but not limited to Carbenicillins, Cefpirome, Meropenem) | | |
| Monobactam | | | |
| Carbapenem | | | |

In summary, the synergy of minimal permeability of the outer membrane together with the expression of multiple efflux pumps determines much of the inherent resistance of *P. aeruginosa* (Driscoll et al., 2007; Strateva & Yordanov, 2009). The efflux pumps can furthermore be upregulated in their expression, leading to a rise of the minimal inhibitory concentration (MIC) of those antibiotics which are substrates of the pumps (Driscoll et al., 2007).

#### 1.3.1.3 AmpC

The struggle with *P. aeruginosa* is furthermore worsened by its ability to express inducible inhibitors of antimicrobial agents. An important example of such inhibitors is the ß-lactamase AmpC. AmpC as a cephalosporinase cleaves the amino bond of the ß-lactam ring, making the resulting product deprived of its antibacterial activity (Nordmann & Guibert, 1998; Strateva & Yordanov, 2009). The *ampC* gene was first discovered in *Ec*. in 1940. Its enzyme was described by Abraham and Chain as the first bacterial enzyme that could effectively

inactivate penicillin (Abraham & Chain, 1940). Besides, *P. aeruginosa* is able to develop resistance to previously susceptible antibiotics when it is exposed to them during treatments. Hence, antibiotic treatment can exert pressure by selecting strains that have acquired mutations or overexpression that give them a survival advantage (Driscoll et al., 2007). As a result, antibiotic treatment can act as a double-edged sword.

### *1.3.2 Acquired resistance mechanisms*

To aggravate matters more, *P. aeruginosa* has a remarkable ability to acquire further resistance through random mutations or horizontal gene transfer, adding to its existing arsenal of resistance and virulence mechanisms (Strateva & Yordanov, 2009). The rate of horizontal gene transfer is comparatively higher in bacteria found in biofilm formations than in those in liquid culture (Donlan, 2001).

#### 1.3.2.1 Inducible resistance mechanisms

In the presence of certain agents or extracellular environmental situations, *P. aeruginosa* is able to induce specific intracellular reactions as a response to inflicted changes. The expression of efflux pumps and enzymes which mediate antibiotic resistance such as *ampC* overexpression can be induced (Strateva & Yordanov, 2009). For example, the presence of ß-lactam antibiotic, in particular imipenem, has been found to induce a 10 times higher expression of *ampC* (Bagge et al., 2002). Thereby indicating that ß-lactam antibiotics as well as ß-lactamase inhibitors can induce the expression of *ampC* and cause self-inflicted resistance to ß-lactam antibiotics (Hanson & Sanders, 1999). Other factors, which can trigger *ampC* overexpression will be discussed in detail in further sections.

## 1.4 Multi-drug resistant (MDR) strains

It has been shown that *P. aeruginosa* is a cunning pathogen, which employs multiple virulence factors as well as intrinsic and acquired antibiotic-resistant mechanisms, making its treatment and eradication a tough task. It is one of the most important pathogens causing nosocomial infections, which are difficult to treat. In addition, multi-drug resistant (MDR) *P. aeruginosa* strains are emerging, which pose a risk of exacerbating infections and limiting antibiotic treatment options. In accordance with this, the World Health Organization (WHO) ranked *P.*

*aeruginosa* with carbapenem-resistant among the top three bacterial species on its priority list of pathogens, for which new antimicrobial agents are urgently needed (Dhar et al., 2018; Tacconelli et al., 2018) . The acronym ESKAPE, stands for six pathogens that are of immense threat for causing persistent nosocomial infections (Mulani et al., 2019). These nosocomial pathogens are ***E****nterococcus faecium,* ***S****taphylococcus aureus,* ***K****lebsiella pneumoniae,* ***A****cinetobacter baumannii,* ***P****seudomonas aeruginosa* and ***E****nterobacter spp*. ("ESKAPE") (Rice, 2008). The emergence of MDR pathogens is caused amongst others by the widespread use of antibiotics, self-medication and as an effect of insufficient or ineffective therapeutic regimes, which fail to eradicate but instead cause for selection of resistant bacteria strains. Thus, making MDR pathogens account for 15.5 % of Hospital Acquired Infections (HAI) worldwide (Mulani et al., 2019; Rice, 2008).

In general, antibiotic therapy involves either the single use of antibiotics or in combination with other antibiotics of a different class (e.g. combination of ß-lactam with fluoroquinolones). Also, the application of compounds to inhibit or circumvent the bacteria's inherent resistance such as in the case of ß-lactamase inhibitors is frequently used (e.g. piperacillin/tazobactam). The rationale thereby is to regain the effectiveness of antibiotics that have become ineffective or to increase their effectiveness through combination of different antimicrobial classes. However, analysis show an annual shrinkage of the list of antibiotics that can effectively be used for treatment. Many antibiotics that showed effectiveness against ESKAPE pathogens by 2010 have now been deemed inept. In addition, resistance against new antibiotic combinations, that have been suggested to replace those previously found as ineffective have been reported (Mulani et al., 2019). Thus, creating a worrisome outlook of the future, in which more antibiotic combinations with increased adverse side effects shall be in use. Already, colistin has been used as the only treatment for some MDR *P. aeruginosa* strains despite its neuro- and nephrotoxic side effects (Chatterjee et al., 2016; Sabuda et al., 2008). Given that, those mostly affected by *P. aeruginosa* or MDR pathogens are vulnerable immunocompromised patients, those with severe burn injuries or ICU

patients, these prospects are alarming. This highlights the necessity of the development of new antimicrobial agents to assist in controlling MDR bacteria.

## 1.5 Previous study relating to this work: Sonnabend et al. (2020)

Many studies aiming at generating novel antimicrobial agents have previously been conducted. Some focuses on finding new adjuvants to recover the activity of existing antibiotics. Others target chromosomally encoded non-essential genes, that gain importance and promote resistance in the presence of therapeutic concentrations of antibiotics (Sonnabend et al., 2020; Srivastava et al., 2018; Strateva & Yordanov, 2009). Such genes are referred to as secondary resistance genes (SRGs) (Jana et al., 2017).

On the quest to discover novel antimicrobial agents, Sonnabend and colleagues purposed to find new secondary genes, which assist in making *P. aeruginosa* resistant to ß-lactam antibiotics (Sonnabend et al., 2020). They used cefepime and meropenem to search for genes, that seemed to be crucial in achieving or maintaining antibiotic resistance against ß-lactams. For this reason, a transposon (Tn)-directed insertion sequencing (TraDIS) approach was conducted. TraDIS is an approach that helps find genes, which are relevant or responsible for growth and thriving under particular conditions or stress. Found candidates were subsequently verified by creating deletion mutants thereof and testing their ability to ß-lactam resistance and sensitivity as well as their *ampC* expression (Sonnabend et al., 2020).

### *1.5.1 P. aeruginosa Strain ID40*

In their study, Sonnabend et al. used the MDR *P. aeruginosa* strain ID40, which is also the model organism with which this study was conducted. ID40 is a MDR hospital isolate (Willmann et al., 2018) with a genome length of approx. 6.9 Mega base pairs (Mbp) which encodes for more than 6.400 open read frames. Moreover, ID40 carries a plasmid with approx. 57.446 bp length and comprises around 59 putative genes (Sonnabend et al., 2020). The resistance profile of ID40 is depicted in Table 2. The most prominent reason for the resistance to ß-lactam antibiotics is the overproduction of the β-lactamase AmpC. The ß-lactam resistance can furthermore be predominantly attributed to a point mutation in the

*dacB* gene encoding for the Penicillin-binding protein 4 (PBP4) (G to A at position 1310 of the coding sequence) which leads to an inactivated PBP4 as explained below in more detail and consequently AmpC overproduction (Sonnabend et al., 2020) (Torrens et al., 2019).

**Table 2: Resistome of ID40.**
Data obtained from (Sonnabend et al., 2020)

| Resistant | Intermediate | Sensitive |
|---|---|---|
| ***ß-Lactam*** | | ***Aminoglycoside*** |
| Imipenem | Meropenem | Amikacin |
| Piperacillin | | Tobramycin |
| Piperacillin/Tazobactam | | Gentamicin |
| Aztreonam | | |
| Ceftazidime, Cefepime | | ***Polymyxin*** |
| ***Fluoroquinolone*** | | Colistin |
| Levofloxacin Ciprofloxacin | | |

Using a TraDIS approach to decipher secondary resistance genes to cefepime and meropenem, Sonnabend and colleagues found many enzymes associated with the modulation and recycling of the peptidoglycan (PG) to significantly influence the occurrence of ß-lactam resistance upon antibiotic treatment (Sonnabend et al., 2020). Such included the lytic transglycosylase (LT) (MltG), the cytosolic permease AmpG, the ß-lactamase AmpC, and the murein (Mur) endopeptidase MepM1. Before these enzymes and their function can be described in more detail, the metabolism of the cell envelope and cell wall synthesis will be discussed.

## 1.6 The bacterial cell envelope

The bacterial cytoplasm is encased by different specific envelopes, allowing it to separate and protect itself from the surrounding harsh and hazardous environment but also enabling selective exchange with the environment. This can be in the form of expulsion of waste products, communication with surrounding microorganisms or the intake of nutrients. In general, bacteria can be classified into two main groups according to the layers of their cell envelopes: namely

Gram-negative and Gram-positive bacteria (named after Christian Gram (1884)) (Silhavy et al., 2010). The cytoplasm of bacteria is surrounded by a symmetric phospholipid bilayer referred to as the inner membrane (IM) (Silhavy et al., 2010).

In-between the IM and the Outer membrane (OM) is the periplasmatic space, which is of aqueous-viscous like consistency due to the densely packed proteins it contains (Silhavy et al., 2010). The periplasmic space acts as a cellular compartment that allows seclusion of potentially harmful enzymes such as alkaline phosphates or RNAse (Silhavy et al., 2010). Hence, the periplasmic space is often viewed on as an evolutional progenitor of the eukaryotic lysosome (De Duve & Wattiaux, 1966; Silhavy et al., 2010). The outer membrane (OM), which surrounds all compartments is an unsymmetrical lipid bilayer, consisting of phospholipids (confined to the inner leaflet) and lipopolysaccharides (LPS) (confined to the outer leaflet) (Kamio & Nikaido, 1976; Silhavy et al., 2010). LPS is linked to endotoxic shock caused by Gram-negative pathogens that can develop during septicaemia (Raetz & Whitfield, 2002; Silhavy et al., 2010).

The thin peptidoglycan (PG) cell wall (approx. 6 nm) of Gram-negative bacteria is embedded in the periplasmic space. The peptidoglycan sacculus acts as a rigid wall, that gives and obtains the shape of the cell and prevents it from swelling under osmotic stress (Silhavy et al., 2010). Therefore, antimicrobial agents targeting the PG can cause cell lysis by disrupting the PG sacculus. Due to the defective cell wall, the plasma membrane fails to withstand the high intracellular turgor pressure been exerted and thereby leads to cell lysis (Silhavy et al., 2010).

The cell envelope of Gram-positive bacteria differs from those of Gram-negative ones in distinct ways. Firstly, by the absence of an outer membrane. As a result, the cell would lack additional stability and protection. Accordingly, Gram-positive bacteria possess an additional thickened PG cell wall, which could be several times thicker than that of Gram-negative counterparts (Silhavy et al., 2010). An exception from the classification into either Gram-negative or Gram-positive groups are the bacteria of the group Mycoplasma, which in general lack a PG cell wall. *P. aeruginosa*, which is the model organism of this study belongs to the Gram-negative bacteria group.

PG has always posed a good target for antibiotic treatment. Widely used antibiotics targeting the cell wall and its metabolisms are ß-lactams, fosfomycin and glycopeptides (Bush, 2012).

### *1.6.1 Structure and synthesis of PG*

The peptidoglycan (murein) cell wall consists of two building blocks (Figure 2): N-acetyl-muramic acid (MurNAc) and N-acetyl-glucosamine (GlcNAc). These are covalently linked by ß-1,4-glycosidic bonds, creating a heteropolysaccharide (Barreteau et al., 2008; Dhar et al., 2018; Sonnabend et al., 2020). Attached to the MurNAc moiety is an oligopeptide chain, in Gram-negative pathogens usually consisting of L-alanine, γ-D-glutamate, meso-diaminopimelic acid, D-alanine and D-alanine (L-Ala-γ-D-Glu-m-DAP-D-Ala-D- Ala) (Glauner et al., 1988).

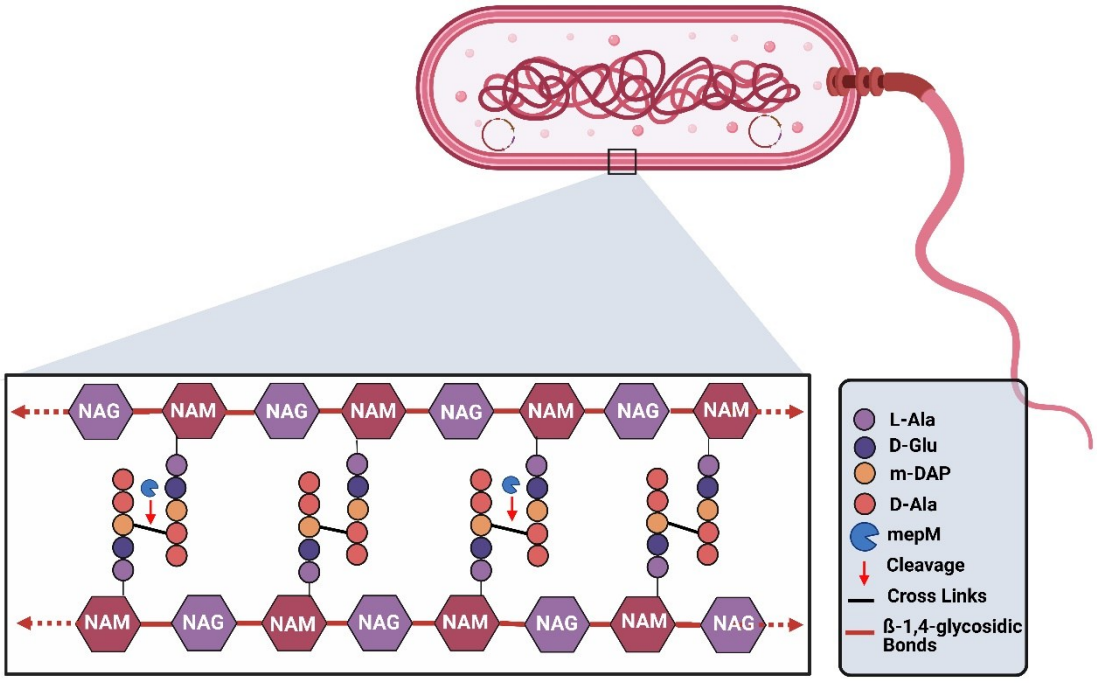


**Figure 2: Simplified illustration depicting the organisation of the PG (murein) sacculus and its structure.**
*In Gram-negative bacteria such as P. aeruginosa, the murein sacculus is located in the periplasm between the OM and the IM. These glycan chains consist of the building blocks N-acetylglucosamine (NAG; purple) and N-acetylmuramyl-pentapeptides (NAM; red). The glycan chains are cross-linked with each other via peptide bonds (black lines) using the peptide residues of the N-acetylmuramic acid moieties (NAM). This creates a mesh-like sacculus that encompasses the entire bacterial surface and provides shape, stability, and protection to the cell. Murein endopeptidases (MepMs; blue Pac-Man figure) enable cell wall remodelling by cleaving the peptide cross-linkage (red arrow), which combines adjacent NAM moieties. Thereby increasing the pores size of the cell wall and releasing PG metabolites as well as facilitating the incorporation of new PG-subunits. Figure was created in BioRender. Aidoo, S. (2023) BioRender.com/n45h697*

These pentapeptide chains are furthermore linked to each other by cross-linking the third amino acid (m-DAP) with the fourth amino acid (D-Ala) of a neighbouring

pentapeptide chain (Schleifer & Kandler, 1972). Thereby, interconnecting adjacent MurNAc-pentapeptides via peptide bonds and creating a firm and ridged mesh-like structure, which encompasses the entire bacteria surface and enables it to withstand environmental and turgor stress (Dhar et al., 2018; Schleifer & Kandler, 1972). Bacteria under normal circumstances are subject to lysis when their murein sacculus is defective or disrupted (e.g. via. Lysozyme or ß-lactam treatment). During the growth, elongation and cell division phase, bacteria remodel their cell wall, which puts them at risk of developing holes or instability in the murein sacculus. Therefore, multiple mechanisms are in place to prevent this risk and enable the incorporation of new PG components without losing cellular integrity (Dhar et al., 2018). Due to the crucial character of the cell wall for the survival of Gram bacteria, it has been the target of many antimicrobial agents such as ß-lactam antibiotics. On this quest, more knowledge about the assembly mechanism, regulation and modulation of cell wall synthesis and its influence on the induction of resistance mechanisms such as AmpC is of utmost importance concerning the battle against ß-lactam resistant pathogens.

### *1.6.2 De Novo synthesis of the murein sacculus*

The cell wall biosynthesis of *Ec.* has been studied extensively and characterized unlike in *P. aeruginosa* where little has conclusively been researched. Bioinformatic analysis however suggest several of *Ec*. enzymes to be homologous to those present in *P. aeruginosa* (Dhar et al., 2018). Following, the cell wall biochemistry of *P. aeruginosa* is been described utilising the terms commonly used for *Ec.* enzymes. Dhar et al. showed in their previous study in detail that the enzymes present in *Ec*. have homologous enzymes in *P. aeruginosa*. The functions that these enzymes perform have been found to be identical (Dhar et al., 2018).

The de-novo synthesis of PG starts in the cytoplasm with fructose-6-phosphate (Figure 3, bottom left). This is converted to GlcNAc- α-6-Phosphate by GlmS (glucosamine-6-phosphate synthetase). Next, several enzyme-directed steps work together to produce uridine-diphosphate (UDP)-GlcNAc. Enzymes involved in these steps are GlmM and GlmU (Dhar et al., 2018; Sonnabend et al., 2020).

In contrast to *Ec*, GlmS in *P. aeruginosa* is regulated by a repressor GlmR (Ramos-Aires et al., 2004), while in *Ec*. both GlmS and GlmU are regulated by a transcriptional factor NagR (Dhar et al., 2018).

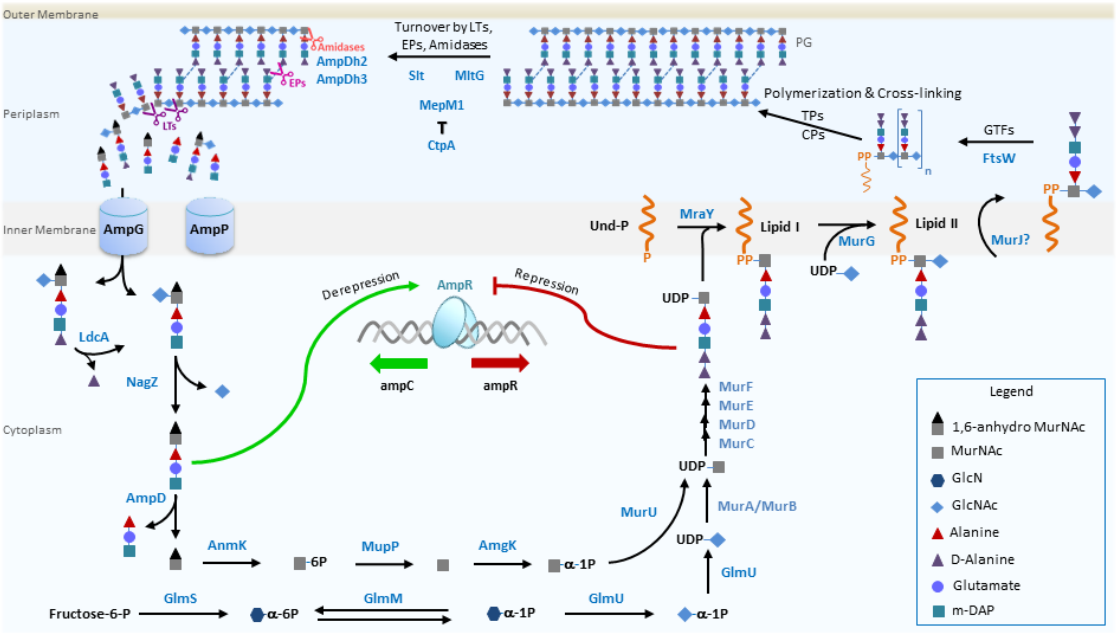


**Figure 3: Illustration depicting PG recycling processes and synthesis pathway of PG metabolites.**
*The murein sacculus is located in the periplasm in between the outer and the inner membrane. The murein sacculus consists of the two alternating peptidoglycans GlcNAc and MurNAc, whereby the MurNAc moiety contains the pentapeptide residue. The peptidoglycan chains are linked into a mesh-like structure through peptide cross linkages, which are typically created between the third and the fourth peptide residues of adjacent MurNAc moieties (meso-diaminopimelic acid → D-Ala). The murein sacculus is under constant turnover, mediated through various enzymes, pores and polymerases, creating an intricate interplay which in turn enables cell response to environmental changes and communication. PG metabolites can be generated via de novo synthesis or through an alternative pathway which recycles PG metabolites from the periplasmatic space. Detailed explanation of both pathways as well as the meaning of enzyme abbreviations are provided in the main text. AmpR, a transcriptional regulator is usually repressed as long as UDP-MurNAc (PG precursor) binds to its effector binding domain. Accumulation of 1,6-anhydroMurNAc (PG turnover metabolite) displaces UDP-MurNAc-pentapeptide from its binding site on AmpR. This results in derepression of AmpR, which in turn takes its active form, regulating the expression of several genes such as ampC (ß-lactamase) (Balasubramanian et al., 2012; Dhar et al., 2018; Sonnabend et al., 2020). Figure obtained from (Sonnabend et al., 2020))*

The resulting UDP-GlcNAc is subsequently converted to UDP-MurNAc by the MurA/MurB enzymes (Dhar et al., 2018; Sonnabend et al., 2020). Following, the Mur ligases MurC, MurD, MurE, and MurF convert the product into UDP-MurNAc pentapeptide by sequential addition of the amino acids (Barreteau et al., 2008). Now, the UDP-MurNAc pentapeptide is transported to the inner leaflet of the IM and attaches to a cytosolic carrier named undercaprenyl pyrophosphate (Und-P), which is arranged as a 55-carbon aliphatic chain (Dhar et al., 2018). The linkage is made by MraY, resulting in the formation of Lipid I (Bouhss et al., 2004; Ikeda

et al., 1991). By attaching of GlcNAc to Lipid I, MurG catalyses Lipid II (undecaprenol-pyrophosphate-UDP-GlcNAc-MurNAc peptide) (Brown et al., 2013; Vollmer & Bertsche, 2008), which in turn is transported into the periplasmic space putatively by the enzymes FtsW and MurJ. (Dhar et al., 2018; Mohammadi et al., 2011; Sham et al., 2014). Several periplasmic enzymes such as high molecular mass penicillin-binding protein (HMM PBP), glycosyltransferases (GTF), transpeptidases (TP), and DD-carboxypeptidase (CPs) incorporate GluNAc-MurNAc pentapeptides into the growing peptidoglycan. (Legaree et al., 2007; Vollmer & Bertsche, 2008). HMM PBP fulfils both transglycosylase and transpeptidase activity. (Dhar et al., 2018)

This de-novo synthesis of PG is sensitive to fosfomycin activity. To bypass this, *P. aeruginosa* utilises the alternative pathway that recycles PG metabolites. The existence of this alternative pathway is thought to be responsible for *P. aeruginosa*'s inherent resistance against Fosfomycin (Sonnabend et al., 2020).

### *1.6.3 PG recycling*

Bacteria usually recycle about 40-50% of their cell wall components and thereby save resources and energy (Dhar et al., 2018; Doyle et al., 1988). Cell wall degradation and recycling commences with the catabolic activity of enzymes such as low-molecular-mass-penicillin-binding proteins (LMM PBP), endopeptidases (EPs), lytic transglycosylases (LTs) and amidases. These enzymes cleave the PG layers and facilitate insertion of new PG components or the degradation thereof (Dhar et al., 2018). In detail, murein (Mur) endopeptidases (EP) such as MepM1 cleaves the cross-linkage between adjacent peptides (Dhar et al., 2018; Vollmer et al., 2008), while LTs such as MltA, MltG or Slt cleave the glycosyl bonds (Lee et al., 2017).

Investigation on *P. aeruginosa* identified 11 LTs, in contrast to *Ec*. which possesses eight lytic transglycosylase enzymes. The LT presented by *P. aeruginosa* are namely MltA, MltB, MltD, MltF, MltF2, MltG, Slt, SltB1, SltB2, SltH/SltB3 and RlpA (Lee et al., 2017). Some enzymes exhibit clear preference in their substrates, e.g. RlpA acts mainly on substrates having no peptide chain

attached (GlcNAc-anhMurNAc) whereas MltB requires the presence of peptides (muropeptide). In general, functional redundancy between the lytic enzymes can be assumed (Dhar et al., 2018).

*P. aeruginosa* harbours a periplasmatic amidase, namely AmpDh2, which is homologue to the amidase AmiD present in *Ec*. Amidases act on the murein sacculus by separating the sugar molecules from the peptide moiety (Dhar et al., 2018; Eggers et al., 2023; Vollmer et al., 2008). Carboxypeptidases are responsible for cleaving the C-terminal amino acids of the peptide chains. LMM-PBP can either act as endopeptidases or carboxypeptidases (Vollmer et al., 2008).

Through the activity of LTs, Eps, LMM PBP, carboxypeptidases and Amidases PG metabolites such as N-acetyl-glucosamine-1,6-anhydro-N-acetyl-muramyl-peptide (GlcNAc-1,6-anhMurNAc-peptides), GlcNAc-anhMurNAc as well as free tri-, tetra-, and pentapeptides are released. (Sonnabend et al., 2020; Vollmer et al., 2008). *P. aeruginosa*. harbours a permeases AmpG, that enables the transport of GlcNAc-1,6-anhMurNAc-peptide into the cytoplasm (Jacobs et al., 1994). Besides AmpG, *P. aeruginosa* possesses another permease referred to as AmpP, whose substrates concerning the transfer of PG metabolites are yet not fully elucidated. Nevertheless, AmpP and AmpG have been found to play a great role as a requirement for the maximum expression of ß-lactamase. (Kong et al., 2010; Perley-Robertson et al., 2016).

In the cytoplasm, the next enzyme that modifies the muropeptides is β- N- acetylglucosaminidase (NagZ). NagZ cleaves the glycosidic bond, resulting in separate units of GlcNAc and 1,6-anhMurNac peptides (Dhar et al., 2018). Under the influence of an LD-carboxypeptidase, commonly known as LdcA, the terminal D-alanine from the oligopeptide is cleaved. (Sonnabend et al., 2020; Templin et al., 1999). Next, the amidases AmpD and AmpDh3 separate the peptides from the sugar moiety, whereby 1,6-anhydroMurNAc (1,6-anhydro-N-acetylmuramic acid) and tri-, tetra- as well as pentapeptides are created (Dhar et al., 2018; Eggers et al., 2023; Zhang et al., 2013). Subsequently, AnmK catalyses the phosphorylation of 1,6-anhMurNAc to MurNAc-6-Phosphate, which in turn is

further processed by MupP, AmgK and MurU to UDP-MurNAc (Gisin et al., 2013; Sonnabend et al., 2020).
Having UDP-MurNAc been an intermediate product of both the PG de novo synthesis and the PG recycling pathway, both pathways converge from this step on leading to the generation of Lipid-II and the integration of new PG components into the PG sacculus as described above (Dhar et al., 2018; Sonnabend et al., 2020).

In summary, the rigid PG cell wall also shows a dynamic character, that enables cell growth and recycling of resources. Thereby also protecting the microorganism and preventing the entry of harmful agents. Such harmful agents are ß-lactam antibiotics, which hampers cell wall synthesis in bacteria. ß-lactam antibiotics are able to bind to the HMM PBP due to their resemblance with its actual substrate the D-Ala-D-Ala residue of the muropeptide. They bind with high affinity to these enzymes, thereby causing for loss of activity of the HMM- PBP and blocking their transpeptidase activity site. This results in reduced cross- linking and subsequent cell lysis. (Bush & Bradford, 2016; Dhar et al., 2018; Strominger & Tipper, 1965).

### 1.7 Inducible ß-lactamase AmpC

In general, Penicilloyl-serin transferase (better known as ß-lactamase) inhibits ß-lactam antibiotics by cleaving the amino bond of the ß-lactam ring, thereby leading to loss of antibacterial activity of the resulting product (Strateva & Yordanov, 2009; Sykes & Matthew, 1976). ß-lactamases are historically classified into 4 molecular classes (Ambler, 1980; Strateva & Yordanov, 2009). *P. aeruginosa* possesses ß-lactamases of all 4 classes, with AmpC belonging to the class C group. This class of ß-lactamase uses a serine-based mechanism in its active centre to inactive ß-lactam antibiotics (Strateva & Yordanov, 2009).

In *P. aeruginosa* AmpC is an inducible chromosomal encoded ß-lactamase (cephalosporinase). *ampC* usually is expressed at a low level, which however is responsible for the intrinsic resistance against many of the early generation cephalosporins and aminopenicillins (Langaee et al., 2000). Moreover, clinically commonly used ß-lactamase inhibitors, including sulbactam, tazobactam and

clavulanic acid, have been found to have no inhibitory effect on AmpC (Nordmann & Guibert, 1998). In addition, it has been postulated that cell wall defects, as an effect of ß-lactam activity can result in increased in-flux of cell wall metabolites into the cytoplasm and thereby upregulate the expression of *ampC.* This is achieved by the transcriptional regulator AmpR. In Wild-Type (WT) strains, AmpR is repressed, leading to a low level of *ampC* expression. (Balasubramanian et al., 2012; Dik et al., 2017). This repressed state however can be altered through the occurrence of mutations or accumulation of activator ligands of AmpR.

### *1.8* AmpR, the regulator of *ampC* expression

The unhindered action of toxins such as ß-lactam antibiotics is prevented by a feedback loop that registers such stress and sets the defence mechanisms in motion. Through the cytosolic intermediates and the rate of PG turnover, the cell is informed about its state, which is followed by counteractive processes. (Mayer, 2019). The inducible *ampC* gene, that encodes for a ß-lactamase (cephalosporinase) is regulated by a transcriptional regulator AmpR, which under normal circumstances exhibits a down-regulative influence on *ampC* expression. AmpR is a 32.6 kDa transcriptional regulator protein with two active domains: a helix-turn-helix DNA-binding domain and an effector-binding domain. *ampC* and *ampR* are two adjacent genes separated by an intercistronic DNA region, to which the DNA-binding domain of AmpR attaches (Dik et al., 2017). The effector-binding domain binds a suppressor ligand (UDP-MurNAc-pentapeptide, a precursor of the PG building block). Activator ligands are the cytosolic muropeptides such as 1,6-anhMurNAc-penta- or tri-peptides deriving from PG recycling processes. UDP-MurNAC-pentapeptide (repressor) has been found to bind with higher affinity to the AmpR effector-binding domain than the activator counterparts (muropeptides). Thus, explaining the usually suppressed state of AmpR, which can be reverted by the accumulation of PG-recycling muropeptides. (Dik et al., 2017; Sonnabend et al., 2020).

In summary, accumulation of the PG biosynthesis intermediate products represses *ampC* expression, while PG degradation metabolite derepresses *ampC* expression, thereby leading to elevated ß-lactamase production.

Overproduction of AmpC can also be achieved by mutations in the recycling or synthesis pathway. Thus, deletion or mutation of the amidases *ampD* leads to high levels of 1,6-anhMurNAc-tri-peptides but low levels of 1,6-anhMurNAc-pentapeptides and is associated with increased activation of AmpR and consequently higher AmpC production (Moya et al., 2009; Torrens et al., 2019). The low levels of anhMurNAc-pentapeptides is probably due to the carboxypeptidase activity of PBP4 (encoded by the *dacB* gene), which converts muropentapeptide precursors into murotetrapeptide precursors (Moya et al., 2009; Torrens et al., 2019). Mutations in *dacB* also have been found to lead to *ampC* overexpression and elevated MIC values for ß-lactam antibiotics (Dhar et al., 2018). Inactivated PBP4 possesses no longer the carboxypeptidase activity. Therefore 1,6-anhMurNAc-pentapeptides can accumulate in the cytosol which leads to a higher activation of AmpR and consequently AmpC overproduction (Balasubramanian et al., 2012; Torrens et al., 2019).
Moreover, it has to be mentioned that AmpR acts as a global transcriptional regulator (Figure 4).

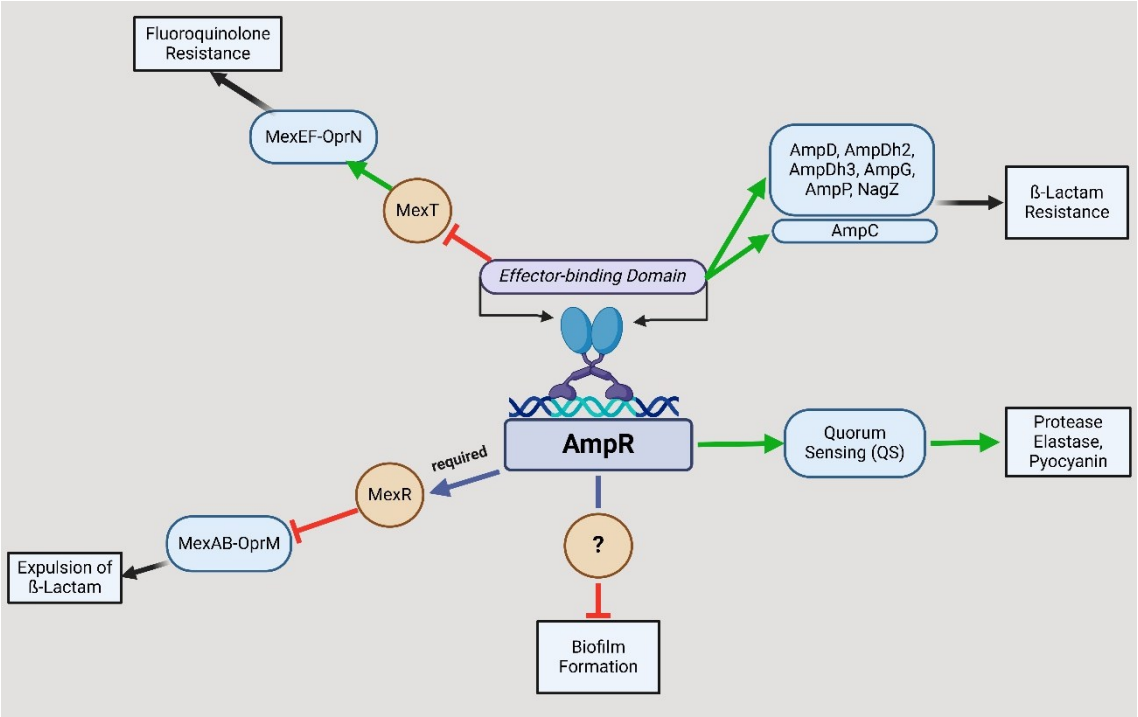


**Figure 4: AmpR regulation and its effect on antibiotic resistance and virulence**
*Data compiled from (Balasubramanian et al., 2012; Dhar et al., 2018). Depicted are a selection of proteins under AmpR regulation. AmpR is a transcription factor that regulates the expression of various effectors involved in antibiotic resistance and virulence. It plays a role in the expression of the amp-genes and the nagZ gene, whose transcripts are important enzymes involved in ß-lactam resistance. The expression of ampC can either be repressed or derepressed*

*depending on the ligand binding at the effector-binding domain of AmpR. AmpR furthermore influences the expression of the efflux pump systems MexEF-OprN and MexAB-OprM via their regulator proteins. AmpR repression or mutation is linked to hyperactivity of these efflux pumps, resulting in reduced susceptibility to their substrates. Moreover, the activity of AmpR is associated with increased production of protease, elastase and pyocyanin via the quorum sensing pathway. Biofilm formation has been postulated to be depressed by AmpR activity through a yet unknown mechanism. Figure was created in BioRender. Aidoo, S. (2023) BioRender.com/r89z380*

For instance, the presence of active AmpR has been described as a requirement for *mexR* expression. MexR is a regulator of MexAB-OprM and represses the expression of this efflux pump (Balasubramanian et al., 2012; Dhar et al., 2018). One of the substrates been expelled by MexAB-OprM are ß-lactams (see Table 1). Figure 4 describes the interaction between AmpR, MexR and ß-lactam resistance. In brief, AmpR locked in its inhibited state through its repressor ligand (UDP-MurNA-pentapeptide) causes for repressed *ampC* expression, which in turn leads to suppressed ß-lactamase activity. Furthermore, active AmpR induces the expression of *mexR*, which in turn inhibits the expression of the *mexAB-oprM* cluster resulting in reduced expulsion of ß-lactam antibiotics. Surprisingly, mutation of *ampR* or *ampC* in the *P. aeruginosa* strain PAO1 leads to nullified ß-lactam resistance, despite the activity of MexAB-OprM. Hereby, highlighting that AmpC carries a greater impact in conferring ß-lactam resistance than the expulsion by the counterpart MexAB-OprM (Dhar et al., 2018).

Furthermore, the efflux pump MexEF-OprN, which expels substances including fluoroquinolones (see Table 1) is positively regulated by its regulator MexT (Dhar et al., 2018). AmpR is able to repress the expression of *mexT*. Hence, AmpR-deficient mutants show comparatively greater resistance to fluoroquinolones than WT strains (Figure 4) (Balasubramanian et al., 2012).

The important role of AmpR in conferring resistance to *P. aeruginosa* has herewith been highlighted. It is an important joint along which many paths are connected and intertwined.

## 1.9 Correlation between enzymes involved in PG modulation and ß-lactam resistance

A correlation between the activity of the enzymes involved in cell wall modulation or biosynthesis and ß-lactam resistance can be assumed and have been shown in several studies. For example, AmpG (permease) deficient *Enterobacteriaceae* were found deprived of their ability to recycle PG metabolites leading to reduced

*ampC* expression (Jacobs et al., 1994; Korfmann & Sanders, 1989). This effect of AmpG was validated by Zamorano and co-workers, who mutated *ampG* in pan-resistant *P. aeruginosa* clinical isolates and thereby could restore their sensitivity to ß-lactam antibiotics (Dhar et al., 2018; Zamorano et al., 2011). Moreover, upon inactivation of *ampD*, 1,6-anhMurNAc-peptides accumulated in the cytoplasm leading to induction of *ampC* overexpression and ß-lactamase overproduction (Jacobs et al., 1995) .This effect was successfully counteracted by mutation of *nagZ* (generates 1,6-anh-MurNAc muropeptides by cleaving the glycosidic bond) in *ampD* deficient mutants, resulting in reversal of *ampC* overexpressing and reduced ß-lactam resistance (Zamorano et al., 2010). Consequently, inhibitors of NagZ were tested as potential candidates for antimicrobial targeting. However, these inhibitors showed affinity also to human glucosaminidases, rendering them unfit for antimicrobial usage (Stubbs et al., 2007).

The correlation between PG metabolites and ß-lactam resistance has additionally been shown in the case of the periplasmatic LT MltG, which is responsible for cleaving the glucosyl bonds between the PG sugar moieties. Sonnabend et al. found an impressive reduction in ß-lactam MIC values upon deletion of MltG in *P. aeruginosa* ID40 strains (see Figure 5). This effect was attributed to decreased AmpC activity of the mutants (Sonnabend et al., 2020). Activity of Bulgecin, a natural inhibitor of Slt and MltG leads similarly to reduced ß-lactam MIC values, thereby validating the findings of Sonnabend et al and highlighting the role of LTs such as MltG in conferring ß-lactam resistance (Dik et al., 2019).

In summary, it appears that many of the enzymes involved in PG metabolism are directly or indirectly involved in the production of the ß-lactamase AmpC. To understand the mechanisms concerning ß-lactam resistance and to develop effective therapies against it, further studies on these enzymes would be of great assistance. These enzymes also provide good targets for controlling ß-lactam resistant pathogens.

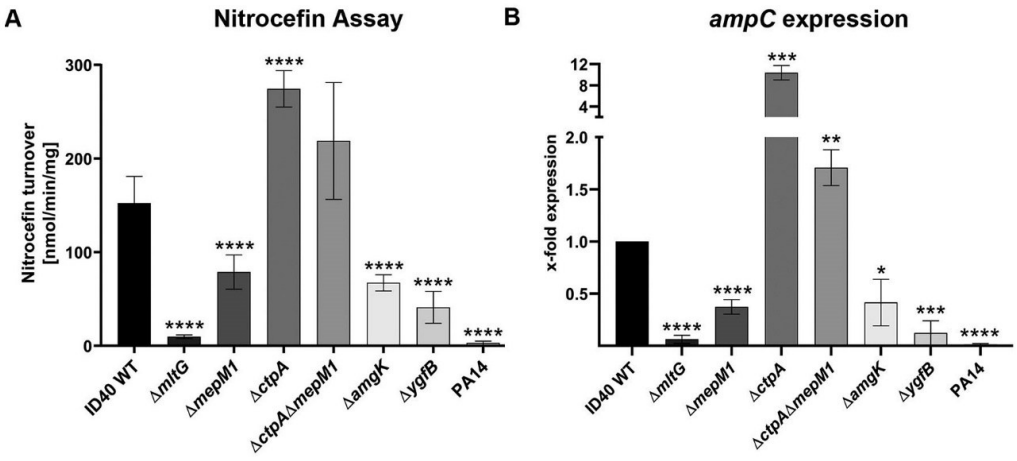


**Figure 5: Impact of different genes involved in PG turnover upon *ampC* expression and activity.**
*Assessment of ß-lactamase activity using a nitrocefin assay (A) and ampC expression in x-fold expression (B). Deletion of the genes mltG, mepM1, and amgK, whose enzymes are involved in PG turnover and recycling show a significant reduction of ampC expression and activity compared to ID40 WT. ctpA deletion increases ampC expression and activity which can partially be reversed by additional deletion of mepM1 (ΔctpA ΔmepM1 double mutant). The P. aeruginosa laboratory strain PA14, which shows susceptibility to all tested ß-lactam antibiotics has nearly undetectable ampC expression and activity. Student's t-test was conducted with the results of the WT set as reference: *, P = 0.05; **, P = 0.01; ***, P = 0.001; ****, P = 0.0001. Data obtained from (Sonnabend et al., 2020), with kind permission for usage by his research group AG Schütz-Bohn (Tübingen)*

## 1.10 Murein endopeptidases (MEPs) and CtpA

In *P. aeruginosa*, murein endopeptidases (MEPs) cleave the peptide cross linkage D-Ala-m-DAP between adjacent muropeptides (Sonnabend et al., 2020). By so doing, MEPs facilitate the incorporation of new GlcNAc-MurNAc-peptides into the PG matrix while simultaneously releasing PG degrading products such as GluNAc-1,6-MurNAc into the cytosol (Dhar et al., 2018; Strateva & Yordanov, 2009). In *Ec*. more knowledge about the functions of Endopeptidases (EPs) have been generated while few is yet known about the function of MEPs in *P. aeruginosa* (Dhar et al., 2018). In *Ec*. three such MEPs have been identified, namely MepM (YebA), MepH and MepS. The genome of *P. aeruginosa* likewise harbours three homologous enzymes, here designated as MepM1 (PA0667, Locus Tag reference strain PAO1), MepM2 (PA3787) and MepM3 (PA4404), which are closely related to MepM (YebA) of *Ec*. Additionally, *P. aeruginosa* encodes homologue endopeptidases to MepH and MepS of *Ec.* which are here designated as MepH1 (PA1198) and MepH2 (PA1199) (Kemper, 2020) medical PhD thesis). In the recent TraDIS approach done by Sonnabend and colleagues, genes of various MEPs such as *mepM1*, *mepM2*, *mepM3* and *mepH2* were identified as secondary resistance genes (SRGs) (Jana et al., 2017; Sonnabend

et al., 2020), which showed involvement in contributing and maintaining ß-lactam resistance. For MepM1, it has in fact been validated that deletion of *mepM1* increased sensitivity to ß-lactam antibiotics (Figure 5) (Sonnabend et al., 2020). Additionally, the carboxy-terminal processing protease (CtpA) has been shown to degrade various EPs, particularly MepM1, MepM3, MepH1 and MepH2, thereby controlling the degree of PG cross-linkage in the murein sacculus (Srivastava et al., 2018; Strateva & Yordanov, 2009). Intriguingly, MepM2 is not a substrate of CtpA, hence MepM2 is not regulated by this protease (Srivastava et al., 2018).

It has previously been shown that loss of the activity of CtpA results in defective type III secretory system (Srivastava et al., 2018). In fact, additional deletion of *mepM1* in a *ctpA*-deficient mutant *(ΔctpA ΔmepM1* double mutant) reverted this effect and partially restored virulence and cytotoxicity. Hence indicating the major role of MepM1 activity in mediating the phenotype of CtpA deficiency (Sonnabend et al., 2020; Srivastava et al., 2018).

The absence of CtpA also leads to reduced rate of cross linking. This is attributed to the accumulation of CtpA substrates such as MepM1, which with the fall of restraint, exert their function hyperactively (Srivastava et al., 2018). In addition to these findings, deletion of *ctpA* (*ΔctpA*) in ID40 strains resulted in elevated *ampC* expression and increased resistance to ß-lactam antibiotics, while loss of *mepM1* has been linked to reduced *ampC* expression and increased susceptibility to ß-lactam antibiotics in ID40 strains (Sonnabend et al., 2020) (Figure 5). Upon further deletion of *mepM1* (Δ*mepM1 ΔctpA* double mutant) this hyper-resistance could be reduced but not fully reverted. The remaining portion of the hyper-resistant phenotype of the Δ*mepM1 ΔctpA* double mutant was attributed to the effect of the other CtpA substrate, which remained hyperactive due to the mutation of *ctpA* (Sonnabend et al., 2020).

Hence, it can be concluded that increased activity of *mepM1* mediates *ampC* expression and thereby promotes ß-lactam resistance (Sonnabend et al., 2020). Thus, it is of great interest to determine whether inhibition of multiple *mepMs* can

result in resistance and phenotype changes and also to identify which of the *mepMs* is the major contributor to these phenotypical changes.

### *1.10.1 Impact of various mepM deletion on ß-lactam resistance*

In a recent study of our research group Kemper J. (Medical PhD thesis) analysed in her dissertation the impact of single, or combined *mepM* gene deletions upon ß-lactam resistance. Her findings are summarized in Table 3 (Kemper, 2020). In brief, single deletion of *mepM1* and *mepM2* increased sensitivity to many of the ß-lactam antibiotics tested, compared to the MDR ID40 wild-type strain. Combined deletion of *mepM1* and *mepM2* (ID40 *ΔmepM1/2)* restored ß-lactam sensitivity for many of the tested ß-lactam antibiotics. In fact, ß-lactam susceptibility was increased for all tested antibiotics. Additional deletion of *mepM3* (ID40 *ΔmepM1 ΔmepM2 ΔmepM3* designated as *ID40 ΔmepM123)* made the mutant sensitive to all tested ß-lactam antibiotics. Thus, highlighting the immense impact, which the activity of MepMs have in contributing to and maintaining ß-lactam resistance. Thereby suggesting, that loss of all three MepMs results in restored ß-lactam susceptibility.

**Table 3: Antibiotic sensitivity of Pa. ID40 and various *mepM* deletion mutants**
*The table summarizes the measured minimal inhibitory concentrations (MICs). Colour code: highlighted in green are the MICs of the deletion mutants, which are lower than the MICs of the WT. Bold green on grey background indicates the MIC values which are lower than the MIC breakpoint according to the current EUCAST Clinical Breakpoint Tables. Red marks the MIC values which are higher than those of the WT. (Table obtained from the dissertation of J. Kemper (Kemper, 2020)).*

| | MIC Breakpoint (µg/L) | | ID40 (WT) | *ΔmepM1* | *ΔmepM2* | *ΔmepM3* | *ΔmepM1/2* | *ΔmepM123* |
|---|---|---|---|---|---|---|---|---|
| | S ≤ | R > | | | | | | |
| Meropenem | 2 | 8 | 8 | 2 – 8 | 4 | 4 – 8 | **≤1 - 2** | **<1 - 1** |
| Imipenem | 4 | 4 | 32 | 16 | 32 | 32 – 64 | 8 | 4 – 8 |
| Cefepime | 8 | 8 | 16 | **8** | 8 - >8 | 16 | **4** | **4** |
| Ceftazidime | 8 | 8 | 32->32 | 16–32 | 32->32 | 32->32 | **8** | **4 – 8** |
| Piperacillin/ Tazobactam | 16 | 16 | 128->128 | 32–64 | 32 – 64 | 64–128 | **8 – 16** | **8 – 16** |
| Aztreonam | 16 | 16 | 16 - 32 | **8 - 16** | 16 | 16 - 32 | **4 - 8** | **4** |

### *1.10.2 AmpC expression in the different mepM mutants*

The reduction in ß-lactam resistance after deletion of various *mepM* genes can be attributed to concurrent behaviour of *ampC* expression. It has been previously discussed that deficiency in *mepM1* activity is correlated to reduced expression

and activity of *ampC* (Sonnabend et al., 2020). Kemper J. added to this knowledge with her results showing that *ΔmepM1* carries the major effect in reducing *ampC* expression and thus reducing ß-lactamase activity. *ΔmepM2* and *ΔmepM3* single mutants did not result in a significant reduction of *ampC* expression (Kemper, 2020). Furthermore, she showed that multi-deletion mutants (double and triple deletions) did not provide a synergistic or additive reduction of *ampC* expression (Figure 6). This implies that MepM1, MepM2 and MepM3 in concert modulate β-lactam resistance not only by modulation of *ampC* expression but in addition also by so far unknown mechanisms.

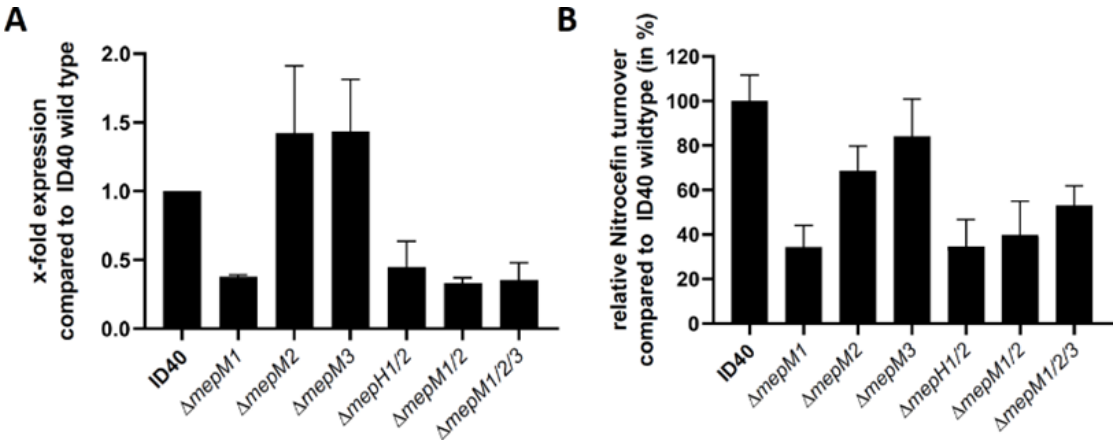


**Figure 6: The *ampC* expression and ß-lactamase activity of different MEP deletion mutants.**
*(A) RT-PCR of RNA isolates. Depicted are the mean and SD of x-fold ampC expression of ID40 (WT) in comparison to the different mutants. (B) Assessment of ß-lactamase activity using a nitrocefin assay. Presented are the mean and SD of relative nitrocefin turnover compared to ID40 WT. (Data are obtained and compiled from the doctoral thesis of Kemper J and Vöhringer K (Kemper, 2020; Vöhringer)).*

### *1.10.3 Correlation between expression of the mexEF-oprN cluster and ß- lactam resistance*

To address how MepM´s contribute to β-lactam resistance, in a first attempt Kathrin Vöhringer performed in her doctoral thesis a proteome analysis of membrane proteins of ID40 and of a *mepM123* deletion mutant (Vöhringer, unpublished). The rationale behind these experiments was based on precedent experiments and findings of others. Srivastava et al. reported that deletion of the MepM1 regulator *ctpA* resulted in defective type III secretory system, which could be reverted upon additional *mepM1* deletion (Δ*mepM1* Δ*ctpA*) (Srivastava et al., 2018). This suggests that increased activity of MepM1 results in reduced cross-linking (= increased PG pore size) which in turn has a negative effect on the

assembly or insertion of secretion proteins that traverse the cell envelope. In accordance with this, studies on *Aeromonas hydrophila* revealed that increased PG pore size (reduced peptide cross-linking) influenced the assembly mechanism of the type II secretion system (Vanderlinde et al., 2017). Conceivably, it can be assumed that loss of various MepMs could alter the PG pore size toward more cross-linkage and thereby influence the assembly and insertion of macromolecular structures.

Proteomic analyses of membrane proteins revealed that loss of *mepM1, mepM2 and mepM3 (ΔmepM123)* leads to altered production rate of several proteins. Among such proteins with increased production were components of the MexEF- OprN efflux pump. In line with this finding, Sonnabend et al. (supplementary data) observed in their TraDIS experiments that Tn insertion in the *mexE* or *mexF* gene, might lead to increased resistance to cefepime or meropenem (Sonnabend et al., 2020). Therefore, it was hypothesized that *mepM123* deletion leads to higher levels of the MexEF-OprN efflux pumps and consequently to reduced β-lactam resistance. Indeed, higher levels of the efflux pump in a *mepM123* deletion mutant could be confirmed. Moreover, it could be demonstrated that additional deletion of the efflux pump cluster in a *mepM123* deletion mutant, partially restores β-Lactam resistance, indicating that MepMs might modulate somehow the protein levels of this efflux pump which in consequence might influence β-lactam resistance. At first sight, this finding seems to be counterintuitive because efflux pumps are exporters of antibiotics. In this case however, β-lactam antibiotics are not a substrate of the MexEF-OprN efflux pump (see Table 1). In addition, efflux pumps export not only antibiotics but also other substrates. Lamarche et al. demonstrated that MexEF-OprN efflux pumps modulate quorum sensing through secretion of a signalling molecule of the HAQ family. Moreover, activation or overproduction of the efflux pumps seems to modulate virulence. They observed upon overproduction of this efflux pump, reduced swarming motility, pyocyanin production and biofilm formation (Lamarche & Déziel, 2011). In line with this another study reported in strains overproducing MexEF-OprN changes in quorum sensing and reduced secretion

of factors (rhamnolipids, pyocyanin and elastase) controlled by the quorum sensing systems of *P. aeruginosa* (Köhler et al., 2001).

Taken together, previous work showed that MepM1, MepM2 and MepM3 contribute to ß-lactam resistance by modulating AmpC and MexEF-OprN production and eventually also by additional yet unknown mechanisms.

### 1.11 Key points aimed to address in this study

In summary, the overall future goal of this project is to assist in the identification and development of new antimicrobial compounds that enhance the susceptibility of MDR *P. aeruginosa* strains to ß-lactam antibiotics by the inhibition of MepM proteins. Since in silico analyses of the MepM structure (Kemper, 2020) suggest, that the catalytic centres of all three MepMs are very similar, it might be feasible to inhibit all three MepMs with one compound. MepMs could therefore already qualify as a drug target. However, if deletion of *mepMs* would also affect virulence, this would furthermore increase the attractivity of MepMs as a drug target. The overproduction of MexEF-OprN together with the potential alteration of AmpR's activity in a *mepM123* deletion background led to the hypothesis that, *mepM123* deletion might possibly affect biofilm production, as well as elastase, pyoverdine and pyocyanin production.

Therefore, the specific aim of this thesis was to answer the following questions:

1. Is the influence of all MepMs equal, or does one specific MepM hold a major role in modulating the abundance of the MexEF-OprN efflux pump?
2. Do MepMs modulate virulent factors such as biofilm formation, elastase, pyoverdine and/or pyocyanin secretion? If yes, which MepMs play here a dominant role?
3. Does deletion of *mepM123* attenuate virulence in a *Galleria melonella* infection model?

# 2 Materials and Methods

## 2.1 Materials

### *2.1.1 Galleria mellonella larvae*

*Table 4: G. mellonella Larvae*

| Species | Origin |
|---|---|
| Galleria mellonella larvae | b.t.b.e. Insektenzucht GmbH, Wörishofen |

### *2.1.2 Bacterial strains*

#### 2.1.2.1 Provided bacterial strains

*Table 5: Provided bacterial strains*

| Strains | Origin |
|---|---|
| ***Pa. ID40*** | |
| ID40 (WT) (multi-resistant bloodstream isolate) | (Willmann et al., 2018) |
| ID40 *ΔmepM1* | (Sonnabend et al., 2020) |
| ID40 *ΔmepM2*<br>ID40 *ΔmepM3*<br>ID40 *ΔmepM1 ΔmepM2*<br>ID40 *ΔmepM1 ΔmepM3*<br>ID40 *ΔmepM1 ΔmepM2 ΔmepM3* | AG. Bohn-Schütz<br>unpublished |
| ID40 *ΔctpA* | (Sonnabend et al., 2020) |
| ID40::*mexE*-HiBiT<br>ID40 *ΔmepM1 ΔmepM2 ΔmepM3::mexE*-HiBiT | AG. Bohn-Schütz<br>unpublished |
| ***Pa. PA14*** | |
| *Pa*. PA14 (WT) (Laboratory *Pa*. strain) | DSM (Nr. 19882) |
| *Pa*. PA14 *ΔmepM1*<br>*Pa*. PA14 *ΔmepM2*<br>*Pa*. PA14 *ΔmepM3*<br>*Pa*. PA14 *ΔmepM1 ΔmepM2*<br>*Pa*. PA14 *ΔmepM1 ΔmepM3*<br>*Pa*. PA14 *ΔmepM1 ΔmepM2 ΔmepM3* | AG. Bohn-Schütz<br>unpublished |

| ***Escherichia coli*** | |
|---|---|
| *Ec*. DH5α | Thermo Fisher Scientific, Schwerte |
| *Ec*. SM10λ pir ($Ca^{2+}$ competent) | (Hmelo et al., 2015) |
| *Ec*. TOP 10 ($Ca^{2+}$ competent) | Thermo Fisher Scientific, Schwerte |
| *Ec*. SM10λ pir pEXTK-*mexE*-HiBiT | AG Bohn-Schütz unpublished |

2.1.2.2 In-frame insertion mutants generated in this work

*Table 6: In-frame insertion mutants generated in this work*

| Strains | Gene alteration |
|---|---|
| ***Pseudomonas aeruginosa*** | |
| ID40 *ΔmepM1::mexE*-HiBiT<br>ID40 *ΔmepM2::mexE*-HiBiT<br>ID40 *ΔmepM3::mexE*-HiBiT<br>ID40 *ΔmepM1 ΔmepM2::mexE*-HiBiT<br>ID40 *ΔmepM1 ΔmepM3::mexE*-HiBiT | Insertion of HiBiT tag at the C-terminal end of *mexE*. |

### *2.1.3 Oligonucleotides*

*Table 7: Primers*

| Primer reference number | Sequence (5' → 3') | Characteristics |
|---|---|---|
| 1703 | ACCGGATCGTCGTGAATG | Flanking primer to verify HiBiT insertion through PCR |
| 1704 | AGAGCATGTTCTCCACCC | |
| 1081 | TCTTCTTGAACAGCCGCC | |

### *2.1.4 Antibodies*

*Table 8: Antibodies*

| Name | Origin |
|---|---|
| Monoclonal mouse α-*E. coli* RNA Polymerase β IgG Antibody (1:1.000) | BioLegend (USA) |

| | |
|---|---|
| Horseradish-peroxidase (HRP) conjugated Rabbit anti-Mouse antibody IgG (H+L) (1:2.000) | Thermo Fisher Scientific Schwerte |

### *2.1.5 Antibiotics*

*Table 9: Antibiotics*

| Name | Manufacturer |
|---|---|
| Gentamycinsulfate | AppliChem, Darmstadt |
| Irgasan | Sigma-Aldrich, Taufkirchen |

### *2.1.6 Enzymes*

*Table 10: Enzymes*

| Name | Reference |
|---|---|
| Deoxyribonucleotide triphosphate (dNTPs) (10mM) | Roche Diagnostics, Rotkreuz (CH) |
| DpnI restriction enzyme | Thermo Fisher Scientific, Schwerte |
| Gibson Assemble master mixture | Kindly provided by Andrea Eipper (Tübingen);<br>5x isothermal (ISO) reaction buffer:<br>➔ 25% PEG-8000, 500 mM Tris-HCl (pH 7.5), 50 mM MgCl2, 50 mM DTT, 1 mM each of the 4 dNTPs and 5 mM NAD<br>Phusion DNA Polymerase<br>From New England Biolabs, Ipswich (UK)<br>T5 Exonuclease (10 U/µl)<br>From Epicentre, Madison (USA)<br>Taq DNA Ligase (40 U/µl)<br>From New England Biolabs, Ipswich (UK) |
| Lysozyme (from Hen Egg) | Sigma-Aldrich |
| Mango Mix™ | Bioline, London (UK) |

### *2.1.7 Buffer solutions*

*Table 11: List of Buffer solutions*

| Name | Composition / Manufacturer |
|---|---|
| 5 x SDS running buffer | 60.55 g Tris<br>288,15 g Glycerine<br>10 g SDS<br>filled to 2 L with dd$H_2O$ |
| 5x TBE buffer | 54 g Tris Base<br>27,5 g Boric acid<br>20 mL of 0,5 M EDTA (pH = 8.0)<br>filled to 1 L with dd$H_2O$ |
| 10 x Western Blot-transfer buffer | 60,6 g Tris<br>288,8 g Glycerine<br>filled to 2 L with dd$H_2O$ |
| 10 x Western Blot wash buffer | 24,2 g Tris<br>180 g NaCl<br>1 M HCl (for pH = 7,4)<br>100 mL Tween-20<br>Filled to 2 L with dd$H_2O$ |
| 4x Laemmli Buffer | Supplemented with 10% ß-mercaptoethanol (BME) (Bio-Rad, Hercules (USA)) |
| DPBS (1x) | Gibco Life Technologies,<br>Carlsbad (USA) |
| Ponceau Red Stain | 0.5 % (w/v) Ponceau S,<br>1 % acetic acid, in dd$H_2O$ |
| Pyridine-Acetic Acid (Pyr/AcOH) Buffer | 4.05 mL Pyridine<br>2.86 mL Acetic Acid<br>Filled to 1L with 993.09 mL ddH2O<br>pH to 5.0 |

### *2.1.8 Culture medium for bacterial cultivation*

*Table 12: Mediums for bacterial culturing*

| **Solid Medium** | **Composition** |
|---|---|
| Lysogeny Broth (LB) agar | 15 g bactoagar<br>10 g Tryptone<br>5 g Yeast-Extract<br>10 g NaCl<br>pH = 7,0 |
| LB Gentamycin 15 Agar | LB agar supplemented with 15 mg/L gentamycin |
| LB Gentamycin 75 Agar | LB agar supplemented with 75 mg/L gentamycin |
| LB Irgasan Gentamycin Agar | LB agar supplemented with 15 mg/L Gentamycin and 25 mg/L Irgasan |
| **Liquid Medium** | **Composition** |
| LB Liquid Medium | 10 g Tryptone<br>5 g Yeast-Extract<br>10 g NaCl<br>Filled to 1 L with $ddH_2O$<br>pH = 7,0 |
| LB-Glycerol-Bouillon (20%)<br>For cryo conservation | 100 mL Glycerol (100%)<br>Filled to 500 mL with LB liquid medium |
| LB Medium<br>Supplemented with IPTG | 1 g Tryptone<br>0.5 g Yeast-Extract<br>1 g NaCl<br>100 mL $ddH_2O$<br>100 µL 1 M IPTG in $ddH_2O$ |

| | |
|---|---|
| M9 minimal medium | 770 mL sterile Ampuwa® water<br>200 mL 5x M9 salts (Sigma-Aldrich, Cat. No: M6030)<br>1 mL 1 M MgSO4<br>3 g D-Glucose<br>0.1 mL 1 M $CaCl_2$<br>10 mL 100x Trace Elements consisting of<br>5 g EDTA<br>0.83 g $FeCl_3$<br>0.084 g $ZnCl_2$<br>0.013 g $CuCl_2$ * 2 $H_2O$<br>0.01 g $CoCl_2$ * 6 $H_2O$<br>0.01 g $H_3BO_3$<br>0.001 g $MnCl_2$ * 6$H_2O$<br>Dissolved in 1 l Ampuwa® pH 7.5 |
| M9 minimal medium without trace elements | ~700 mL Ampuwa®<br>200 mL 5x M9 salts (1 M MOPS)<br>1 mL 1 M $MgSO_4$<br>0.1 mL 1 M $CaCl_2$)<br>filled to 1 L with Ampuwa ®<br>0.4% (w/v, final concentration) glucose added prior to usage form a 20% stock solution |
| MOPS minimal medium | 500 mL Ampuwa®<br>100 mL 1 M MOPS stock solution (0.1 M final)<br>100 mL 10x $Na_2$-Succinate stock solution (0.4 M)<br>10 mL 100x $NH_4Cl$ (0.93 M)<br>1 mL 1000x NaCl (5 M)<br>10 mL 100x $KH_2PO_4$ (0.22 M) |

| | |
|---|---|
| | 1 mL 1 M $MgSO_4$<br>100 µL 10.000x $FeSO_4$ (36 mM)<br>Fill up with Ampuwa® to 1 L<br>Sterile filtration (0.22 µm Filter)<br>All stock solutions were generated with Ampuwa® water as the solvent. |
| S.O.C - Medium<br>Nutrient-rich medium for recovery of transformed bacterial cells | 2 % Tryptone<br>0,5 % Yeast Extract<br>10 mM NaCl<br>2,5 mM KCl<br>10 mM $MgCl_2$<br>10 mM $MgSO_4$<br>20 mM D-Glucose |
| Succinate minimal medium | 6 g $K_2HPO_4$<br>3 g $KH_2PO_4$<br>1 g $(NH_4)_2SO_4$<br>0.2 g $MgSO_4$ * $7H_2O$<br>4 g succinic acid<br>1.1 g NaOH<br>Dissolved in Ampuwa®<br>pH adjusted to 7.0 with NaOH<br>Fill up to 1 L with Ampuwa®<br>Sterile filtration (0.22 µm Filter) |

### *2.1.9 Components of the minimal media*

*Table 13: Components of the minimal media*

| **Media** | **Chemical** | **Final concentration in media [mM]** |
|---|---|---|
| Succinate minimal medium | KP (Potassium Phosphate) | 56.4 |
| | $(NH_4)_2SO_4$ | 7.57 |
| | $MgSO_4$*$7H_2O$ | 1.66 |
| | succinic acid | 33.87 |

| | | |
|---|---|---|
| MOPS minimal medium | MOPS | 100 |
| | Succinate | 40 |
| | $NH_4Cl$ | 9.3 |
| | NaCl | 43 |
| | $KH_2PO_4$ | 2.2 |
| | $MgSO_4$ | 1 |
| | $FeSO_4$ | 0.0036 |
| M9 minimal Medium without Trace Elements | Phosphate-Buffer | 69.8 |
| | $NH_4Cl$ | 18.7 |
| | NaCl | 8.55 |
| | $MgSO_4$ | 1 |
| | CaCl2 | 0.1 |
| | Glucose | 2.22 |

### *2.1.10 Solutions*

*Table 14: Liquid solutions created for this study*

| Solution | Composition |
|---|---|
| 1% Crystal violet solution (CV) | 1 g Crystal violet powder<br>20% (v/v) Ethanol<br>80% DI water |
| 33% acetic acid | 33 % (v/v) acetic acid<br>66 % $ddH_2O$ |
| Buffer K | 50 mM Triethanolamine<br>250 mM Sucrose in $ddH_2O$ |

### *2.1.11 Chemicals*

*Table 15: List of chemicals*

| Name | Manufacturer |
|---|---|
| Acidic acid | Carl Roth, Karlsruhe |
| Agar agar | Carl Roth, Karlsruhe |
| Ampuwa® | Fresenius Kabi GmbH, Homburg |
| ß-mercaptoethanol (BME) | Applichem, Darmstadt |

| | |
|---|---|
| Beef extract | BD Biosciences, Freiburg |
| Blue Block PF (10x) | SERVA Electrophoresis GmbH, Heidelberg |
| Boric acid | Sigma-Aldrich, Taufkirchen |
| Chloroform | Merck, Darmstadt |
| Crystal Violet powder | Sigma-Aldrich, Taufkirchen |
| $FeSO_4$ | |
| Gene ruler 1 kb plus DNA Ladder | Thermo Fisher Scientific, Schwerte |
| Glycerine | Merck, Darmstadt |
| $K_2HPO_4$ | Sigma-Aldrich, Taufkirchen |
| $KH_2PO_4$ | |
| $MgSO_4*7H_2O$ | |
| MOPS | |
| $Na_2$-Succinate | |
| $(NH_4)_2SO_4$ | |
| Orange G Dye | |
| PageRuler$^{TM}$, prestained protein ladder | Thermo Fisher Scientific, Schwerte |
| Protease inhibitor | Roche Diagnostics, Rotkreuz (CH) |
| Pyochelin I and Pyochelin II (0,5mg/mL) | Toronto Research Chemicals |
| Pyocyanin from *Pa*. ≥98% (HPLC) | Sigma-Aldrich, Taufkirchen |
| Pyoverdines from *Pa*. >90% (HPLC) (25 mg/mL) | Sigma-Aldrich, Taufkirchen |
| Pyridine, EMSURE® ACS,Reag. Ph Eur | Merck, Darmstadt |
| SeaKem® LE Agarose | Lonza, Basel (CH) |
| Skimmed milk powder | TSI Consumer Goods GmbH, Zeven |

| | |
|---|---|
| Succinic acid | Sigma-Aldrich, Taufkirchen |
| SYBR safe DNA gel stain (0,01 %) | Thermo Fisher Scientific, Schwerte |
| Triton X-100 | Sigma-Aldrich, Taufkirchen |
| TRIS | Applichem, Darmstadt |
| Trypton | Applichem, Darmstadt |
| Tween-20 | Bio-Rad, Hercules (USA) |
| Yeast extract | Carl Roth, Karlsruhe |

### *2.1.12 Consumables*

*Table 16: Consumables*

| **Product** | **Manufacturer** |
|---|---|
| BD-Micro Fine™ + Demi Syringe ($^1/_2$ U) | BD, Heidelberg |
| Columbia agar plate with Sheep blood | Thermo Scientific, Schwerte |
| Cuvettes (plastic), 1,5 mL | SARSTEDT, Nümbrecht |
| Eppendorf cups (1,5 mL) | SARSTEDT, Nümbrecht |
| Eppendorf cups (1,5 mL, 2 mL) Safe lock | Eppendorf, Hamburg |
| Falcon tubes (15 mL), conical bottom | Greiner Bio-One, Frickenhausen |
| Falcon tubes (50 mL), conical bottom | Corning Life Sciences, Corning (USA) |
| Injekt® Solo disposable syringes (2 mL, 5 mL, 10 mL) | B. BRAUN (Hessen) |
| Inoculation loops, blue | Greiner Bio-One, Frickenhausen |
| Cryo-tubes, 1,5 mL | Sarstedt, Numbrecht |
| Microplate, 96-well, transparent, F-Bottom Chimney well | Greiner bio-one, Frickenhausen |
| Microplate, 96-well, Black, F-Bottom Chimney well | Greiner bio-one, Frickenhausen |
| Nitrocellulose Membrane, Cytiva Amersham™ Protran™ | Cytiva Europe GmbH, Freiburg |

| | |
|---|---|
| Nunc™, F96 Microplate, non-treated, white | Thermo Fisher Scientific, Schwerte |
| Nunc™- MaxiSorp™ 96-well ELISA microplate | |
| Nunc™ Immuno TSP lids | |
| Parafilm® M Sealing Film | Brand, Wertheim |
| Petri dishes | Greiner Bio-One, Frickenhausen |
| Pipette tips, 10 µL | Brand, Wertheim |
| Pipette tips, 200 µL | Sarstedt, Numbrecht |
| Pipette tips, 1000 µL | Greiner, Frickenhausen |
| Polystyrene reagent tube (14 mL), Round bottom, sterile | Corning Life Sciences |
| Reaction tubes for PCR (0,2 mL), 8 strip tubes with attached dome-shaped cup | Biozym, Oldendorf |
| Mini-PROTEAN® TGX precast gels (4-20%) | Bio-Rad, München |
| Serological pipettes (5 mL, 10 mL, 25 mL, 50 mL) | Corning Life Sciences |
| Whatman filter paper | Merck Darmstadt |

### *2.1.13 Food mixture for G. mellonella*

*Table 17: Food mixture for G. mellonella*

| **Name** | **Manufacturer** |
|---|---|
| Beeswax | Mixed-Store.de, Ilshofen |
| Corn grits | Rapunzel Naturkost, Legau |
| Dried yeast flakes | |
| Glycerine, EMSURE® Ph Eur | Merck, Darmstadt |
| Honey | Stöckmann Honig, Gödenstorf |
| skimmed milk powder | TSI Consumer Goods GmbH, Zeven |
| Wheat meal | Rapunzel Naturkost, Legau |

### *2.1.14 Kits*

*Table 18: Kits*

| Name | Manufacturer |
|---|---|
| EnzChek™ Elastase Assay Kit | Thermo Fisher Scientific, (Schwerte) |
| EnzChek™ Protease Assay Kit (red fluorescence) | |
| Kapa HiFi PCR Kit | Roche Diagnostics, Rotkreuz (CH) |
| Monarch® Plasmid Miniprep Kit | New England Biolabs GmbH, (Frankfurt) |
| Nano-Glo® HiBiT Blotting System | Promega Corporation, Fitchburg, (USA) |
| Nano-Glo® HiBiT Lytic Detection System | |
| QIAGEN® *DNeasy UltraClean Microbial* Kit | QIAGEN GmbH, (Hilden) |
| SideroTec™-Total assay Kit | Accuplex Diagnostics Ltd., (Ireland) |
| *Wizard® SV Gel and PCR Clean-Up System* Kit | Promega Corporation, Fitchburg, (USA) |

### *2.1.15 Equipments*

*Table 19: Instruments and devices*

| *Device* | *Type* | *Manufacturer* |
|---|---|---|
| BioPhotometer | | Eppendorf, Hamburg |
| Centrifuge | 5430R | Eppendorf, Hamburg |
| Centrifuge | Multifuge 3S-R | Heraeus, Hanau |
| Centrifuge (Mini) | Rotilabo | Roth, Karlsruhe |
| Manual Microsyringe Pump with Digital Display | DMP | World Precision Instruments, Inc. (USA) |
| Electrophoresis System | Mini PROTEAN Tetra Cell | Bio-Rad, Munich |
| Electroporation System, | Gene Pulser II | Bio-Rad, Munich |
| FastGene FAS-V | | Nippon Genetics, Düren |
| Gel electrophoresis-Documentation System | BioDoc Analyze | Biometra, Göttingen |
| Gel electrophoresis-Gasket and system | Mini-Sub Cell GT | Bio-Rad, Munich |

| | | |
|---|---|---|
| Gel tray | 7x10 cm | Bio-Rad, Munich |
| Gel tray | 15x10 cm | Bio-Rad, Munich |
| Heating Block | Thermomixer comfort | Eppendorf, Hamburg |
| Ice Machine | AF 156 | Scotsman Ice Systems, Vernon Hills (USA) |
| Incubator | B6420 | Heraeus, Hanau |
| Incubation Shaker | Ecotron | INFORS HT, Graz |
| Integra Multi Pipette (electrical) | VIAFLO | INTEGRA Biosciences GmbH (Biebertal) |
| Integra pipette tips | Green choice Inserts | |
| Label Printer | Dymo 450 | Dymo/Newell brands, Sandy Springs (USA) |
| Magnetic Heating Stirrer | MR 3002 | Heidolph, Schwabach |
| Microwave | Micromat | AEG, Frankfurt a.M. |
| Multi Pipette | Xplorer | Eppendorf, Hamburg |
| Nanodrop One Spectrophotometer | | Thermo Fisher Scientific |
| NanoQuant Plate™ | | Tecan Trading AG |
| pH meter | Mettler Toledo™ FiveEasy | Thermo Fisher Scientific |
| Photometer | Bio Photometer | Eppendorf, Hamburg |
| Pipettes (2,5 µL, 10 µL, 20 µL, 100 µL, 200 µL, 1000 µL) | Reference; Research plus | Eppendorf, Hamburg |
| Pipetting Aid (electrical) | Accujet pro | NeoLab, Heidelberg |
| Power Supply | PowerPac 200/300 | Bio-Rad, München |
| Precision balance | EG 4200-2NM | KERN & SOHN GmbH |
| Rocking Shaker | Assistant RM5 | Karl Hecht, Sondheim |
| Sterile Bench | BDK-S 1200, | Weiss, Sonnenbühl |

| | | |
|---|---|---|
| | 1300 | |
| Tecan-microplate reader | Infinite M200 Pro | Tecan Group, Crailsheim |
| Thermocycler for PCR | C1000 Touch | Bio-Rad, München |
| Vortexer | Vortex Relax top | Heidolph, Schwabach |
| Water Bath | WB 10 | Memmert, Schwabach |
| Western Blot Imager | Fusion Solo S | Vilber, Eberhardzell |

### *2.1.16 Software*

*Table 20: Software*

| **Name** | ***Manufacturer*** |
|---|---|
| Adobe Photoshop CS6 | Adobe Systems, Mountain View (USA) |
| BioRender | Science Suite Inc., Toronto (Canada) |
| EndNote | Thomson Reuters, New York City (USA) |
| GraphPad Prism 9.4.1 | GraphPad Software, San Diego (USA) |
| i-control 1.11 (for Tecan infinite reader) | Tecan, Crailsheim |
| ImageJ | Java, National Institutes of Health (USA), (Rueden et al., 2017) |
| Microsoft Office | Microsoft, Redmond (USA) |
| SnapGene | GSL Biotech LLC, Chicago (USA) |

## 2.2 Methods

### *2.2.1 Bacteria strains and growth conditions*

Unless otherwise stated, bacteria were cultured by inoculating frozen cryo-cultures into 5 mL of lysogeny broth (LB) and incubated overnight at 37°C with continuous agitation of 200 revolutions per minute (rpm). For cultivation on LB plates, cryo-culture was spread on LB plates with an inoculation loop and incubated overnight at 37°C without agitation. Bacterial growth on LB plates containing antimicrobial additives was also performed at 37°C without agitation. Bacterial cultures for detection of pyoverdine secretion were cultured at 30°C for 24 hours with agitation (200 rpm).

Depending on the targeted cell density, subcultures were generated in two different standardized ways. The overnight cultures were either diluted to an optical density $(OD)_{600}$ of 0.1 or diluted 1:20 with fresh LB and incubated for 2 hours at 37 C with shaking (200 rpm).

### *2.2.2 Photometric measurement of bacteria cell count*

To provide standardized sample conditions for comparison of assays, the bacterial cell count was determined and adjusted based on the optical density at the wavelength 600 nm ($OD_{600}$). For this purpose, bacterial culture was diluted in fresh LB-medium or DPBS (Dulbecco's Phosphate Buffered Saline) and vortexed for proper mixture. The $OD_{600}$ was measured with a photometer. An $OD_{600}$ of 1 corresponded to a cell count of $10^9$ *Pseudomonas* bacteria cells per mL. Bacterial cultures were adjusted to desired ODs using following formula:

$$V_1 * c_1 * D = V_2 * c_2$$

$$\rightarrow V_1 = \frac{V_2 * c_2}{D * c_1}$$

$V_1$ = volume of the culture

$c_1$ = measured $OD_{600nm}$

$V_2$ = final desired volume

$c_2$ = final desired $OD_{600nm}$

$D.$ = dilution factor

### *2.2.3 Storage of bacterial strains as cryo-cultures*

Bacterial strains were preserved at -80°C in LB medium supplemented with 20 % glycerol. 5 mL of overnight cultures were pelleted at 5000*g for 5 min. The supernatant was discharged, and the pellet resuspended in 3 mL of LB+20% glycerol. 1 mL aliquots of this suspension were filled into cryo tubes and frozen immediately.

### *2.2.4 1 % agarose gel electrophoresis*

Gel electrophoresis uses electrical current to separate DNA fragments according to their sizes for purification and visualization. Nucleic acid gel electrophoresis was performed by first preparing a 1 % (w/v) agarose solution using SeaKem® LE Agarose and 0.5 % (v/v) TBE (Tris-Borat-EDTA) buffer. Next, the agarose solution was boiled and supplemented with 4.5 µL of SYBR safe DNA gel stain. Then the warm solution was poured into the gel tray and an electrophoresis comb corresponding to the number of needed wells was inserted. After cooling and solidifying, the gel was placed into a gel electrophoresis-gasket (Bio-Rad) and immersed into 0.5 % TBE buffer. The wells were then filled with 7 µL of PCR product and 5 µL of gene ruler 1 kb plus. The gene ruler consists of a standardized mix of DNA fragments which later allowed matching of the separated DNA fragments to their respective sizes. Electrophoresis then ran for 45 minutes (min) at 110 Volt (V) and variable current. Upon completion, the DNA fragments were visualized using a Gel Documentation System (Biometra). We often used gel electrophoresis to separate DNA fragments after polymerase chain reaction.

### *2.2.5 Polymerase chain reaction (PCR)*

PCR is an enzyme-dependent method that enables *in-vitro* amplification of DNA fragments with the aid of appropriate up- and downstream primers. In this work, PCR was performed to screen for successful mutagenesis and to generate up and down fragments for mutagenesis vectors. Genomic DNA (gDNA) or supernatant of lysed bacterial culture served as a template. General components of the PCR reaction are stated in Table 22. The Thermocycler (C1000 Touch) with the following general settings was employed.

*Table 21: PCR settings*

| Stage | Temperature (°C) | Time [min] | Repeats |
|---|---|---|---|
| 1. Initial Denaturation | 95 | 5 | 1x |
| 2. Denaturation<br>3. Annealing<br>4. Extension | 95<br>54 - 70<br>72 | 0.5<br>0.5<br>1 | 30x |
| 5. Final Extension<br>6. Infinite Hold | 72<br>4 | 5<br>∞ | 1x |

*Table 22: General Components of the PCR reaction*

| Compound | Amount per PCR tube | |
|---|---|---|
| 2x Mango Mix™ | 7.5 | µL |
| Forward Primer (10 µM) | 0.5 | µL |
| Reverse Primer (10 µM) | 0.5 | µL |
| $H_2O$ | 3.5 | µL |
| DNA sample | 3 | µL |

### *2.2.6 Mutagenesis to obtain mexE-HiBiT insertion mutants.*

To assess the influence of MepMs upon the abundance of MexE-OprN efflux pump, we sought to detect MexE by connecting chromosomally to the *mexE* gene a gene fragment encoding a HiBiT tag. For this purpose, the plasmid pEXTK-*mexE*-HiBiT was used. pEXTK-*mexE*-HiBiT carries 744bp homologous to the 3´ end of *mexE* followed by 24bp encoding a Glycin-Serin linker, 33bp encoding the HiBiT tag, a Stop codion and 942 bp homologous to the downstream flanking DNA sequence of the *mexE* gene. For the selection process during mutagenesis the plasmid carries a gentamicin resistance cassette and an IPTG inducible Thymidinkinase (Figure 7). The plasmid was transferred by conjugation as described below. For this purpose, the donor strain *Ec.* SM10λ pir strain containing pEXTK-*mexE*-HiBiT was used.

2.2.6.1 Bi-parental mating

Overnight culture of the donor strain (*Ec.* SM10λ pir strain containing pEXTK-*mexE*-HiBiT) and various recipient strains (*P. aeruginosa* ID40 *mepM* deletion mutants) were grown. 200 µL of the cultured donor and 400 µL of the cultured recipient were combined and pelleted at 10000 g for 1 min. The pellet was re-suspended in 100 µL of LB, then spotted onto a non-selective LB agar plate and incubated overnight at 37°C. The next day, the mating mix was scraped off the plate and re-suspended into 2 mL of LB. 100 µL and 20 µL of this suspension mix was plated on LB selection plates containing Irgasan (25 ng/mL) as selection against *E. coli* and Gentamycin (75 ng/mL). Only those *P. aeruginosa* cells having incorporated the mutator plasmid through the first crossover (Figure 7) were able to grow on these selection plates.

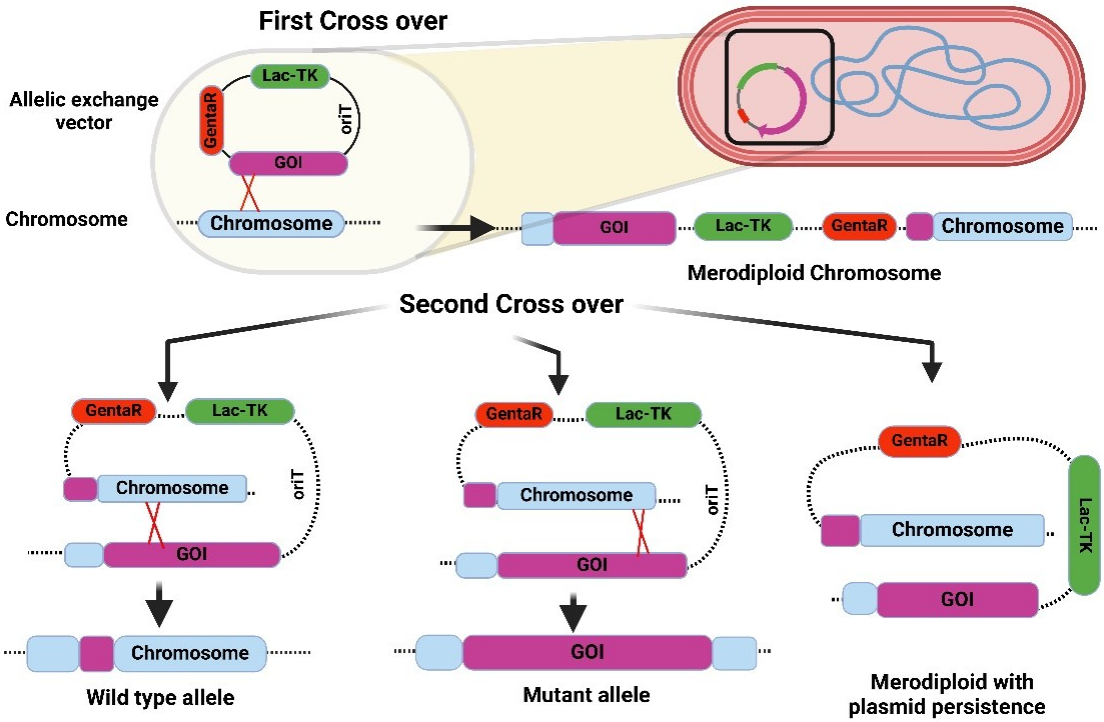


**Figure 7: Schematic depiction of the two-step allelic exchange.**
*First, a suitable allelic exchange vector containing the gene of interest (GOI) is created. The DNA flanking regions of the GOI are homologous to the up- and downstream region of the chromosomal insertion site. Genes for counterselection such as a thymidine kinase under a Lac operator (Lac-TK) and antibiotic resistance against Gentamycin (GentaR) are also included. During mating of the donor (Ec.) and recipient cells (Pa.), horizontal gen transfer of the allelic exchange vector occurs. After vector transfer a first crossover can occur. This results in merodiploid cells carrying both chromosomal alleles and plasmid-encoded alleles. Depending on the location of the second crossover, three distinct outcomes can result: (i) restoration of the wild type allele or (ii) insertion of new gene information leading to a mutant allele. A third outcome occurs when the plasmid persists resulting in resistant merodiploids. These merodiploids can be detected by their resistance to Gentamycin. Figure was adapted from (Hmelo et al., 2015) and created in BioRender. Aidoo, S. (2023) BioRender.com/w77h669.*

Single colonies of these cells were then streaked on LB plates and incubated at 37°C overnight to enable a second crossover. Resulting single colonies were then picked and inoculated into LB containing 1 mM IPTG (Isopropyl β-D-1-thiogalactopyranoside) to induce expression of the thymidine kinase under a Lac operator and incubated at 37°C with shaking (200rpm) for approx. 5 hours. For counter-selection, this bacterial culture was later streaked on LB plates enriched with Azidothymidine (AZT, 200 µg/mL) and incubated at 37°C overnight. Cells having completed the second crossover survived on this selection media as they did not express thymidine kinase converting AZT to the genotoxic DNA chain terminator. Therefore, using the same inoculation loop, single colonies of these survivals were streaked first on LB plates supplemented with gentamycin (75 ng/mL) and then on non-selective LB plates. *P. aeruginosa* cells having lost their vector after the second crossover showed growth on the LB plate only but not on the Gentamycin (75 ng/mL) plate. Single colonies with this growth pattern were selected for PCR verification of a gene insertion of the coding sequence (CDS) for HiBiT at the 3´end of the *mexE* gene.

#### 2.2.6.2 Colony PCR and gel electrophoresis

Several of the resulting Gentamycin-sensitive single colonies after the second crossover were selected for screening. They were first resuspended individually into 50 µL of distilled water and subsequently lysed at 95°C for 5 minutes. About 3 µL of the lysed bacterial suspension and the respective primer pair were combined. Later, colony PCR was performed with the following reaction conditions according to the PCR program described in Table 21. The annealing temperature was adjusted to 54°C.

*Table 23: Colony PCR compounds*

| Compound | Amount per PCR tube |
|---|---|
| 2x Mango Mix™ | 7.5 µL |
| Primer Forward 1703 (10 µM) | 0.5 µL |
| Primer Reverse 1081 (10 µM) | 0.5 µL |
| $H_2O$ | 3.5 µL |
| Lysed bacterial suspension | 3 µL |

Evaluation of the PCR products was done via gel electrophoresis. Primer 1703 binds in the coding sequence (CDS) of *mexE* while primer 1081 binds in the CDS of the HiBiT-Tag. Therefore, only those colonies exhibiting the HiBiT insertion showed a band with a fragment length of 236 base pairs (bp).

2.2.6.3 Obtaining genomic DNA (gDNA)

After the first verification of insertion mutant, a second round of verification was performed. For this purpose, putative *mepM* mutant clones in which *mexE* was now replaced with *mexE*-HiBiT were cultivated in 5 mL LB-medium overnight at 37°C. Genomic DNA (gDNA) was then extracted from 1.8 mL of these cultures using the *DNeasy® Ultraclean® Microbial* kit following its manual. The concentration of obtained gDNA was measured with a NanoDrop spectrophotometer (Thermo Scientific). PCR was again performed this time with 20 ng gDNA per reaction. The primer pairs 1703/1081 and 1703/1704 were employed. Subsequent agarose gel electrophoresis separated the DNA fragments accordingly. While the primer pair 1703/1081 resulted in a 236 bp fragment only when the HiBiT gene was inserted correctly, the primer pair 1703/1704 on the other hand showed a 501 bp fragment indicating the insertion of a HiBiT CDS or 444 bp fragment indicating no HiBiT insertion.

*Table 24: PCR compounds for amplification of gDNA template*

| **Compound** | **Amount per PCR tube** | |
|---|---|---|
| 2x Mango Mix™ | 7.5 | µL |
| Primer Forward 1703 (10 µM) | 0.5 | µL |
| Primer Reverse 1704 or 1081 (10 µM) | 0.5 | µL |
| $H_2O$ | 5.5 | µL |
| gDNA 20ng | 1 | µL |

Verified *mepM*::*mexE-HiBit* mutants were then stored in LB medium containing 20% glycerol at - 80°C for further use.

### *2.2.7 Luciferase Assay*

An option to verify and quantify MexE-HiBiT production in the generated *P. aeruginosa* mutants encoding MexE-HiBiT proteins was by employing the

Nano-Glo® HiBiT Lytic Detection System. MexE-HiBiT fusion proteins interact with LgBiT (provided in the kit) due to the high affinity of HiBiT to LgBiT. This results in a functional luciferase complex. Upon adding of an appropriate substrate (provided in the kit), the substrate is converted to a product with simultaneous emission of photons (Figure 8), which could be detected and quantified with an appropriate device (here: TECAN reader) Due to linear correlation between luciferase activity (light emission) and the amount of HiBiT, the amount of a protein fused to HiBiT can be semi-quantified.

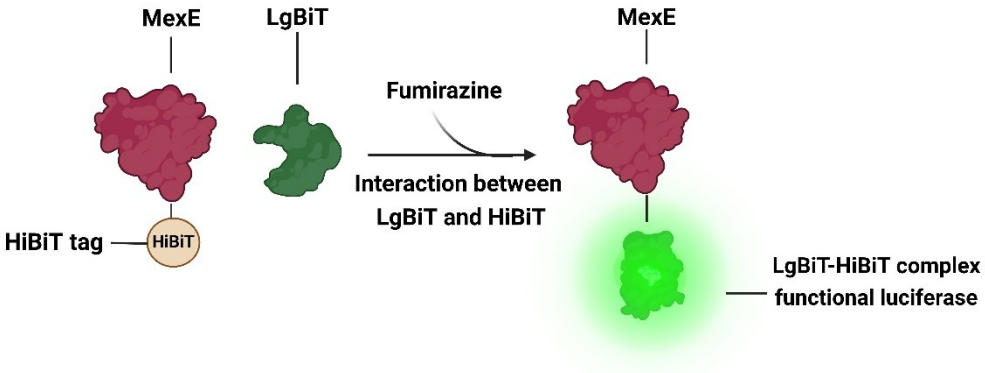


**Figure 8: Schematic depiction of the interaction between LgBiT and HiBiT**
*The Nano-Glo® HiBiT Lytic Detection System enables detection and quantification of proteins fused to a HiBiT tag. Interaction of HiBiT with LgBiT due to their high affinity to each other results in a functional luciferase complex (LgBiT-HiBiT). This complex now is able to convert a provided substrate (fumirazine) under simultaneous light emission. This chemiluminescence signal can be detected with appropriate devices. This figure was created in BioRender. Aidoo, S. (2023) BioRender.com/w94z186.*

#### 2.2.7.1 Obtaining cytosol extracts

*P. aeruginosa* strain ID40 and its various *mepM* mutants carrying a HiBiT tag version of the *mexE* gene were cultured overnight in 5 mL of LB medium. Subcultures were generated by diluting the overnight culture 1:20 (overnight culture: LB medium) and incubated for approx. 2 hours at 37°C with agitation (200 rpm). Subcultures were later centrifuged at 4000*g for 5 min, the supernatants decanted, and the pellets resuspended in 1 mL DPBS solution. The suspension was again pelleted at 10000*g for 1 min and resuspended in 1 mL of DPBS. This step was to ensure, that residues of the supernatants were removed. Next, the OD of the suspensions were determined. To ensure an equal cell count in all samples following formula was utilised to calculate the volume of bacteria suspension needed to obtain a final $OD_{600}$ of 1 ($10^9$ *Pa*. cells per mL).

$$\frac{100}{OD_{measured}} = V_{bacterial\ suspesion}\ [\mu L]$$

This calculated volume was filled into Eppendorf cups and centrifuged at 10000*g for 1 min. In order to prevent loss of cells, majority of the supernatant was first carefully removed with a pipette, then re-centrifuged for 1 min at 10000*g. Finally, the supernatant was completely removed with a precision pipette. The pellet was resuspended in 500 µL of supplemented Buffer K (see Table 25) and incubated for minimum 60 min on ice.

*Table 25: Compounds used for supplementing Buffer K*

| Compound | Final concentration in supplemented Buffer K |
|---|---|
| DNAse | 10 µg/ml |
| Lysozyme | 20 µg/ml |
| Protease inhibitor | 10 mM |
| $MgCl_2$ | 1 mM |
| 0,5 % EDTA | 1 mM |
| Triton X-100 | 0.5 % |

After lysis, 50 µL of the lysate was transferred into a 96-welled non-transparent microplate. Samples were measured in triplicates to minimize technical inaccuracies. The provided Lytic Buffer from the Nano-Glo® HiBiT Lytic Detection System was supplemented with LgBiT (ratio 1:100) and fumirazine (ratio1:50). 50 µL of this supplemented Lytic Buffer was added to each well and incubated for 10 minutes while shaking. Finally, the luciferase activity was measured employing a TECAN reader with the following settings: Mode Luminiscence; Attenuation automatic, Integration time 500 ms. Subsequent statistical analysis was performed using the software program GraphPad Prism 9.

### *2.2.8 Western Blot*

Western blots were performed to visualize differences in the abundance of MexE-HiBiT protein in the generated MexE-HiBiT encoding *mepM*-mutants. For this purpose, overnight cultures were cultivated as described above [2.2.1]. Subcultures were generated by diluting the overnight cultures in fresh LB medium

at a ratio of 1:20 (overnight culture: fresh LB medium). This was incubated for 2 hours at 37°C with shaking (200 rpm).

2.2.8.1 Harvesting of the proteins

First, the $OD_{600}$ of the subculture was determined as described above [2.2.2]. According to the following formula, the volume of water and Laemmli buffer needed to lyse 1 mL subculture was determined:

$$\frac{OD * 0{,}1}{2} * 1000\mu L$$

1 mL of the subculture was centrifuged at 16000*g for 1 min, the supernatant was completely removed by pipetting followed by resuspending of the pellet in the calculated volume of water and Laemmli buffer. Equal amounts were used, while water was added first followed by Laemmli buffer. The suspension was vortexed vigorously and incubated at 95 °C for 10 minutes to lyse the bacteria.

2.2.8.2 SDS PAGE and Protein transfer

To visualize and analyse the abundance of MexE per sample, 10 µL of each sample and 5 µL of PageRuler™ Prestained Protein Ladder were loaded into the gel of a Mini-PROTEAN® TGX precast gel (4 – 20%). After assembly of the chamber (Mini PROTEAN Tetra Cell), electrophoresis was performed at 110 V for 60 min or until the dye front reached the bottom of the gel.

Whatman filter papers and Nitrocellulose membrane fitting the size of the SDS gel were pre-cut. The Whatman filter papers and the sponge were submerged under transfer buffer to have them soaked. Care was taken on only touching the Nitrocellulose membrane at its edges with the help of a tweezer, to prevent unwanted protein staining. The SDS gel was freed from the precast chamber, trimmed if necessary and transferred unto the Nitrocellulose membrane. Adhesion force aided at this step. The blotting sandwich was assembled inside the gel holder cassette (Figure 9) and relocated into the western blot tank filled with cold transfer buffer. Transfer was performed under constant stirring with a magnet stirrer and 350 mA for 60 min at 4°C.

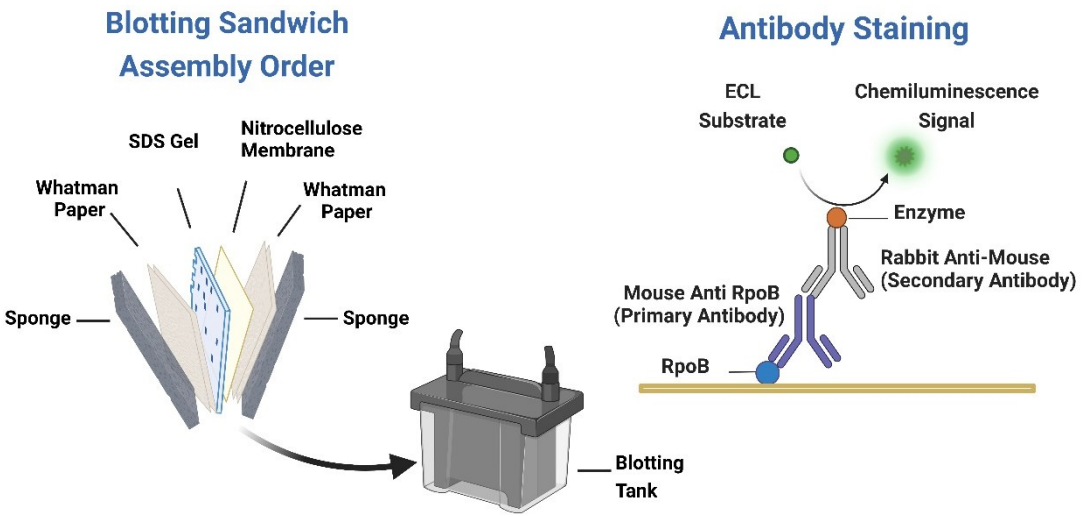


**Figure 9: Schematic depiction of a western blot assembly and Antibody staining**
*The proteins of the lysed cell culture are beforehand transferred unto an SDS gel and separated by SDS PAGE. Sponge, Whatman paper, the proteins containing gel and a nitrocellulose membrane are arranged as depicted and assembled inside a gel holder cassette, which in turn can be placed into the blotting tank. The protein bands can thereby be transferred from the gel to the membrane. These protein bands are later visualized by immunostaining of the membrane. First the primary antibody binds to the target protein (RpoB). The secondary antibody is an enzyme-linked antibody with affinity for the first antibody, which converts an added substrate enabling detection of chemiluminescence. This figure was created in BioRender. Aidoo, S. (2022) BioRender.com/f18x152*

### 2.2.8.3 Ponceau Staining

After transfer was completed, the Nitrocellulose membrane was placed into Ponceau Red Stain for 5 minutes and shaken gently on the rocking shaker (Hecht Karl™). Hereafter, the stained membrane was rinsed multiple times with DI-water until only the protein bands were visible. Chemiluminescence was captured with an Imager (Vilber). The bands of the marker were traced with a pencil. The membrane was separated into two portions since two different detection methods were utilised. The upper membrane portion contained the stain for RpoB and was used to detect RpoB as a loading control, while the lower part of the membrane contained and was used to detect the MexE-HiBiT protein stain. Membranes were placed into separate petri dishes.

### 2.2.8.4 Detection of HiBiT-Tag on the MexE-HiBiT membrane portion

The membrane was covered with TBS-Tween and gently shaken for 5 minutes. The Nano-Glo® HiBiT Blotting System was used for detection and visualization of the HiBiT tag according to the manufacturer´s description (Figure 8). The luminescent signal resulting from the activity of the formed luciferase complex

(HiBiT-LgBiT complex) was captured with the Imager (Vilber) using appropriate programme settings.

2.2.8.5 Blocking, Antibody staining and Imaging of the RpoB membrane portion

The membrane portion containing the RpoB protein was first covered with 5 mL of Blue Block solution and gently shaken overnight at 4°C. Alternatively blocking of the membrane could be done at room temperature for an hour. Both methods were applied depending on our time capacity.

After blocking, 5 µL of Mouse Anti-RNA-polymerase (primary antibody) was added to 5 mL Blue Block solution and the membrane was incubated therein for 60 min at room temperature under gentle shaking. The liquid was then discharged, and the membrane washed three times for 5 min with TBS-T. Subsequently, 5 mL of Blue Block solution supplemented with 2,5 µL of Rabbit anti-Mouse IgG (secondary antibody) conjugated to HRP was added. This was incubated for 60 min at room temperature under gentle shaking. The membrane was washed thrice as described to remove unbound secondary antibodies. Then, the membrane was washed again with DPBS for 5 min. For imaging, an equal volume of Clarity™ Western ECL substrates were combined and 200 µL of this mixture was added onto the membrane. Chemiluminescence was detected using the Imager (Vilber).

### *2.2.9 Biofilm assay*

The biofilm assay included culture cultivation for 2 days and staining of the resulting biofilm, which enabled measurement and comparison of the amount of biofilm been produced (Figure 10). It was assumed that deletion of the *mepM* gene would affect biofilm production and result in comparably lower biofilm productions. The biofilm production of *Pa*. ID40 and its *mepM* mutant strains were examined.

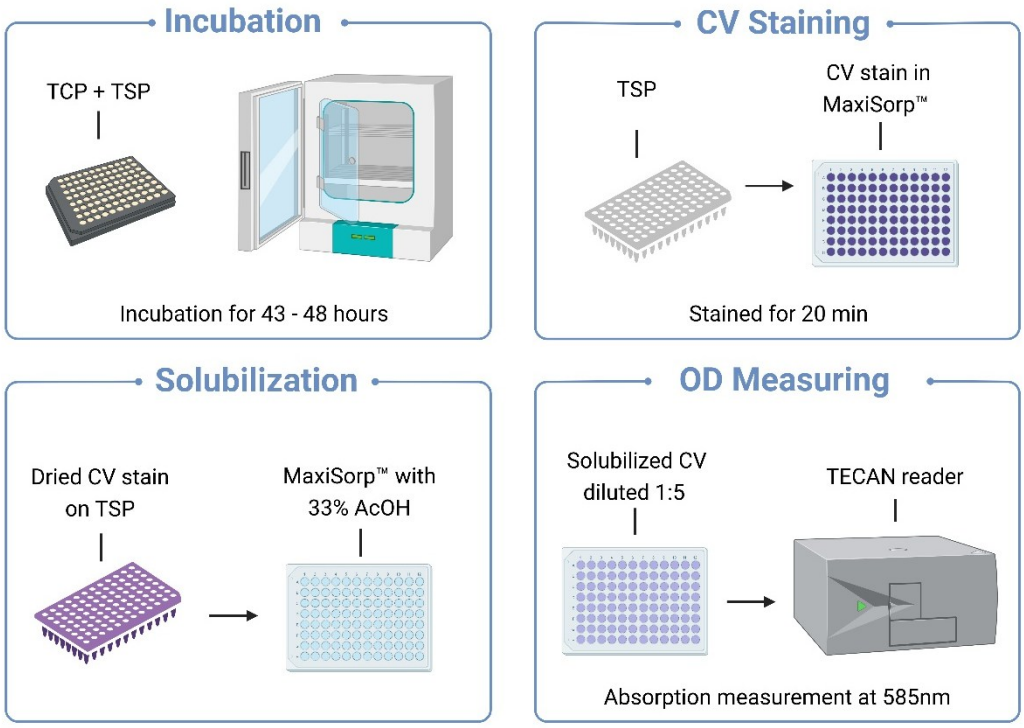


**Figure 10: Schematic representation of biofilm assay**
*Depicted is a schematic workflow of our biofilm assay. First, overnight cultures were generated, which were later diluted into subcultures with an $OD_{600}$ of 0.1. The incubation process involved 2 incubation steps: (i) filling of the subcultures into a 96-welled microplate (TCP), covering with a TSP lid and then incubating at 37°C for two hours. (ii) Transferring of the TSP lid onto a second TCP microplate filled with fresh LB medium and incubating for 43-48 hours at 37°C. CV staining was done by transferring the TSP lid with biofilm attached to it to a microplate filled with 1% crystal violet solution for 20 minutes of staining, followed by a washing series in DI water and drying for up to 60 min. The dried CV was solubilized by transferring the TSP lid onto a microplate filled with 33% acetic acid, followed by a 1:5 dilution. Finally, the $OD_{585}$ of the resolving solution was monitored with a TECAN reader. Figure was created in BioRender. Aidoo, S. (2022) BioRender.com/e80t051*

#### 2.2.9.1 Preparing of culture for biofilm assay

Overnight cultures of the desired bacterial strains were cultured at 37°C with shaking (200 rpm). The overnight cultures were diluted with fresh LB medium to obtain an $OD_{600}$ of 0.1 using following formula:

$$\frac{1}{OD_{600}} * V_1 = V_2$$

$V_1$ = final volume [µL]

$V_2$ = required volume [µL] of overnight culture for $OD_{600}$ = 0,1

200 µL of each sample were filled into a 96-welled Nunc™, non-treated microplate (TCP). Samples were filled in quadruples, sextuples or nonuples, depending on the number of strains examined together on the same microplate. To minimize the edge effect and prevent it from affecting the results, the outer

wells were filled with LB medium and later omitted or used as blanks during data analysis. The microplate was covered with a Nunc™ Immuno TSP lid (TSP) and incubated for 2 hours at 37°C without agitation. The wells of another TCP were each filled with 200 µL of LB medium. The TSP from the incubated culture was transferred unto the new TCP filled with fresh LB medium and incubated at 37°C without agitation for 43 – 48 hours. Care was taken to avoid contamination during the transfer of the TSP.

2.2.9.2 Staining of the biofilm with crystal violet solution (CV)

After completion of the 2-day incubation period, a Nunc™ MaxiSorp™ 96-welled microplate (MaxiSorp) was filled with 1% crystal violet solution (CV), 230 µL per well. The TSP from the incubated culture was transferred into the CV and stained at room temperature for 20 min. Furthermore, two MaxiSorp™ plates were filled with deionized water (DI water). Each well received 250 µL of DI water. The stained TSP was transferred onto the MaxiSorp™ plate filled with water for washing. The washing step was repeated twice, then was the stained TSP lid left to dry at room temperature for 45 – 60 min.

2.2.9.3 Solubilizing crystal violet stain and measuring the optical density

Another MaxiSorp™ plate was filled with 230 µL of 33% acetic acid. TSP with dried crystal violet stain was placed into it and incubated at room temperature till the crystal violet stain was completely dissolved off the TSP. Careful shaking of the TSP aided at this step. Solubilized crystal violet was again diluted 1:5 in 33% acetic acid. For this, in a new MaxiSorp™ plate, 40 µL of solubilized crystal violet was added to 160 µL of 33% acetic acid. The absorption at 585 nm ($OD_{585}$) was measured in a TECAN reader.

### *2.2.10 Elastase activity assay*

This assay was performed to analyse a potential effect of MepM inhibition upon the secretion or the activity of the virulent factor elastase. For this purpose, *Pa.* ID40 and *Pa.* PA14 as well as their *mepM* deletion mutants were cultured overnight. Since an $OD_{600} \geq 2$ was desired, the bacteria were cultured for at least 18 hours. Cultures showing cell density below $OD_{600} = 2$ were re-cultured for a longer period. The EnzChek™ Elastase Assay Kit was used according to the

manufacturer's protocol. First, the provided solutions were brought into reasonable aliquots and stored as instructed. To compose the assay, stock solutions were diluted according to instructions to gain 1x working solutions. For positive control, a 2x concentrated working solution of elastase (from porcine pancreas) was prepared. This would later be diluted to a 1x working solution upon adding of the buffer and DQ$^{TM}$-elastin substrate.

The respective strains of interest were cultured overnight. After determining the $OD_{600}$, the cultures were pelleted at 4000*g for 5 minutes. The resulting pellet was discharged, and the supernatant was filtered with 0,22 µM filters to remove cells and cell particles. The fluid was stored on ice until further usage. The filtered supernatants (enzyme samples) were diluted with LB medium or buffer solution to generate different concentrations of enzyme samples. The aim was to obtain dilutions, at which the enzyme activity of the samples would be in the range of those of the positive control and would allow data analysis. The concentrations used in this study are as follows:

*Table 26: Elastase Assay - Dilution of enzyme samples*

| ***Pa*. ID40 and PA14 strains** | **Elastase positive control** | |
|---|---|---|
| Dilution of supernatants | Elastase working solution, 2x concentrated [U/mL] | Final concentration of Elastase per well [U/mL] |
| No | 0.5 | 0.25 |
| 1:10 | 0.25 | 0.125 |
| 1:50 | 0.125 | 0.06 |
| 1:100 | - | - |

A black 96-welled microplate was filled by adding 50 µL of 1x reaction buffer to 100 µL of enzyme samples or Elastase (positive control). Each sample was filled in duplicates to minimize technical inaccuracies. For negative control, the enzyme sample was replaced with either 100 µL of LB-medium or 1x buffer solution. To ensure a simultaneous start of the reaction in all wells, 50 µL of the DQ$^{TM}$-elastin substrate was added using a multi-pipetting device. Fluorescence intensity,

indicating the elastase activity, was measured immediately after addition of the substrate using a TECAN reader. The excitation / emission settings were 505 / 515 nm.

After measuring, a growth curve was generated using the elastase reference standards provided in the kit (Figure 11). These elastase reference samples generated an initially almost linear curve, which flattened out with time, resembling a logarithmic curve (Figure 11 only shows the initial linear section). In order to deduce the elastase activity of the bacteria strains in U/mL from the results of the elastase reference, the initial linear section of the graph of the reference samples was used to generate a calibration equation translating the increase in fluorescence over time into elastase activity in U/mL. The time point 30 minutes (approx. middle of the linear curve) was chosen as reference with which the linear regression was generated. Furthermore, a best-fit linear equation was also generated, which was utilised to determine the elastase activity of the bacteria strains. All calculations were performed in GraphPad Prism 9.

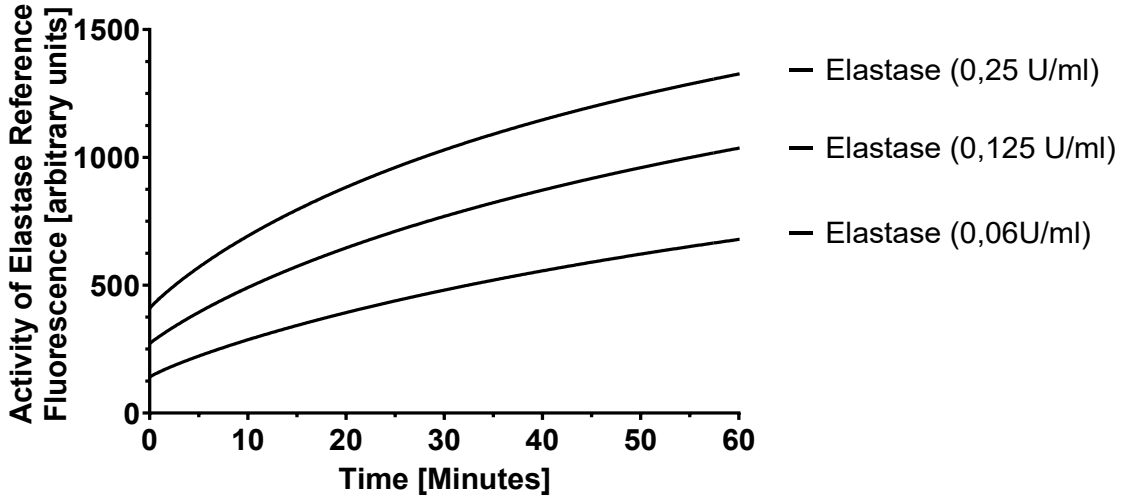


**Figure 11: Standard curve of the elastase reference at different concentrations**
*Presented is the ability of the elastase reference sample to cleave the DQTM-elastin substrate into a fluorescence-emitting substrate, indicating its activity. Higher fluorescence intensity representing higher elastase activities. The elastase reference samples generated a graph resembling a logarithmic curve. Starting with an initially linear growth, which flattened out over time. Here only the initial linear section is shown. Three elastase reference concentrations were created: 0.06 U/mL, 0.125 U/mL and 0.25 U/mL.*

### *2.2.11 Protease activity assay*

This assay was used to measure besides elastase also all other proteases secreted by *P. aeruginosa* and to assess the influence of *mepM* deletion on the

level of protease secretion. *Pa.* ID40 (WT) and *Pa.* PA14 (WT) as well as their *mepM* deletion mutants were cultured overnight. The EnzChek™ Protease Assay Kit (red fluorescence) was used according to its protocol, which is very similar to that of the EnzChek™ Elastase Assay. Therefore, bacterial cultivation and handling was as described in section 2.2.10. The provided solutions were first brought into reasonable aliquots and stored as instructed. To gain 1x working solutions, the stock solutions were diluted according to instructions. For positive control, a 2x concentrated working solution of Elastase (from the EnzChek™ Elastase Assay Kit) was prepared according to its manual and as described in section 2.2.10. Through pilot experiments, we noticed that *Pa*. PA14 strains showed higher protease activity than *Pa*. ID40 strains. For this reason, supernatants of *Pa*. PA14 strains were diluted differently in comparison to supernatants of ID40 strains (see table 26):

*Table 27: Protease Assay - Dilution of enzyme samples*

| ***Pa*. ID40 strains** | ***Pa.* PA14 strains** |
|---|---|
| Dilution of supernatants | |
| No<br>1:10<br>1:50 | No<br>1:10<br>1:100<br>1:1000 |

100 µL of the dilutions as well as of the elastase sample (positive control) were filled into a black 96-welled microplate. Each sample was filled in duplicates. Negative controls consisting of LB-medium or 1x digestion buffer were included. To ensure a simultaneous reaction onset in all wells, a multi-pipetting device was used to add 100 µL of BODIPY TR- X solution to all wells. Fluorescence intensity, indicating protease activity was measured by a TECAN reader immediately after adding of the BODIPY TR- X solution. The expected excitation / emission maxima were at approx. 589 / 617 nm.

### *2.2.12 Pyocyanin secretion assay*

Pyocyanin (PYO) was extracted from the bacterial cultures, remaining after the biofilm assay. This allowed comparison of culture colouration, biofilm production and pyocyanin secretion of the same bacterial culture samples. Also, a comparison of these characteristics between the wild type and different mutation strains of *Pa*. ID40 was possible. Bacterial culturing and handling were as described in section 2.2.9. (Biofilm assay), with the only exception being that samples were always filled in sextuples into the 96-welled microplate. Only *Pa*. ID40 wild type and its *mepM* mutant strains were analysed.

#### 2.2.12.1 Pyocyanin extraction and quantification

After complete incubation of 2 days, cultures originating from the same bacterial strain were combined in a reaction tube. Pipetting and vortexing helped to dissolve biofilms and solid portions of the culture before measuring of the $OD_{600}$. Samples were centrifuged at 10000*g for 2 min and then sterile filtered using 0,22 µM filters. PYO extraction from the supernatant was performed according to previously described methods (Alayande et al., 2018; Essar et al., 1990; Frank & Demoss, 1959; O'Malley et al., 2004). In brief, 250 µL of Chloroform was added to 500 µL of each supernatant. This was vortexed at maximum speed for 5 min and subsequently centrifuged for 2 min at 10000*g. 200 µL of the resulting blue organic layer (bottom layer) was filled into new reaction tubes. Care was taken to ensure that none of the aqueous layer (LB) transferred into the reaction tube. To the blue chloroform extract, 100 µL of 0.5% HCl was added and vortexed at maximum speed for 5 min, followed by centrifugation at 10000*g for 2 min. PYO was extracted into the aqueous HCl layer which turned from blue to reddish upon acidification. The characteristic absorption maxima of PYO dissolved in 0.2 M HCl (0.1 – 0.2 N HCl) have been previously described to be at approx. 204, 242, 277, 387.5 and 521.5 nm. (El-Fouly et al., 2015; Ohfuji et al., 2004; Watson et al., 1986). Our PYO dissolved in HCl was confirmed and quantitated via UV-Vis Spectrophotometer. Its characteristic absorption maxima laid at 277, 388 and 520 nm. The absorption values of the PYO extracts at 520 nm were determined with the UV- Vis Spectrophotometer To minimize the effect of technical

inaccuracies, 2-6 technical replicates per strain were conducted for all four independent experiments.

2.2.12.2 Determining the concentration of PYO in µg/mL

In accordance with previously described methods (Alayande et al., 2018; Essar et al., 1990), where it has been postulated that multiplication of the absorption value at 520 nm according to following formula, reveals the concentration of PYO in µg/mL, we determined the concentrations of our PYO extracts.

$$C_{PYO} = A_{520} * 17{,}072$$

C: = Concentration in µg/mL

A: Absorption

The mean of the resulting concentration values of the technical replicates per strain and per experiment were then analysed using GraphPad Prism 9.

### *2.2.13 Pyoverdine Secretion assay*

Pyoverdine is a characteristic siderophore produced by *P. aeruginosa* strains and acts in acquisition of iron. According to the recommendation of literature (Filloux & Ramos, 2014) different culture media were used, which promised to trigger and increase PVD secretion, enabling its measurement. During our preliminary experiments, liquid media of MOPS, M9 minimal medium, and succinate medium (all iron-free) were tested. Succinate medium however, prevailed over the other media due to its display of the typical green-fluorescent colour of pyoverdine in its *P aeruginosa* overnight cultures. To start, liquid LB overnight cultures of *Pa*. ID40 WT and its *mepM* mutant strains were diluted 1:10 in succinate minimal media (iron free) by adding 500 µL of overnight cultures grown in LB medium to 4,5 mL of succinate minimal medium and incubated for 24 hours at 30°C with agitation (200 rpm). The 24-hour cultures were again diluted 1:10 in succinate minimal medium and incubated at 30°C for 24 hours with agitation (200 rpm). Traces of iron from the initial LB culture were minimized by the multiple dilution step. $OD_{600}$ measurements were performed after each incubation step.

2.2.13.1 Quantification of Pyoverdine

After centrifugation and filtration with 0,22 µM filters, the supernatants were diluted 1:10 in Pyridine-Acetic Acid (Pyr/AcOH) buffer. The absorption spectrum of this dilution was monitored from 180 to 800 nm utilising a UV-Vis spectrophotometer. Iron-free pyoverdine has characteristic absorption maxima at 380 nm. In the presence of iron molecules, pyoverdine forms a complex with iron and its absorption maxima shifts to 400 nm. The concentration of PVD was determined with the Lambert-Beer equation:

$$C_{PVD} = \frac{A}{\varepsilon * d}$$

$C_{PVD}$ = Concentration of PVD [mol/L]

$A$ = Absorbance

$\varepsilon_{380}$ = 16500 L/(mol*cm)

$\varepsilon_{400}$ = 1900 L/(mol * cm)

$d$ = 1 cm

### *2.2.14 SideroTec™-Total assay*

The SideroTec™-Total assay enables by colourimetric testing the detection of siderophores or iron chelators in liquid media. It could be used with both unfiltered cell culture or cell-free media and has a pH optimum of pH = 6 – 8. Turbidity and microorganisms in the sample could interfere with and hinder the correct reading of colour change. Therefore, our samples were sterile filtered after incubation. The assay was performed according to the manufacturer´s instructions. In brief, the standard siderophore stock provided in the kit was diluted using a dilution series. 500 µL of the provided standard stock was given into a reaction tube. 250 µL of this was diluted 1:2 in 250 µL of supplied diluent. This two-fold dilution was repeated 6 times (see Table 28). An eighth reaction tube served as a negative control with a standard concentration of 0 µM/L and was filled with diluent only.

*Table 28: Dilution series of SideroTec™-Total standard stock*
*Table adapted from the SideroTec™-Total Assay protocol available in the kit.*

| Reaction tube number | Volume of standard stock [µL] | Volume of diluent [µL] | Dilution series | Final Concentration of standard [µg/mL] |
|---|---|---|---|---|
| T1 | 500 | 0 | - | 100 |
| T2 | 0 | 250 | 250µL of T1 | 50 |
| T3 | 0 | 250 | 250µL of T2 | 25 |
| T4 | 0 | 250 | 250µL of T3 | 12,5 |
| T5 | 0 | 250 | 250µL of T4 | 6,25 |
| T6 | 0 | 250 | 250µL of T5 | 3,1 |
| T7 | 0 | 250 | 250µL of T6 | 1,5 |
| T8 | 0 | 250 | - | 0 |

*Pa*. ID40 and its *mepM* mutant strains were examined. 100 µL of cell-free supernatant of overnight cultures and 100 µL of dilution of standards were filled in separate wells of a 96-well microplate provided in the kit. Samples were loaded in duplicates.

The catalyst solution contained in the kit was diluted 1:10 in Dye reagent. To ensure a simultaneous onset of the reaction, an electric multi-pipetting device was used to add 100 µL of supplemented dye reagent solution to each well. The plate was incubated at room temperature for 12 min and then placed in a microplate reader to measure the OD at 620 – 630 nm.

A standard curve was generated using the results obtained from the standard dilutions. The final concentration of the standard dilutions was plotted on the x-axis, while on the y-axis, $1/OD_{620-630}$ of the standard dilutions were plotted. The mathematical formula of the resulting linear standard curve was used to determine the concentration of siderophores present in the bacterial samples. The formula was as follows:

$$y = m * x + c$$

$$\rightarrow x = \frac{(y - c)}{m}$$

$$\rightarrow concentration\ of\ Siderophore = \frac{\left(\frac{1}{OD} - background\ signal\right)}{slope}$$

*y* = 1/OD of the sample

*m*= slope

*x* = concentration of Siderophore in the sample

*c* = y-intersect = background signal

### *2.2.15 Virulence test with Galleria mellonella larvae*

*Galleria mellonella (G. mellonella)* are greater wax moths or honeycomb moths. Their larvae provide an alternative model for studying general effects of bacterial infection and virulence. They are easily accessible, simple in husbandry and are not subject to ethical constraints. The larvae were supplied by b.t.b.e. Insektenzucht GmbH. Upon arrival, they were released from their provided food box and sorted by size into fresh food boxes and incubated at 30°C without agitation until usage.

The strains used for the infection series were *Pa*. ID40 (WT), ID40 Δ*mepM*1 Δ*mepM*2 and ID40 Δ*mepM*1 Δ*mepM*2 Δ*mepM*3. These strains were cultured overnight at 37°C then brought to an $OD_{600}$ = 0.1 to create subcultures. Subcultures were generated by incubating diluted bacterial suspension for 2 hours at 37°C with agitation. After pelleting of the subcultures and discharging of the supernatants, the pellet was dissolved in 1 mL of DPBS and kept on ice. For *Pa*. PA14 strains a cell count of $5*10^2$ and $10^3$ bacteria per mL DPBS was desired. For *Pa*. ID40 strains concentrations between $10^3$ and $1.6*10^5$ cells/mL were aimed for.

Active larvae of the same size were selected by sight and infected with exactly 10 µL of bacterial dilution. Syringe (BD-Micro Fine™) and precision injection tools (Manual Micro syringe Pump) were used. Groups of 8-20 larvae were injected with different infection doses. Larvae that lost hemolymph or were injured were

discharged and not included in the analysis. Infected larvae were kept in petri dishes with food and incubated for 5 days at 37°C. They were examined daily and those found dead (showing discoloration and no movement upon touch stimulation) were noted and discharged by freezing at -20°C and autoclaving. After day 5, the infection series was ended and evaluated.

To determine the actual concentration of bacteria present in the dilutions injected into each larvae, a colony forming unit (CFU) determination was performed. 100 µL of each dilution was plated on blood agar plates (Columbia plates) and incubated overnight at 37°C without agitation. 2 plates were inoculated per dilution. CFU was determined and viewed as the actual bacterial concentration per dilution.

We plotted the survival ratio after 5 days against the logarithm of the infection dose. Next, we fitted the data to the following equation $Y=100/(1+x/LD_{50})$ using a nonlinear regression in GraphPad Prism 9:

$$y(x) = \frac{100}{1 + \frac{x}{LD_{50}}}$$

With $y(x)$ being the survival rate after 5 days for the infection dose $x$ and $LD_{50}$ being the lethal infection dose at which 50% of the infected animals are dead after 5 days.

Also, non-linear regression curves and statistics using extra sum-of-square F test were performed with the Null hypothesis of one curve fits all data sets (i.e. data of ID40 WT and ID40 ∆*mepM1/2* or ID40 WT and ID40 ∆*mepM123* could be explained with the same fit). Finally, the $LD_{50}$, $R^2$ and the 95% confidence interval of $LD_{50}$ were compared with each other. These statistical analyses were conducted with GraphPad Prism 9.

# 3 Results

The rationale of this study has been elucidated extensively in the introduction section, which led to the following three questions this study aims to address: (i) identifying the mechanisms that contribute to reduction of ß-lactam resistance upon *mepM* deletion, thereby determining *mepM*-deletion constellations that exhibit the major impact, (ii) analysing the influence *mepM* deletion exerts on virulence and (iii) elucidating possible attenuation of lethality upon co-deletion of *mepM*. In this section, we present our results assessing these questions.

## 3.1 Modulation of the abundance of the efflux pump MexEF-OprN by MepMs

In previous studies, it could be shown that deletion of *mepM1* moderately reduced ß-lactam resistance to various ß-lactam antibiotics, which furthermore was associated with reduced *ampC* expression and ß-lactamase activity (Sonnabend et al., 2020). If in addition to *mepM1* also *mepM2* and *mepM3* were deleted (Δ*mepM123)*, resistance to various ß-lactam antibiotics could be broken, but this effect is not explainable solely by further reduction of *ampC* expression (Kemper, 2020) (Figure 6). Based on proteome data, prior to this study evidence was provided that deletion of *mepM123* indeed leads to an increased abundance of MexE, indicating a higher abundance of the MexEF-OprN efflux pump in the cell envelope. Moreover, it could be demonstrated that additional deletion of the *mexEF-oprN* operon in the *mepM123* deletion mutant, partially restores resistance to ß-lactam antibiotics. Consequently, a positive correlation between MexEF-OprN overexpression due to deletion of *mepM123* and increased ß-lactam susceptibility can be drawn.

These findings raised the question of whether one distinct murein endopeptidase modulates the abundance of the MexEF-OprN efflux pump. To address this question, the aim was to semiquantify MexE levels using a luciferase assay and to visualize the abundance of MexE by Western blot analysis. As a first step to achieve this goal, *mepM* deletion mutants were generated encoding a MexE-HiBiT fusion protein. The HiBiT-tag is a small peptide, that consists of 11 amino acids, which binds with high affinity to the larger LgBiT subunit to create a

functional luciferase (Schwinn et al., 2018). Upon addition of LgBiT and an adequate substrate (furimazine) to previously lysed bacteria, the LgBiT-HiBiT protein complex (HiBiT is connected to MexE) is formed which converts the substrate to a product under light emission. The light emission can then be detected and evaluated. The strains ID40::*mexE*-HiBiT, ID40 ∆*mepM1*::*mexE*-HiBiT, ID40 ∆*mepM2*::*mexE*-HiBiT, ID40 ∆*mepM3*::*mexE*-HiBiT, ID40 ∆*mepM1/2*::*mexE*-HiBiT, ID40 ∆*mepM1/3*::*mexE*-HiBiT and ID40 ∆*mepM123*::*mexE*-HiBiT were generated by allelic exchange as described in section 2.2.6. Successful mutagenesis was finally verified by PCR using the primers mentioned in section 2.1.3 (Oligonucleotides). Figure 12 presents an exemplified PCR gel electrophoresis verifying the successful integration of *mexE*-HiBiT in all strains used in this experiment. With the primer pair for upstream and downstream the gene, PCR products of approx. 500 bp length were expected, while a combination of upstream and inside primers were expected to generate PCR products of approx. 237 bp length.

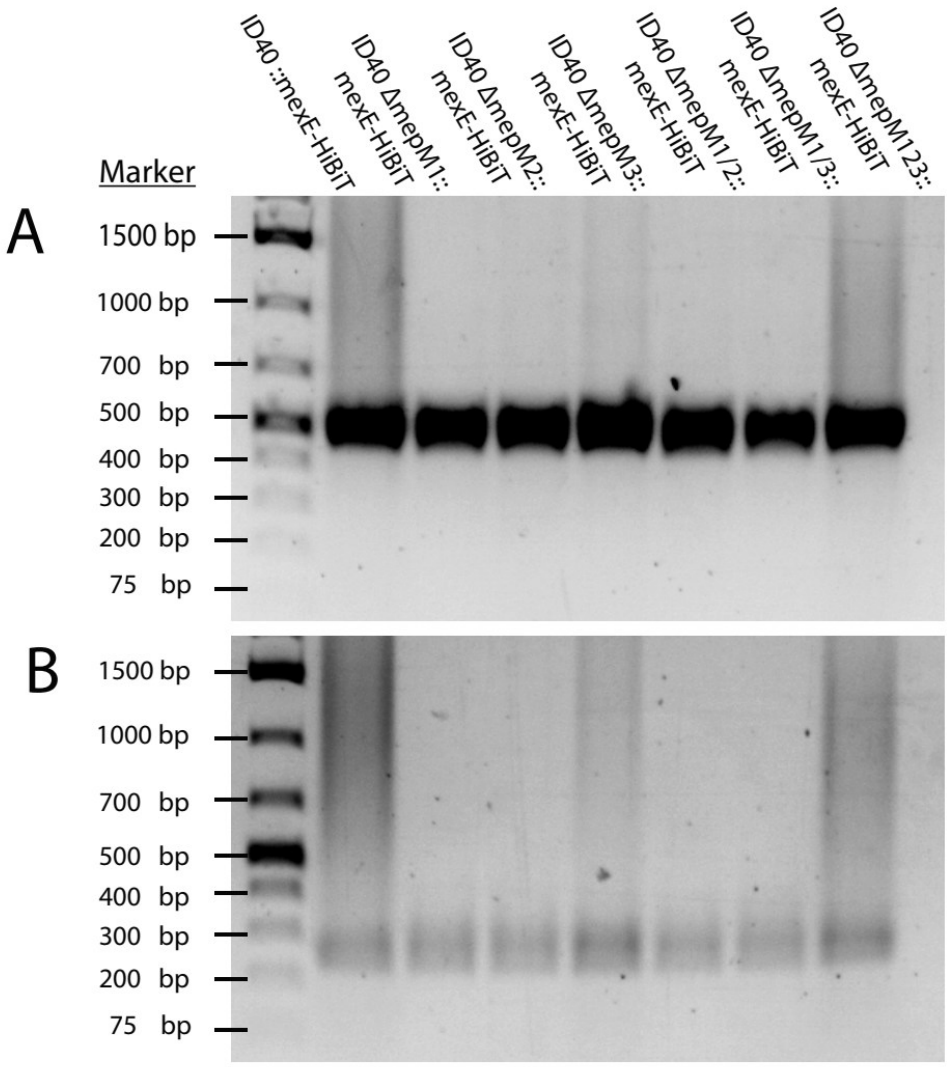


**Figure 12: PCR gel electrophoresis verifying the successful integration of *mexE*-HiBiT into ID40 strains**
*Depicted is a PCR gel electrophoresis verifying the successful mutagenesis of mexE-HiBiT mutants of the ID40 WT and mepM deletion strains. DNA marker and ladder as specified. (A) Upstream and downstream primers generated a DNA fraction of approx. 500 bp. (B) Upstream and inside primer led to a truncated DNA fraction of 237 bp. bp = base pairs*

### *3.1.1 Determining MexE levels in mepM deletion mutants by luciferase assays*

For the luciferase assay, subcultures of overnight cultures were incubated for 2h at 37°C, then centrifuged and the supernatant thereof discharged. The cell pellets were resuspended into D-PBS and washed by multiple centrifugation and resuspension steps to minimize traces of the LB supernatant. Equal count of bacteria according to their $OD_{600}$ values were lysed with 500 µL of supplemented buffer K (see Table 25) and incubated therein for 60 minutes on ice. In a 96-well plate, 50 µL of lysate was added to 50 µL of lytic buffer provided in the Nano-Glo® HiBiT Lytic Detection System kit. After a 10 minutes incubation period at room temperature under constant shaking, the luciferase activity was measured via a TECAN reader. Four individual experiments were conducted, with 3 replicates per experiment. Each replicate was measured twice with an interval of 120 seconds to identify and minimize technical inaccuracies. The cumulative results of the luciferase activity level were evaluated and visualized as x-fold change in comparison to ID40 WT (Figure 13).

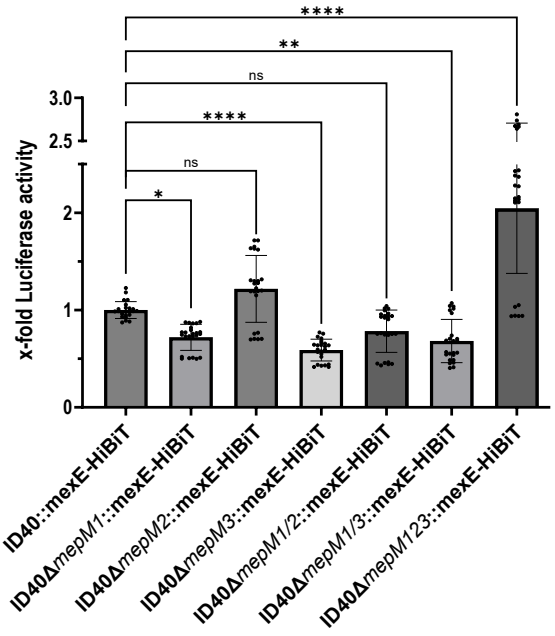


**Figure 13: Quantification of MexE abundance via luciferase assay.**
*Indicated Pa strains were cultured overnight in LB. Same cell counts of bacteria were lysed and luciferase activity was measured. Presented are the mean of the x-fold change which was normalised to the WT ID40 as well as the SD of four independent experiments, each with three replicates and each replicate technically measured twice. One-way ANOVA test was performed to determine statistical differences between the means of the mutant strains in comparison to that of the WT. ns = not significant = p > 0,05; * = p ≤ 0,05; ** = p ≤ 0,01; **** = p ≤ 0,0001.*

In comparison to *Pa*. ID 40 WT, single deletion of *mepM2* shows a tendency to increase MexE-levels. This elevation of the abundance of MexE-HiBiT failed to reach statistical significance. On the contrary, *mepM1* and *mepM3* deletion resulted in a significant reduction of MexE levels ($p < 0,05$ and $p < 0,0001$ respectively). However, this effect seems to be counteracted by additional deletion of further *mepM* genes. Upon deletion of *mepM1* in addition to *mepM2 (∆mepM1/2)*, MexE levels come to lay in-between the levels of *mepM1* and *mepM2* single deletion, showing an insignificant reduction of MexE levels compared to the WT. Double deletion of *mepM1* in addition to *mepM3* (*ΔmepM1/*3) slightly increases MexE levels to lay in-between that of the respective single deletion mutants. Interestingly, deletion of all three *mepMs* leads to a striking increase in MexE abundance above that of *mepM2* deletion mutant. Indicating that multiple deletion of the *mepM* genes rather leads to increasement in MexE abundance. Taken together, the murein endopeptidases MepM1 and MepM3 compared with MepM2 seem to modulate the levels of MexE controversially. While loss of MepM1 and MepM3 might slightly decrease MexE levels, MepM2 does the opposite and shows a tendency to increase MexE levels. Finally, this finding indicates that the amount of MexEF-OprN efflux pumps in the cell envelope seems to be determined by the interplay of all three MepMs. Next, we aimed at confirming the MexE levels deduced by the luciferase assay with Western blot analysis.

### *3.1.2 Determining MexE levels in mepM deletion mutants via Western blot*

To visualize the impact of *mepM* deletion on MexE abundance, Western blots were conducted as described in material and methods. Four independent experiments were performed to reduce inaccuracies. Figure 14 summarizes the results of three Western blot experiments. The thickness and intensity of a band represents the quantity of proteins detected. Therefore, the thicker or darker the band, the higher the protein count, thereby indicating a higher MexE abundance for this sample. A comparison of bands from different samples is then legitimate when the load of the samples with their bacteria count are nearly identical. The RNA polymerase subunit ß (RpoB) served here as a loading control. Sample load was checked prior to comparison of protein bands. RpoB has a molecular weight

of about 180 kDa, while MexE together with the HiBiT tag could be detected at approx. 50 kDa.

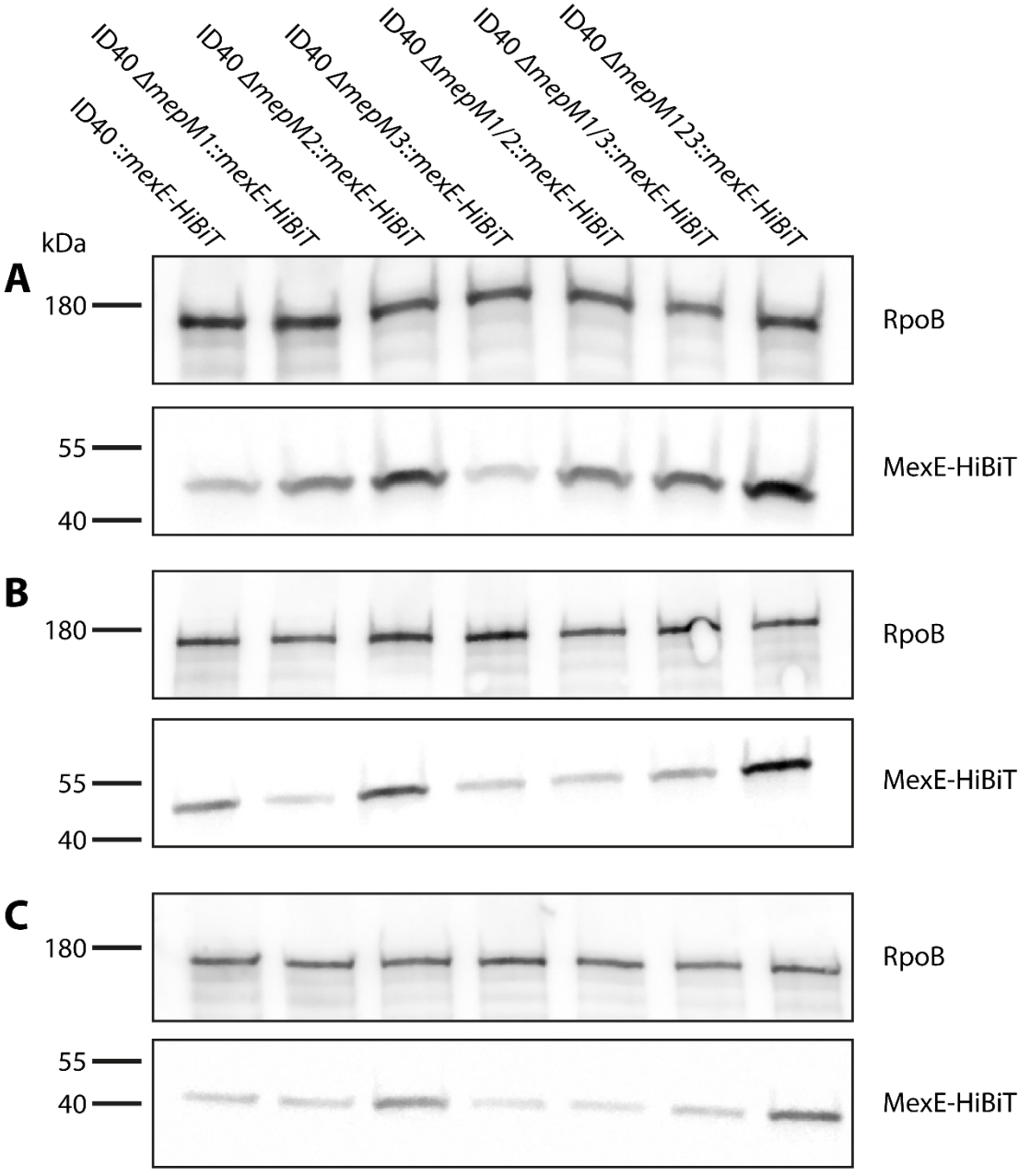


**Figure 14: Western blot examining *mexE*-HiBiT expression.**
*Shown are the protein bands of RpoB and MexE-HiBiT of ID40 WT and the mepM-deletion mutants. The RpoB band acts as a loading control. The results of three independent experiments (A-C) are shown as an example.*

In each experiment, the RpoB bands were of similar boldness and intensity, suggesting identical sample load and bacteria count. ID40 (WT) was set as the reference, to which the protein levels of the mutant strains were compared. The Western blot results visibly show a higher band intensity and thickness for

ID40 *ΔmepM2* and ID40 *ΔmepM1ΔmepM2 ΔmepM3 (ΔmepM123)* mutants. Indicating a higher abundance of MexE in these mutant strains. Of the single deletion mutants, *ΔmepM2* invariably shows high band intensities, indicating higher amounts of MexE than the reference. While the band intensities of *ΔmepM1* samples varied in between slightly lower to similar intensities as the reference ID40, *ΔmepM3* samples bands are on average of less intense as those of the reference.

Of all the deletion mutants, ID40 *ΔmepM123* shows the highest band intensities. These intensities are visibly higher than those of *ΔmepM2* samples. The results of ID40 *ΔmepM1 ΔmepM2 (ΔmepM1/2)* samples varied. Of the four biological replicates, *ΔmepM1/2 samples* twice have band intensities slightly higher and twice slightly lower than those of the reference. The band intensities of ID40 *ΔmepM1 ΔmepM3 (ΔmepM1/3)* fluctuates between being slightly higher or slightly lower than the reference. The intensity levels of ID40 *ΔmepM1/3* and ID40 *ΔmepM1/2* (when they are higher than the reference) are however constantly lower than that of ID40 *ΔmepM2.*

In summary, ID40 *ΔmepM123* shows the highest intensity level, followed by ID40 *ΔmepM2*. ID40 *ΔmepM1/2* and ID40 *ΔmepM1/3* show slightly elevated band intensity levels which are however lower than that of ID40 *ΔmepM2*. ID40 *ΔmepM1*, ID40 *ΔmepM3* and ID40 WT (reference) have the lowest intensity levels. Among the single deletion mutants, *ΔmepM2* seems to have the highest influence on MexE levels and promotes abundance thereof. In double mutant constellations this effect of *ΔmepM2* is weakened by additional *mepM1* deletion. A deletion of the three murein endopeptidases leads to a higher abundance of MexE, which correlates positively with increased sensitivity to ß-lactam antibiotics. This result supports the results of the luciferase assay conducted with the same bacteria samples. Now after evaluating the effects of *mepM* deletions on MexE levels, we sought to address the impact of *mepM* deletions on virulence associated phenotypes such as biofilm formation.

## 3.2 Impact of *mepM* deletion on biofilm formation as a virulence factor

*P*. *aeruginosa*'s capability of forming biofilms which are impenetrable for antibiotics has been reported. They hereby impede antibiotic targeting and treatment. This assay intends to address the impact of *mepM* deletions on biofilm production. For this purpose, an equal cell count of $OD_{600}$ = 0.1 were generated and cultured 43 -48 hours at 37°C. Resulting biofilm was stained with Crystal Violet (CV) then resolubilized into 33%-AcOH. Following, the $OD_{520}$ thereof was monitored.–Figure 15 shows the cumulative results of all biofilm assays. Six independent experiments were performed with each strain having 4 – 9 replicates per experiment. In case of contamination, the contaminated wells showed both cultural colour variation as well as highly elevated $OD_{520}$ values, which differed from the uncontaminated wells containing the designated strains. These contaminated wells were exclusion from the analysis. The $OD_{520}$ was quantified by a TECAN reader. The raw data represented a 1:5 dilution of the initial resolubilized CV staining, the OD values were therefore subsequently multiplied by 5 to calculate back to the undiluted values.

### *3.2.1 Creating x-fold change data normalized to WT*

For each experiment separately, the $OD_{520}$ values (calculated, undiluted values) of the WT samples were summed up to create a statistical mean. The x-fold change was calculated by dividing each OD value (calculated, undiluted value) by the overall mean of the WT samples. The following formula was used:

$$\frac{calculated\ undiluted\ OD_{520}\ value}{Overall\ mean\ of\ WT\ samples}$$

The $OD_{520}$ value (calculated, undiluted values) of every sample including those of the WT and all mutant strains were individually divided by the overall mean of the WT samples. x-fold change expression provides results, which enable direct comparison of the value of the WT samples with those of the other strains. Values below 1.0 indicated a lower and values above 1 a higher biofilm production in

comparison to the WT. A reduction in biofilm production was observed in all *mepM* deletion mutant strains when compared to the WT. (Figure 15 A)

### *3.2.2 Comparison of biofilm production*

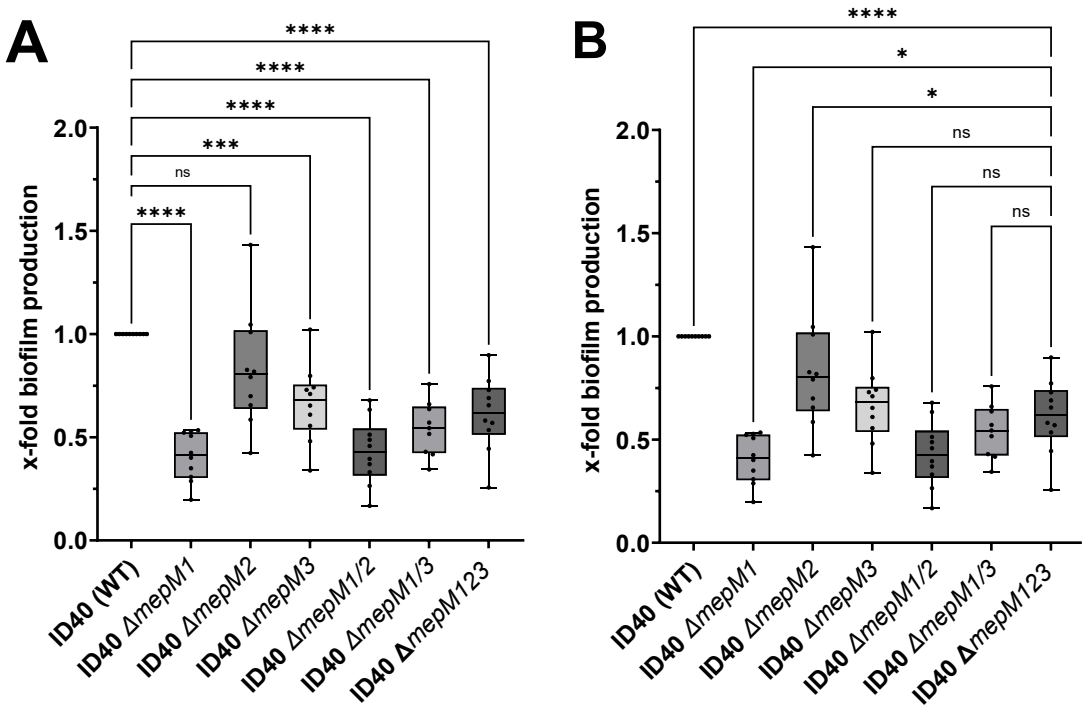


**Figure 15: x-fold biofilm production**
*Similar inoculums of bacteria cells were first cultured in a 96-well plate with a TSP lid. After biofilm had formed and attached to the TSP lid, the TSP lid was stained with Crystal violet (CV) stain. CV was dried, resolubilized in 33%-AcOH, then diluted 1:5. The $OD_{520}$ was measured. Depicted is the x-fold biofilm production in comparison with the Pa. ID40 WT of 6 individual experiments, each containing 4-9 replicates per strain. The mean and SD are presented. One-way ANOVA was performed with (A) the mean of ID40 WT set as reference with which all other means were compared. (B) The mean of ID40ΔmepM123 is set as a reference. ns = not significant = p > 0,05, * = p ≤ 0,05; *** = p < 0,001, **** = p < 0,0001*

In summary, our results show a decrease in biofilm production in all *mepM* deletion mutant strains compared to the WT strain (Figure 15 A). Due to the high number of experiments performed, most statistical differences were of high significance ($p < 0.0001$). While *mepM1* deletion has the strongest effect on biofilm production, *mepM2* deletion leads only to a slight decrease. Deletion of *mepM3* results in a 1.47-fold reduced biofilm production (mean x-fold biofilm production of Δ *mepM3* = 0.678*).* Upon double deletion of *mepM1* in addition to *mepM2*, the strong effect *ΔmepM1* has on the reduction of biofilm production is slightly diminished. ID40 *ΔmepM1/2* shows 2.22-fold lower biofilm production compared to the WT (mean x-fold biofilm production 0.4498). This effect is still

smaller than that of *ΔmepM1* mutant, which has a 2.46-fold reduction of biofilm formation compared to the WT (means of x-fold biofilm production 0.405). The double mutant ID40*ΔmepM1/3* also shows in comparison a 1.77-fold reduction in x-fold biofilm production. ID40*ΔmepM123* shows 1.6-fold lower biofilm formation. Of the multi-mutation strains, ID40*ΔmepM1/2* has the lowest biofilm production level, followed by ID40*ΔmepM1/3*, which in turn is closely followed by the triple mutant ID40*ΔmepM123.*

In summary, *mepM1* deletion contributes strongly to reducing biofilm production while *ΔmepM2* shows only a slight effect. Also, single deletion of *mepM3* reduces biofilm formation, but this effect is minor in contrast to that of *mepM1* deletion. Upon double mutation, the effect of single *mepM1* deletion is slightly diminished, perhaps due to a counteracting effect through *mepM2* or *mepM3* deletion. Triple *mepM* deletion leads to 1.51-fold higher biofilm production levels compared to that of the single *mepM1* deletion (mean x-fold biofilm formation *ΔmepM1* = 0.405 vs. mean x-fold biofilm formation *ΔmepM123* = 0.612). Nevertheless, the level of biofilm production thereof is still lower than that of the WT ($p<0.0001$) and of the single *ΔmepM2* mutant ($p=0.0006$) (Figure 15 B). In conclusion, *mepM1* deletion massively hampers biofilm production and additional deletion of further *mepM* genes leads to a counteraction of this effect. Of note, biofilm formation might not be the only virulence trait affected by deletions of *mepM* genes. Hence, we investigated the effects of *mepMs* upon secreted virulence factors such as elastases, proteases and siderophores.

### 3.3 Impact of *mepM* deletion on secreted factors related to virulence.

An existing correlation between the levels of MexEF-OprN efflux pumps and that of various virulence factors can be assumed. Certain intracellular signalling molecules, which facilitate transcriptional regulation of virulence factors such as elastase and pyocyanin (PYO) are subject to the influence of MexEF-OprN expression. Having MepMs (endopeptidases) been involved in the cleavage of peptidoglycan (PG) cross-linkage, MepMs may affect the sizing of PG pores and the assembly of secretion systems. Additionally, they may influence the migration of proteins from the inner to the outer membrane. Consequently, *mepM* deletion

seemingly may affect the secretion of virulence factors in two ways. Firstly, by increasing the MexEF-OprN expression levels and thus mitigating altered levels of certain intracellular signalling molecules leading to changed levels of various virulence factors. Secondly, by influencing the PG pore size by the level of density of cross-linkages or by influencing the migration or assembly of relevant protein (complex). Therefore, further objective of this study was to assess possible effects *mepM* deletion might pose on elastase secretion. We hypothesized that *mepM* deletion would noticeably affect secretion levels.

### *3.3.1 Elastase secretion and activity assay*

To assess if and to which extent secretion of elastase is altered by *mepM* deletion, liquid bacteria cultures were analysed. First, cell-free supernatant was obtained by centrifugation and filtration, then the EnzChek™ kit was utilised to detect and determine the level of elastase activity.

The strain ID40 showed upon initial testing nearly undetectable elastase secretion levels. (Figure 16 A) This observation can be attributed to the minimal expression level of *lasB* (gene encoding for elastase) in ID40. Unpublished transcriptome data of our working group showed that *lasB* mRNA expression of ID40 is negligible compared to those of the widely used lab strain PA14. In line with the transcriptome data, it can be concluded that ID40 hardly secretes LasB.

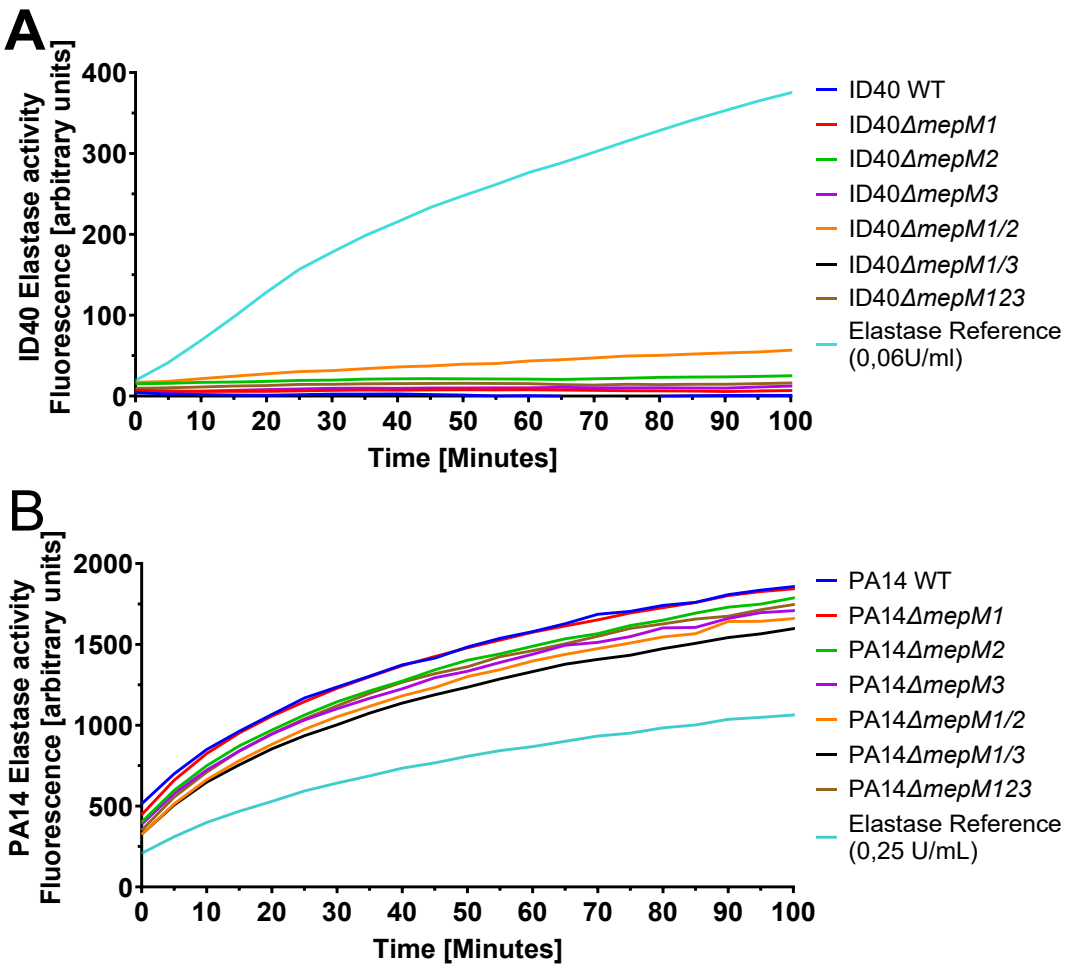


**Figure 16 Comparison of the activity of secreted elastase by PA14 and ID40 strains.**
*Presented is the fluorescence intensity of ID40 (A) and PA14 (B) strains representing the measured elastase activities. Depicted are the values of one experiment as a visual example. Colour coding as specified. While PA14 shows fluorescence intensities above those of our highest reference elastase concentration (0.25 U/mL), ID40 barely manages to reach detectable activity. The fluorescence intensity of all ID40 strains are far below that of our lowest Elastase concentration (0.06 U/mL)*

To still be able to investigate whether in principle MepMs influence elastase, secretion assays were performed with PA14 and its *mepM* mutation strains. The elastase activity in U/mL of the PA14 strains (Figure 17) was calculated using the standard curve of the elastase reference standards as stated in section 2.2.10.

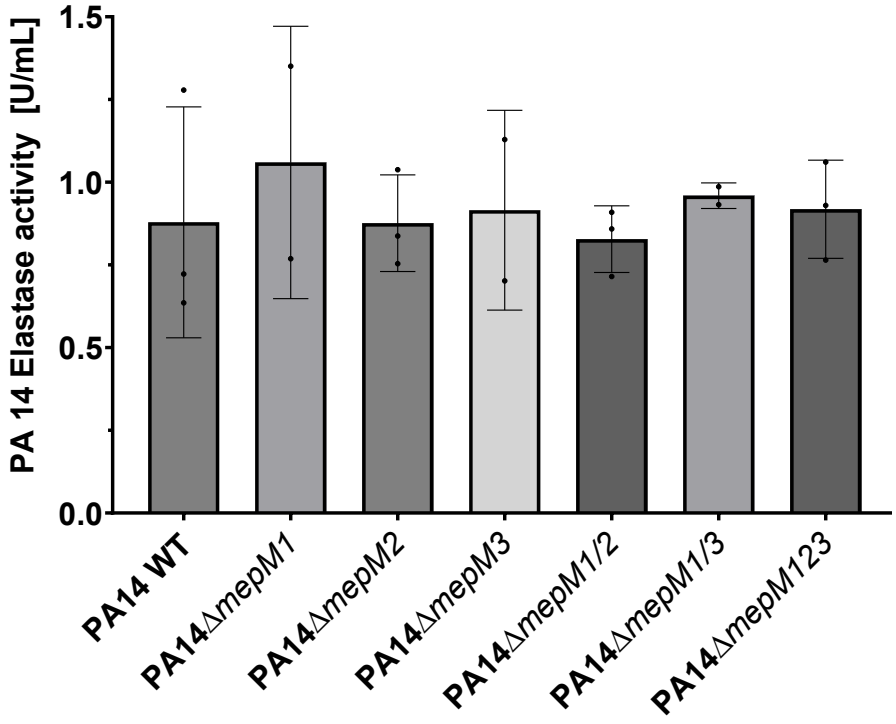


**Figure 17: Comparison of PA14‘s elastase activity:**
*DQ$^{TM}$-elastin substrate from EnzChek$^{TM}$ -kit was added to cell-free supernatants of PA14 WT and its mepM deletion strains. In the presence of elastase, DQ$^{TM}$-elastin is cleaved into a fluorescence-emitting substrate. The fluorescence intensity representing the elastase activity of the sample was detected photometrically ($OD_{520}$). The actual activity of elastase for each sample was calculated by utilising the equation of the elastase standard curve we generated. Depicted are the means and SD of 2 – 3 independent experiments. No significant difference was detectable upon One-way ANOVA statistical testing.*

Figure 17 depicts a comparison of PA14‘s elastase activity. In account to the visibly minor fluctuations in elastase activity, it can be concluded that *mepM* deletion in either constellation applied has no considerable effect or significant influence on the elastase activity of PA14 strains (Figure 17). Herewith also indicating that no measurable difference in the elastase concentration of PA14 upon *mepM* deletion can be expected. However, the execution of this assay was subject to measurement inaccuracies, which nevertheless had no effect on the overall results and conclusion of this assay. The measurement inaccuracies were due to difficulties of adding the DQ$^{TM}$-elastin substrate simultaneously into all wells, thus the reaction could not commence simultaneously for all samples. The samples of the strains PA14 *ΔmepM1*, PA14 *ΔmepM3* and PA14 *ΔmepM1/3* were often affected and started with a maximum delay of 30 - 45 seconds. Consequently, any difference resulting from this short time delay can be deemed neglectable. Having examined the effect of *mepM* deletion upon elastase activity,

we proceeded to check for further effects of *mepM* deficiency on other virulent factors such as protease.

### *3.3.2 Protease secretion and activity assay*

The protease assay was conducted with both ID40 and PA14 and their various *mepM* deletion strains. As was the case with the elastase assay, ID40 strains showed here again neglectable protease activity rendering its experimental results unpractical for analysis. Hence only PA14 was evaluated. For the protease assay cell growth of minimum $OD_{600} \geq 2$ was required (Kohler et al., 2001). To eliminate possible influence that different cell densities could have on the results, the cultures were prior adjusted to a similar cell count using fresh LB medium prior to harvesting. Cultures were then centrifuged, and sterile filtered. Similar to the methods of the elastase assay, first cell-free supernatants were generated, then transferred into a 96-well plate together with a digestion buffer and the BODIPY TR- X solution provided in the EnzChek™ Protease Assay Kit (red fluorescence). Due to lack of a protease enzyme standard solution, we utilised here the elastase enzyme solution provided in the EnzChek™ kit to generate a standard curve. This was feasible since elastase is also able to cleave the substrate provided by the Protease Assay Kit. Therefore, the detected protease activity would be the equivalence of elastase activity. Fluorescence intensity, representing the protease activity was measured by a TECAN reader immediately after adding of the BODIPY TR- X solution. The expected excitation/emission maxima laid at approx. 589/617 nm. The evaluation of the experimental data was carried out in accordance with the evaluation method described for the elastase assay. Four independent experiments were conducted, each consisting of 2 technical replicates. Figure 18 A depicts the individual experimental means and the overall means of the results. No significant difference in protease activity between the various strains could be observed.

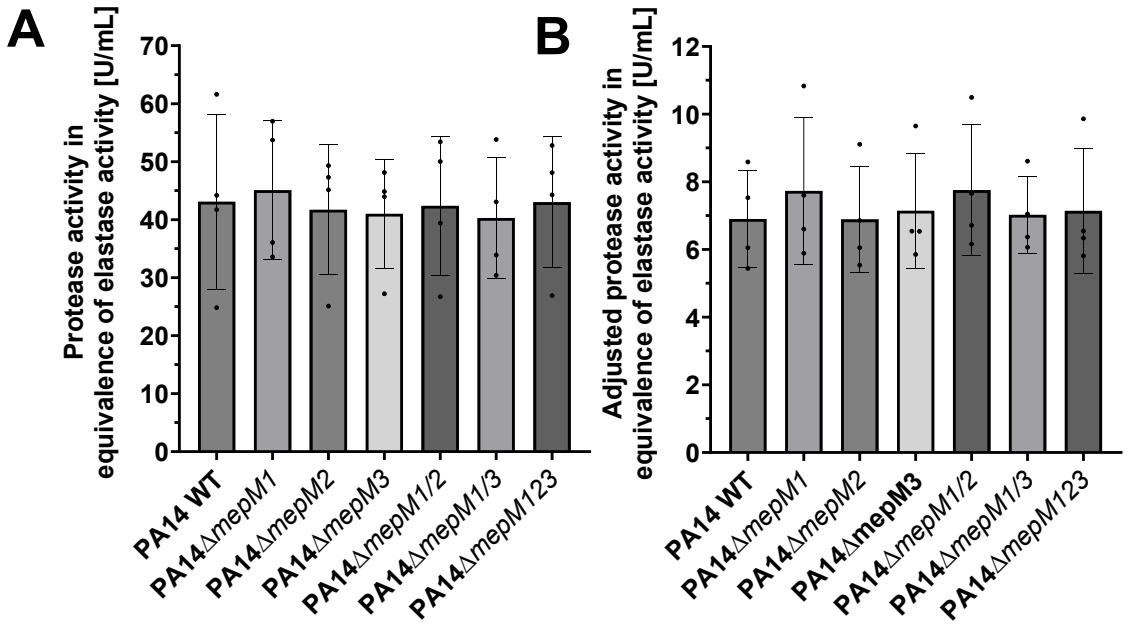


**Figure 18: Protease activity of PA14 strains with and without equalization to cell growth**
*Depicted are the overall mean and SD of four individual experiments addressing the protease activity of PA14 WT and mepM deletion strains. As an alternative to a protease reference sample, the elastase enzyme solution provided in the EnzChek™ kit was utilised. This was used to generate a standard curve and a calibration linear curve. The determined protease activities are therefore equivalence of the elastase activity (A) Protease activity of four individual experiments. (B) Protease activity adjusted to the cell count (OD) at the time of harvest of the respective samples. OD values of experiments 1 & 2: $OD_{600}$ = 2, experiments 3: $OD_{600}$ = 2,5, experiment 4: $OD_{600}$ = 3,5.*

To minimize any interference resulting from different cell growth, we normalized the protease activity to the cell growth (OD at harvest, i.e. $OD_{600}$ = 2, for experiments 1 & 2, $OD_{600}$ = 2.5 for experiment 3 and $OD_{600}$ = 3.5 for experiment 4). This resulted in a minor alteration of the data but presented no significant difference (Figure 18 B). To conclude, deletion of the *mepM* genes, as tested in this study has no effect on *Pseudomonas aeruginosa's* secretion or activity of protease. In contrast to the limitations with the elastase assay, here inaccuracies in measurements were carefully avoided. Next, we investigated the secretion of virulent factors such as siderophores and pyocyanin, upon *mepM* deletion.

### *3.3.3 Macroscopic assessment of culture supernatants*

The biofilm assay repeatedly showed colouration differences between the cultures of the various ID40 strains (Figure 19). This phenomenon was only seen in biofilm cultures incubated without shaking at 37°C for at least 43 hours in LB medium. Cultures from the same bacterial strains with identical mutations that were shaken or incubated in different mediums such as minimal medium (M9) or

MOPS medium did not show this colour variation. Furthermore, respective PA14 strains incubated similarly in LB also showed no colour variation despite measurable biofilm formation. This suggests that the reason for colour differences may be specific to ID40 and not general for *Pseudomonas* species. We hypothesize that this may be due to differential gene expression or mutations specific to ID40.

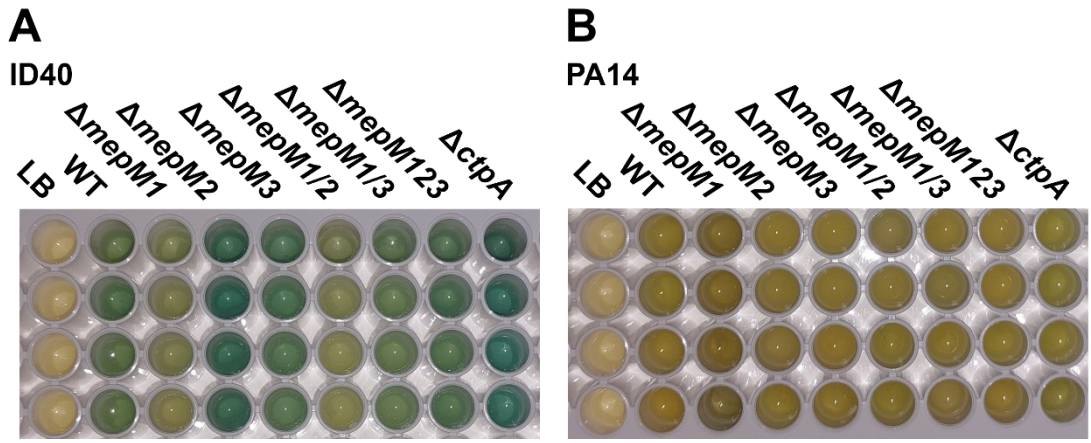


**Figure 19: Colour variation of ID40 and PA14 strains in biofilm assay.**
*ID40 WT* (A)*, PA14* (B) *WT and their mepM mutant strains were cultured for 2 days according to biofilm assay protocol. In contrast to PA14, ID40 samples displayed a spectrum of greenish cultural colouration, which was only seen after cultivation in LB- medium for an extended time. As a negative control LB medium alone (LB) is shown.*

Consequently, the question arises, whether the colour variation is due to differences in secretion of coloured products, resulting from the effect of specific *mepM* deletions. Such colourful secretion products are pyocyanin and siderophores, which are known to be important virulence factors of *P. aeruginosa*. Their role in aggravation of infections can be assumed. Since the *mepM* genes encode for endopeptidases involved in the regulation and recycling of the cell wall, the deletion of one or more of these endopeptidases may impair or affect the integrity of the cell wall and impact its secretion function. We aimed at examining the effect *mepM* deletions may have on pyocyanin and siderophore secretion.

### *3.3.4 Pyocyanin secretion and quantification assay*

First, pyocyanin (PYO) extraction and quantification was conducted using the bacterial cultures, which remained after removal of the biofilm attached to the TSP plate (used in biofilm assay). Thus, we could compare the colouration of the culture, the biofilm production level and the PYO secretion of the same culture samples.

For this, cultures of the same bacteria strain were transferred from the 96-well plate into a combined tube, vortexed and the $OD_{600}$ thereof measured. Samples were then centrifuged and subsequently, the supernatant sterile filtered to obtain cell-free supernatants. PYO extraction was performed according to previously described methods (section 2.2.12). Briefly, 250 µL of chloroform was added to 500 µL of the supernatant. This was vigorously vortexed at maximum speed for 5 minutes and then centrifuged. The chloroform layer (bottom layer) absorbed PYO and turned blueish-coloured. 200 µL of the chloroform extracts were transferred into new reaction tubes and supplemented with 100 µL of 0,5 % HCl. This again was vigorously vortexed at maximum speed for 5 minutes and then centrifuged. PYO was extracted into the aqueous HCl layer and turned from blue to reddish upon acidification. PYO dissolved in HCl was confirmed and quantitated via UV-Vis Spectrophotometer. Its characteristic absorption maxima laid at 277, 388 and 520 nm. Figure 20 shows the graphs of a PYO reference (undefined concentration) and an individual experiment and illustrates these characteristic peaks.

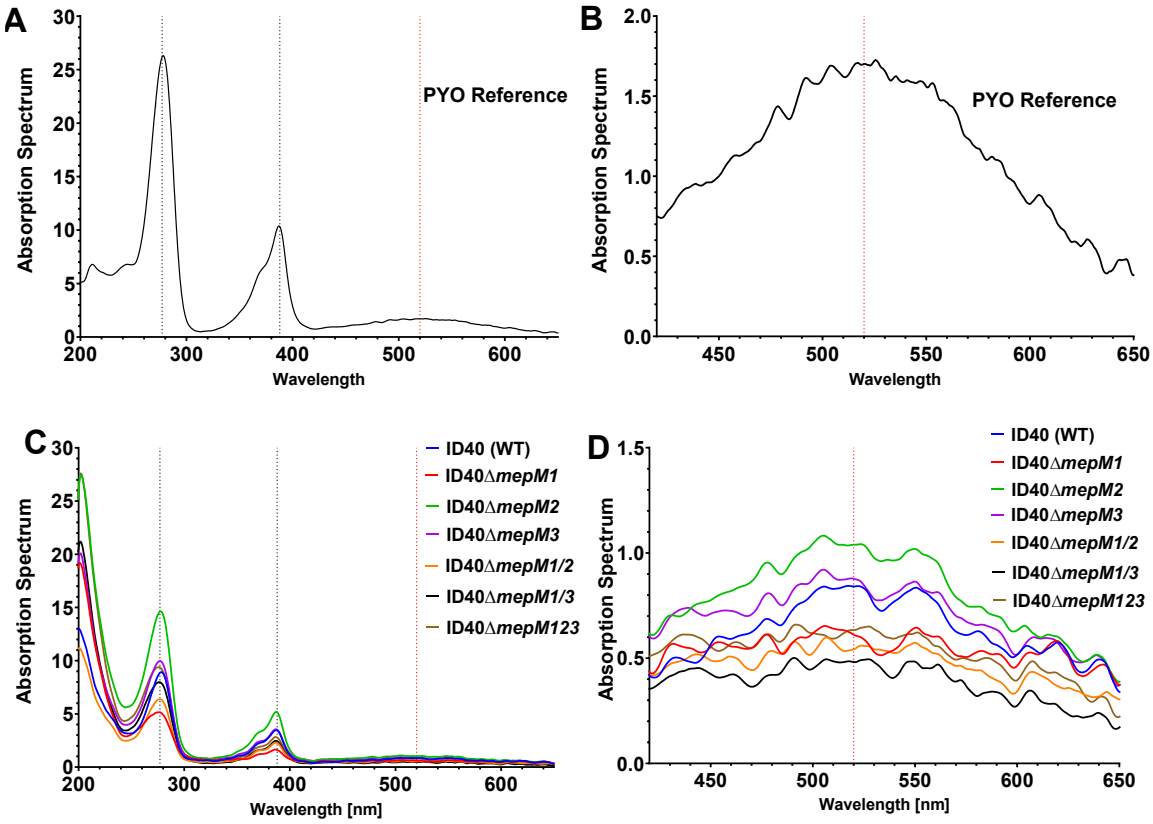


**Figure 20: Absorption spectrum of an individual experiment.**
*Depicted are the absorption spectrums of a PYO reference sample in 0,5% HCl (A & B, concentration unknown), ID40 (WT) (blue) and the mepM mutation strains (C & D, colours as specified). B & D are enlarged regions of A & C. The characteristic absorption maxima of PYO at 277 nm, 388 nm and 520 nm are highlighted with dotted vertical lines. Absorptions below 260 nm were assumed to be influenced by absorption of traces of residual substances extracted simultaneously from the supernatants.*

The absorption values of the PYO extracts at 520 nm were determined with a UV- Vis Spectrophotometer, then converted into a concentration [µg/mL] as stated in section 2.2.12. We first determined the PYO concentration of each strain. To minimize the effect of technical inaccuracies, 2-6 technical replicates per strain were conducted for all four independent experiments. The mean of these technical replicates per strain and per experiment were then analysed.

Although the comparison of PYO concentration secreted by the various ID40 strains revealed tendential differences, no significant differences could be observed (Figure 21). While deletion of *mepM1* reduced in tendency PYO production, deletion of *mepM2* or *mepM3* increased in tendency PYO production. The triple deletion mutant showed also slightly increased PYO secretion compared to the ID40 WT.

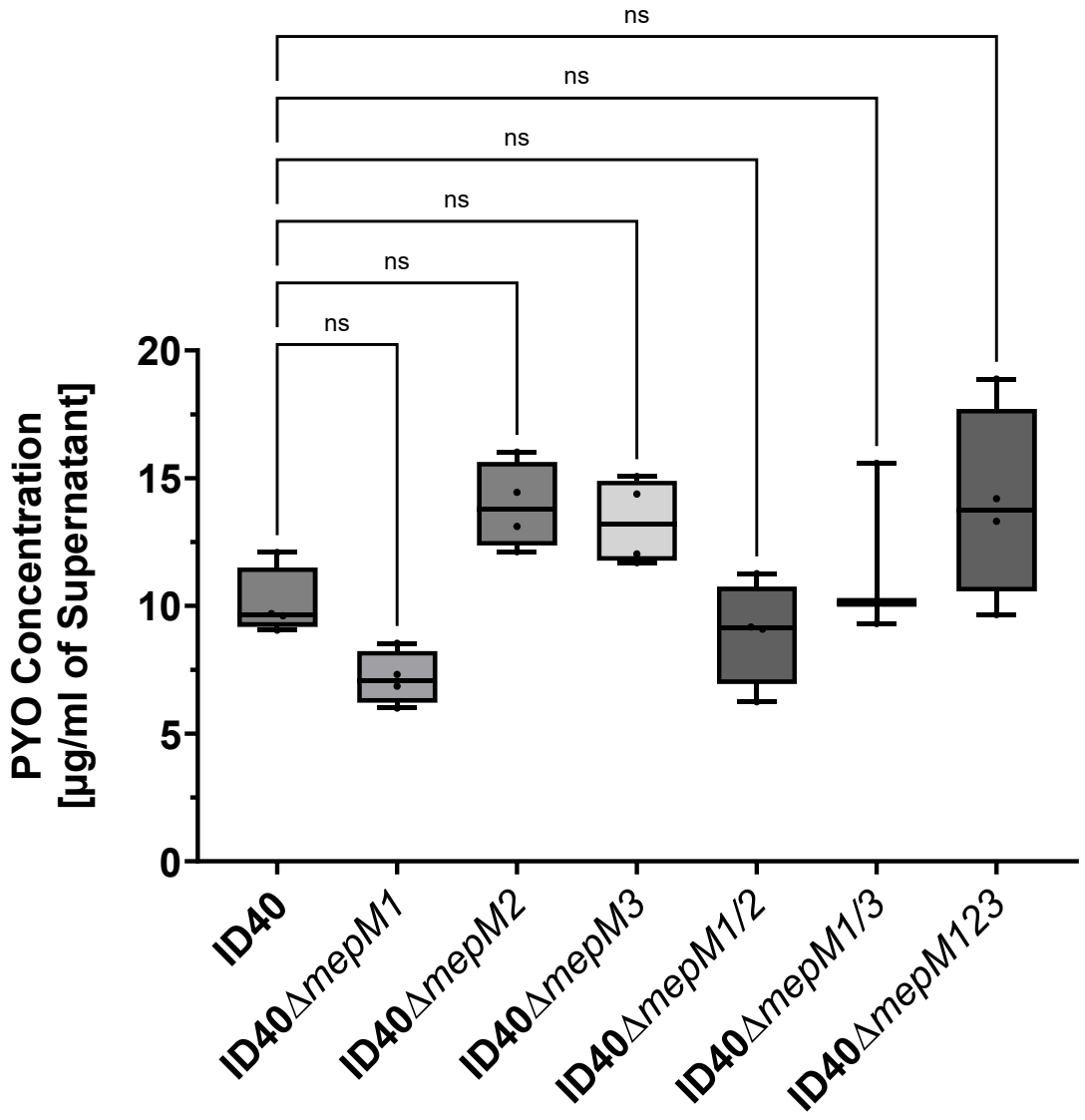


**Figure 21: PYO Concentration [µg/mL] of supernatant**
*Presented are the combined results of four independent experiments showing the PYO concentration [µg/mL] of ID40 WT and the mepM mutant strains. The Absorption values at 520nm were calculated with given formula to obtain the concentration of PYO in µg/mL. ID40 ΔmepM1 and ID40 ΔmepM1/2 show decreased PYO concentrations (7.18 and 8.94 µg/mL respectively) compared to ID40 WT (10.1µg/mL) Single mutation of mepM2 or mepM3 and the double and triple mutations show increased PYO concentrations. Depicted are the means and SD.*

The $OD_{600}$ of the bacteria samples showed comparable growth ranging between $OD_{600}$ = 0.9 to 1.9. It was assumed that this minor difference in OD measurement could be neglected as effect of possible technical inaccuracies. However, to be sure that this is the case, the influence of growth differences was considered, and

each mean of all technical replicates was divided by its $OD_{600}$ value (Figure 22).

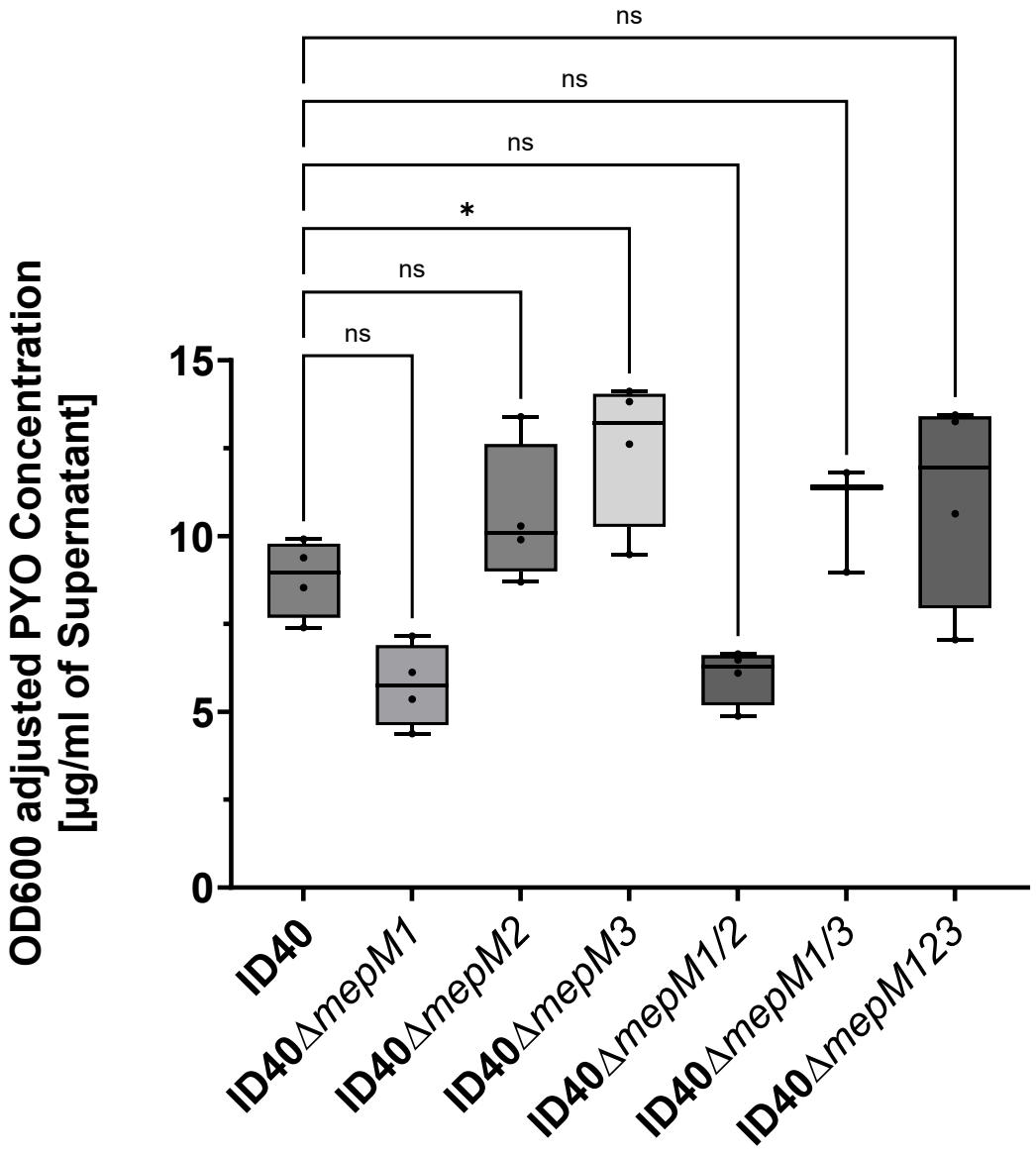


**Figure 22: PYO Concentration [µg/mL of supernatant] in relation to sample's cell density.**
*Presented are the combined results of four independent experiments showing the PYO concentration [µg/mL] of ID40 WT and the mepM mutant strains after extraction. The means of all technical replicates per strain and experiment were determined. To consider the influence of growth differences, every value was subsequently divided by its $OD_{600}$ value. ID40 ΔmepM1 and ID40 ΔmepM1/2 show decreased PYO concentrations (5.75 and 6.03 µg/mL respectively) compared to ID40 WT (8.81 µg/mL) Single mutation of mepM2 or mepM3 and the double and triple mutations show increased PYO concentrations. Depicted are the means and SD.*

As shown in Figure 22, taking growth differences into account only marginally alters the results and leads to only a significant increased PYO production in the *mepM3* deletion strain.

Proceeding, we further looked for a correlation between *mepM* deficiency and pyoverdine secretion or activity rate.

### *3.3.5 PVD secretion and quantification assay*

Pyoverdine (PVD) aids in the acquisition of iron in *P. aeruginosa*. strains. To further investigate the influence *mepM* deletion has on the secretion of coloured products, the PVD secretion was examined more closely. Liquid media used here, which promised to trigger and increase the PVD secretion of bacteria, enabling its measurement were MOPS, M9 minimal medium, and succinate medium (all iron-free). For this purpose, liquid LB overnight cultures were diluted 1:10 into the iron-free minimal media and incubated at 30°C overnight. These overnight cultures again were diluted 1:10 in fresh iron-free minimal media to minimize traces of iron in the growth medium. This again was incubated at 30°C overnight. Cell growth was low due to the minimal media character ($OD_{600}$ ≤ 1). Figure 23 shows the colour spectrum resulting from these experiments under UV light (365 nm). The cultures were of bright neon green or blue colour and fluorescent, indicating the presence of PVD amongst other products. The results suggest that the composition of the medium determines the type of colourful products which are secreted. Perhaps, the medium also interacts differently with the secretion products, evoking different colour impressions.

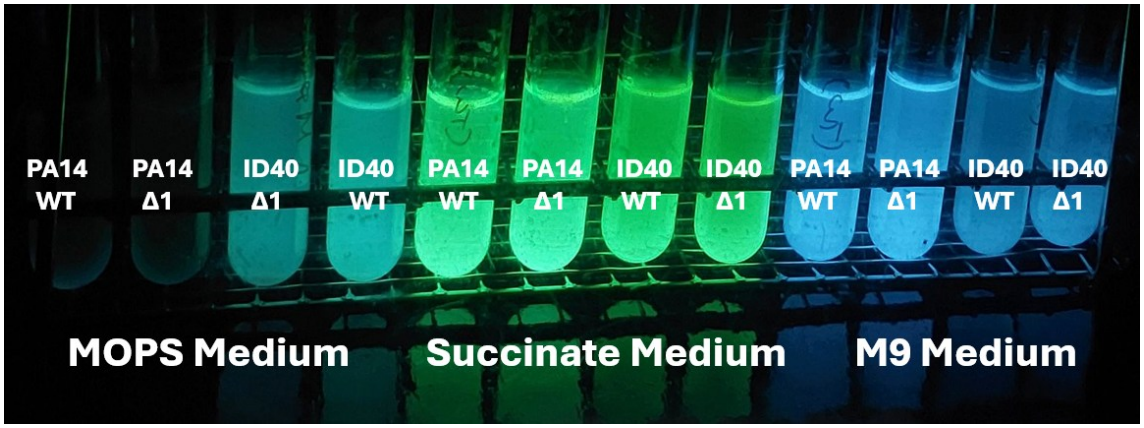


**Figure 23: Fluorescent nature of ID40 and PA14 in different minimal media.**
*Presented is a preliminary experiment with overnight cultures of ID40 and PA14 WT and their ΔmepM1 (Δ1) strains conducted in the iron-free minimal media MOPS (left) succinate (middle) and M9 (right). under UV light (365 nm). The cultures appeared translucent and green/blue fluorescent with exception of the PA14 strains in MOPS medium, which were visibly emerald green coloured in day light but showed no fluorescence under UV light (far left) This suggests that the composition of the medium may determine the kind of secreted colourful products. Used strains include PA14 WT, PA14 ΔmepM1 (PA14 Δ1), ID40 WT and ID40 ΔmepM1 (ID40 Δ1).*

PA14 (WT) and PA14 *ΔmepM1* generated fluorescent cultures with the succinate minimal medium (green) and M9 minimal medium (blue) but not with the MOPS medium. With the MOPS medium, the medium of both PA14 strains tested

appeared greenish (emerald) under daylight. ID40 (WT) and ID40 *ΔmepM1* showed fluorescent colours in all media: MOPS (blue), succinate (green) and M9 (blue). These results indicate that both the media composition and the bacterial species determine the colour appearance due to the secreted products. Due to the fact that green fluorescent colour was characteristic for PVD, we chose to further investigate the green fluorescent media of the succinate iron-free medium over the other two media. This decision was also supported by the low growth in the M9 medium rendering its results inaccurate. This can be explained by the fact that *P. aeruginosa* is a non-fermenting bacterium. Hence *Pa.* is not able to grow on glucose as sole carbon source as used in our M9 media.

Subsequent to incubation, the final cultures were centrifuged, sterile filtered and diluted 1:10 into Pyridine-Acetic acid (Pyr/AcOH) buffer. Using a spectrophotometer, the absorption spectrum of iron-free PVD was monitored and its characteristic absorption maxima at 380 nm was examined. Each sample was measured multiple times to obtain multiple technical replicates. The mean of the replicates per experiment was generated and used to determine the concentration of PVD secreted. The concentration of PVD was determined with the Lambert-Beer equation as stated in section 2.2.13. Having the samples been diluted 1:10 in Pyr/AcOH-Buffer prior, the resulting PDV concentration was then multiplied ten-fold and then converted from the unit mol/L into µM/mL of supernatant. The combined concentrations of secreted PVD from the four independent experiments are depicted in Figure 24. No statistically significant difference was reached upon one-way ANOVA testing.

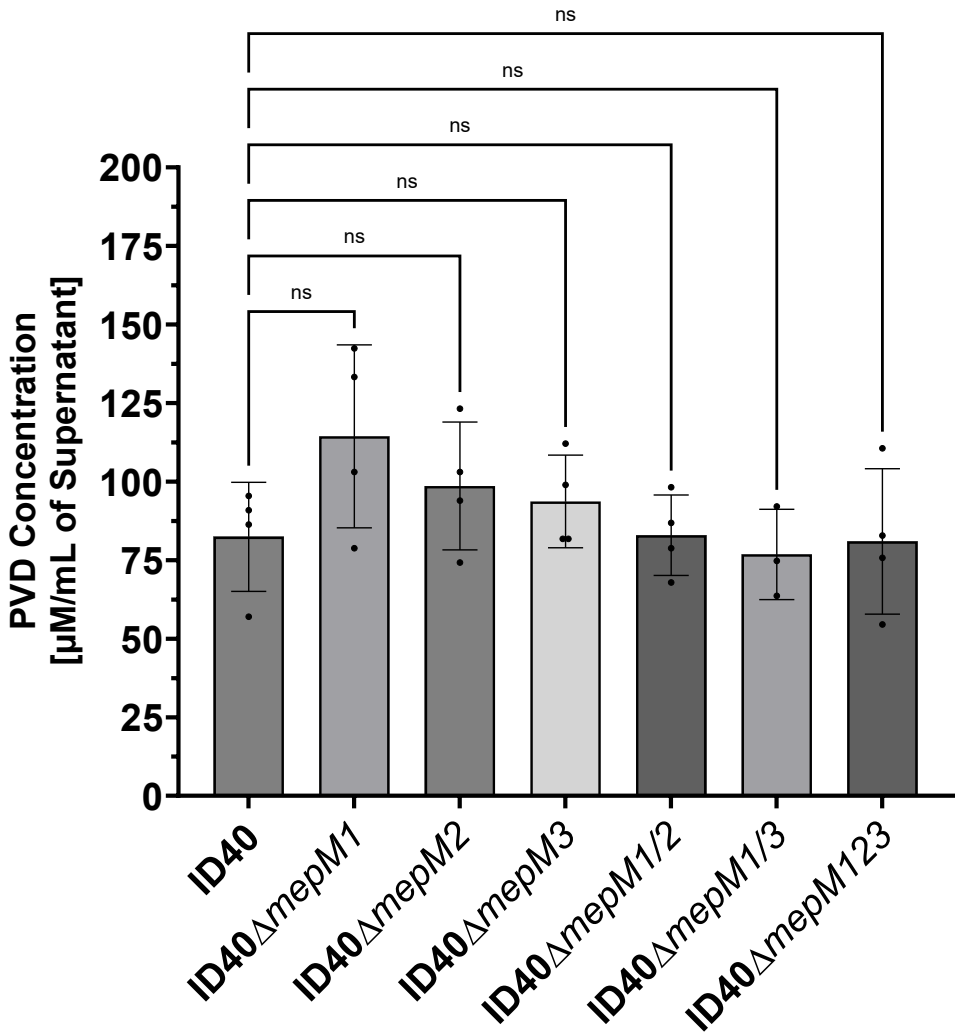


**Figure 24: Concentration of PVD per mL of supernatant**

*Supernatant of overnight cultures (in iron-free succinate minimal medium) were diluted 1:10 in Pyr/AcOH-Buffer. With a spectrophotometer, the absorption spectrum of iron-free PVD was monitored at its characteristic absorption maxima at 380 nm. Presented are the combined results from four independent experiments. The mean of each experiment is shown as a black dot. The overall mean and SD (error bars) are depicted. Single mutation of mepM gens results in a rise of PVD concentration. ΔmepM1 has the highest effect hereof. Double and triple deletion of mepM genes reach levels of PVD concentration comparable to that of ID40 WT. The differences are not statistically significant upon one-way ANOVA testing. In conclusion, no difference is found in-between ID40 WT and the various mepM deletion strains according to PVD secretion.*

ID40's concentration was designated as a reference to which all other values were compared. ID40 *ΔmepM1* shows 1.4-fold higher concentrations than the reference, representing the strain with the highest measured PVD concentration. While ID40 *ΔmepM2* shows 1.2 times higher PVD concentrations than the reference, ID40 *ΔmepM3* shows 1.14-fold higher concentrations.

Of the multi-mutation strains, ID40 *ΔmepM1 ΔmepM2*, ID40 *ΔmepM1 ΔmepM3* and ID40 *ΔmepM1 ΔmepM2 ΔmepM3*, no significant difference in PVD

production was observed compared to the WT. This suggests that *mepM1* deletion results in a though non-significant but considerable rise in PVD secretion. The same is true for single *mepM2* or *mepM3* deletion. Additional *mepM* deletions in form of multi-deletions seem not to affect PVD secretion. The small range from 76 µM/mL to 114 µM/mL in-between which all concentrations are found together with the fluctuations observed and the absence of statistical significance, suggests that no difference is detectable in-between ID40 WT and the various *mepM* deletion strains according to PVD secretion. This leads to the conclusion that MepMs might have no impact on PVD production.

After assessing the secretion of pyoverdine, we sought to address the global secretion of siderophores in general in our PA strains.

### 3.4 SideroTec Assay

We aimed to investigate whether *mepM* deletion influenced *Pa*. ID40's secretion of siderophores or impaired its siderophores activity in general. For this purpose, the SideroTec assay kit, which detects siderophores and iron chelators in liquid media was utilised. 100 µL of cell-free supernatant of overnight cultures grown in LB medium and 100 µL of Catalyst-Dye reagent were combined in a transparent 96-well plate. To obtain a standard curve for comparison, the supplied standard reagent was processed similarly (see section 2.2.14) and filled into the plate. The plate was incubated at room temperature for 12 minutes, later the OD was monitored from 620 – 630 nm in a microplate reader. The microplate reader determined the OD value of each sample, which was in turn used for the analysis.

For evaluation, the final siderophore concentration, which was present in the wells was plotted on the x-axis, while on the y-axis, 1/OD of the standard dilutions were plotted. Four biological replicates were created, each consisting of up to two technical replicates per sample. One standard curve was generated, using the data generated with the standard reagent during the first biological replicate. The mathematical formula as stated in section 2.2.14, which was derived from the linear standard curve was used to determine the concentration of siderophores in all bacterial samples.

For the sake of better comparison, the resulting data was converted into an x-fold change (see section 3.2.1 creating x-fold change data). Thus, the concentration of ID40 was set as a reference to which all other values were compared. Figure 25 presents the combined data of all four independent experiments. No significant difference in x-fold siderophore concentration levels was detected.

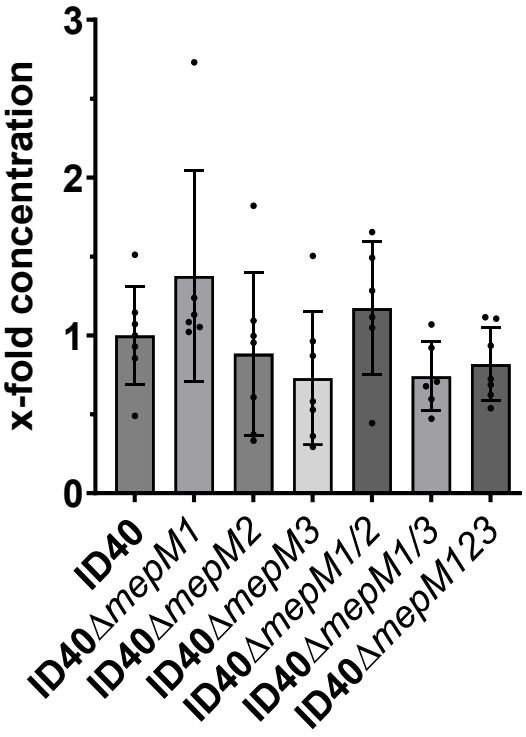


**Figure 25: Concentration of siderophore in x-fold change.**
*Presented is the x-fold change of the siderophore concentrations detected for each strain. The concentrations of siderophore were calculated with the help of the OD values measured and the enzyme standard curve. Slight differences are obvious, which failed to reach significance besides large fluctuations and minor differences between the mean values. Depicted are the means and SD (error bars) of four biological replicates, each consisting of up to 2 technical replicates per sample.*

ID40 Δ*mepM 1* shows slightly higher x-fold siderophore concentration compared to the reference (ID40 WT) and hereby represents the strain with the highest x-fold siderophore concentration. Whereas ID40 Δ*mepM2* presents lower x-fold siderophore concentration levels (mean = 0.88 arb. units), ID40 Δ*mepM3* shows even lower levels (mean = 0.73 arb. units). Of the multi-mutation strains, ID40 Δ*mepM1* Δ*mepM2* shows the highest x-fold siderophore concentration, which lies slightly above that of the WT but lower than that of Δ*mepM2*. ID40 Δ*mepM1*Δ*mepM3* and ID40 Δ*mepM1*Δ*mepM2*Δ*mepM3* depict lower siderophore concentration rates (0.74 and 0.82 arb. units respectively). Since the $OD_{600}$

values of all cultures were comparable with no strain showing higher growth rates, adjusting of the data to the growth rate was not applied.

Although slight differences were obvious, they failed to reach significance due to large fluctuations and minor differences between the mean values. It was therefore concluded that the siderophore secretion and activity between ID40 (WT) and the various *mepM* deletion strains are similar and MepMs do not contribute to the modulation of siderophore secretion. After focusing on the effects of *mepM* deletions on specific virulent factors such as biofilm, PYO and PVD, we now set out to investigate virulence in general and lethality of *mepM* deficient PA strains.

### 3.5 Virulence test with *G. mellonella* larvae

Virulence testing with larvae of honeycomb moths (*G. mellonella*) was conducted to explore whether the deletion of *mepM* generally affects the bacteria's virulence. We hypothesized that *mepM* deletion would lead to altered virulence and lethality.

Following bacteria strains PA14 WT, PA14 Δ*mepM*1 Δ*mepM*2 (PA14 Δ*mepM*1/2) and PA14 Δ*mepM*1 Δ*mepM*2 Δ*mepM*3 (PA14 Δ*mepM*123) as well as *Pa*. ID40 WT, ID40 Δ*mepM*1 Δ*mepM*2 (ID40 Δ*mepM*1/2) and ID40 Δ*mepM*1 Δ*mepM*2 Δ*mepM*3 (ID40 Δ*mepM*123) were used in this infection model. Equal count of bacterial cells ($OD_{600}$ = 0.1) were incubated for 2 hours followed by pelleting and discharging of the supernatant. Desired cell counts between $5*10^2$ and $10^3$ bacterial per mL DPBS for *Pa*. PA14 strains and concentrations between $10^3$ and 1.6 * $10^5$ bacterial per mL for *Pa*. ID40 strains, were created by diluting in DPBS.

The larvae were infected with precisely 10µL of bacteria dilutions by injection through the hind legs then incubated with food supply at 37°C for five days. Those found dead upon daily examinations were discharged and noted. The bacteria dilution was plated on blood agar plates to determine the precise count of bacteria injected. To determine the survival rate, groups of 8-20 larvae were injected with different infection doses. Even at the lowest bacterial concentration of $10^3$, corresponding to 10 bacteria cells per inoculum, all *G. mellonella* larvae infected with PA14 strains died, irrespective of their *mepM* mutations. This observation

suggests that PA14 strains are more lethal than ID40 strains for *G. mellonella*. With all PA14 infected larvae dead irrespective of the concentration or mutation strain, no sensible analysis of the data or comparison could be drawn, leading to neglecting of the PA14 data and a greater emphasis placed on data generated with ID40 infection models (Figure 26). We plotted the survival ratio after 5 days against the logarithm of the infection dose. Data analyses and statistics performed are as stated in section 2.2.15.

With $y(x)$ being the survival rate after 5 days for the infection dose $x$ and $LD_{50}$ being the lethal infection dose at which 50% of the infected animals are dead after 5 days. Obvious displays of high variations and partially conflicting values in the survival rates could be seen. Nevertheless, it distinctly shows that an increase in infection dose (concentration of bacteria infected) is positively correlated with lower survival rates of the *G. mellonella* larvae and vice versa. This effect is consistent and could be observed in all tested ID40 strains and mutations.

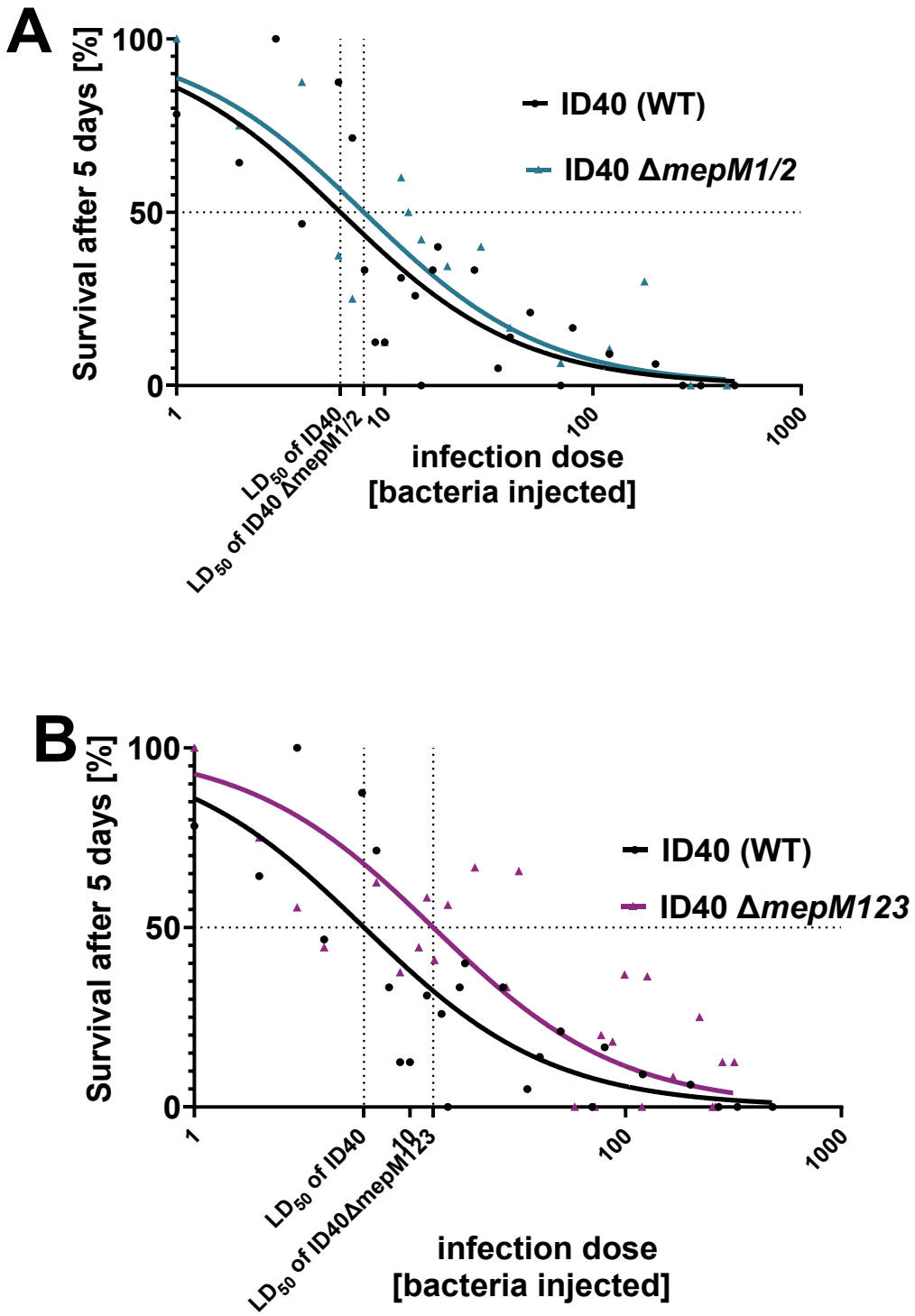


**Figure 26: Lethality of Pa. ID40 in a *G. mellonella* larvae infection model**

*G. mellonella larvae were infected with a defined cell count of Pa. ID40 (WT), Pa. ID40ΔmepM1/2 or Pa. ID40ΔmepM123 and incubated with food supply at 37°C for up to 5 days post-infection. Depicted are the survival rate in percentage after 5 days (y-axis) and the confirmed infection dose (x-axis). To determine the survival rate for each dose 8-20 animals were infected, and the infection dose (CFU) was determined. Colour coding as stated. The $LD_{50}$ values are highlighted. Figure A: ID40 ΔmepM1/2 possessed a slightly higher $LD_{50}$ value than the WT. Thereby indicating to be less pathogenic or lethal than the WT. In Figure B ID40 ΔmepM123 shows a significantly higher $LD_{50}$ value than the WT (12.8 vs. 6.1). Thereby suggesting being significantly less pathogenic or lethal than the WT.*

The non-linear regression curves (Figure 26) and statistics performed suggest a significant difference between ID40 (WT) and ID40 Δ*mepM123* (Table 29), indicating that with all caution, ID40 Δ*mepM123* might be slightly less virulent than ID40 (WT). The differences between ID40 (WT) and ID40 Δ*mepM1/2* are marginal and failed to reach statistical significance.

*Table 29: Comparison of $LD_{50}$, $R^2$ and the 95% confidence interval of Figure 26*
*Emphasized is the $LD_{50}$ of the non-linear regression of Figure 26. The P value was estimated using extra sum-of-square F test with the Null hypothesis of one curve fits all data sets (i.e. data of ID40 WT and ID40 ΔmepM1/2 or ID40 WT and ID40 ΔmepM123 are the same). This is been compared to the $R^2$ (goodness of fit), and the 95% confidence interval of Figure 26.*

| | **Strain** | | |
|---|---|---|---|
| | **ID40 (WT)** | **ID40 Δ*mepM1/2*** | **ID40 Δ*mepM123*** |
| **$LD_{50}$** | 6.124 | 7.938 | 12.83 |
| **$R^2$** | 0.681 | 0.687 | 0.602 |
| **95% Confidence interval $LD_{50}$** | 4.061-9.006 | 4.741-13.030 | 7.808-20.600 |
| **P value** | - | 0.399 | 0.018 |

# 4 Discussion

On the quest to discover new antimicrobial methods to target and treat MDR *P. aeruginosa* infections in human hosts, previous research findings suggested enzymes involved in the turnover of the bacterial cell wall such as MepMs as potential candidates (Dhar et al., 2018; Sonnabend et al., 2020). It has recently been validated that the family of murein endopeptidases (MepM) play an important role in mediating ß-lactam resistance to the MDR *P. aeruginosa* strain ID40. Using a TraDIS approach, several murein endopeptidases, namely MepM1, MepM2, and MepH2, were identified as possible drivers of resistance to cefepime and meropenem. The *mepM1* gene was later confirmed to contribute to ß-lactam resistance via modulation of the expression level of the chromosomally encoded ß-lactamase AmpC, whose expression level is furthermore regulated by AmpR (Dhar et al., 2018; Sonnabend et al., 2020). Subsequent work by Kemper J. ((Kemper, 2020) Dr. med thesis) showed that *mepM2* and to a lesser extent also *mepM3* contribute to ß-lactam resistance. However, deletion of these genes showed no reduction in *ampC* expression. Thereby implying that the contribution mediated by *mepM2* or *mepM3*, in contrast to that of *mepM1*, is seemingly not associated with the modulation of *ampC* expression. It was further shown that double deletion of *mepM1* and *mepM2 (*Δ*mepM1/2)* as well as a triple deletion of *mepM1*, *mepM2* and *mepM3* (Δ*mepM123*) was able to reduce ß-lactam resistance to a much higher extent than the single mutants. However, these studies revealed that this observed reduction in ß-lactam resistance was not explainable by reduced *ampC* expression alone. Further, yet unknown mechanisms must be involved here. Therefore, as an interim conclusion, it can be stated that the contribution of MepM1, MepM2 and MepM3 to ß-lactam resistance is mediated on the one hand by MepM1 causing for increased *ampC* expression levels and on the other hand by other yet unknown mechanisms.

An aim of the medical doctoral thesis of Vöhringer K. ((Vöhringer, unpublished) Dr. med thesis) was to identify these still unknown yet potential mechanisms of ß-lactam resistance. In this context, it was investigated whether the triple deletion

Δ*mepM123* would change the composition of membrane proteins. Proteomic analyses led to the hypothesis that triple deletion could lead to an abundance of the efflux pump MexEF-OprN. This expectation was confirmed by Western blot analyses and quantifications. Furthermore, it was shown that the reduction in β-lactam resistance caused by triple deletion of MepMs could be partially restored by additional deletion of the *mexEF-oprN* operon. These results indeed suggest that in addition to MepM1 mediated modulation of *ampC* expression, MepM mediated modulation of MexEF-OprN expression may also contribute to ß-lactam resistance.

### 4.1 *mepM* deletion affects the abundance of MexEF-OprN

Based on these preliminary studies, the question then aroused whether the modulation of the abundance of the efflux pump MexEF-OprN by MepMs can be assigned to individual MepMs. For this purpose, as a reporter system, strains were successfully generated in which the *mexE* gene was chromosomally modified as a HiBiT-tagged *mexE-HiBiT* gene, which stood under the control of the native promoter.

If both Western blot analysis and the semiquantification of MexE-HiBiT are taken into account, one can clearly state that the triple deletion mutant Δ*mepM123* shows significant increased abundance of MexE-HiBiT. However, only an approximately two-fold increase of MexE-HiBiT level can be observed in such a triple deletion. As a reverse conclusion these findings suggest that the presence of MepM1, MepM2 and MepM3 in concert leads to reduced levels of MexE. Since the genes *mexE*, *mexF* and *oprN* are located on the same operon, it can be deduced that this holds true for the whole efflux pump. It is noteworthy to state that compared to MepM2, MepM1 and MepM3 seem to have an opposite effect on MexE levels: loss of *mepM1* or *mepM3* results in a significant reduction of MexE-HiBiT levels in comparison to the WT, while deletion of *mepM2* leads to a non-significant increase of MexE-HiBiT levels. The presence of MepM2 seems to have a negative impact on MexE levels, indicated by the finding that in all mutants where MepM2 is present (Δ*mepM1*, Δ*mepM3*, Δ*mepM1/3*) the MexE levels are lower and, in the mutants where MepM2 is absent (Δ*mepM/2*, Δ*mepM123*) MexE

levels are higher. To explain the higher MexE levels in Δ*mepM123* compared to that of Δ*mepM2* one could postulate that either MepM1 or MepM3 might also have a rather negative impact on MexE levels. According to the present data one could assume that MepM3 has also a rather negative impact on MexE levels. To validate this assumption, it would be necessary to measure MexE abundance in a *mepM23* deletion mutation. If the hypothesis that MepM2 and MepM3 would have a negative impact on MexE would be correct, a *mepM23* deletion should show similar or even higher (if MepM1 would activate) MexE levels than the *mepM123* deletion mutant. To summarize, the presence of MepMs does affect the abundance of the MexEF-OprN efflux pump present in the cell envelope in a manner yet not fully elucidated.

The activity of all MepMs acting in concert might be greatly important for the controlling of the incorporation and consequently for the abundance of efflux pumps in the cell envelope. The collapse of all three MepMs might cause an imbalance enabling an easier incorporation of the MexEF-OprN efflux pump, resulting in highly elevated MexE-HiBiT levels. In this case, it would be of interest to further investigate in more detail, whether the incorporation of other transmembrane proteins and whole complexes are similarly influenced by the activity of MepMs. In line with this hypothesis, experiments of Vanderlinde and co-workers on *Aeromonas hydrophila* throw light upon a possible relationship between the activity of PG turnover enzymes and the assembly of transmembrane complexes. They reported that increased PG pore size (reduced peptide cross-linkage mediated by enzymes such as MepMs) influenced the assembly mechanism of the type II secretory system (Vanderlinde et al., 2017). Moreover, Srivastava and colleagues reported that the absence of CtpA (carboxy-terminal processing protease), which cleaves its substrates (MepM1, MepM3, MepH1 and MepH2) leads to high levels of these MepMs. They observed as a consequence defective incorporation of the type III-secretion system (T3SS) and consequently less secretion of the T3SS effectors ExoT and ExoS paired with reduced virulence (Kemper, 2020; Srivastava et al., 2018). Bringing the literature together demonstrate that the regulation of murein endopeptidases has

consequences for the incorporation of transmembrane complexes as shown here for the MexEF-OprN efflux pump as a further example beside the T3SS.

At this point we hypothesize that MepMs influence mostly the incorporation of the efflux pump. However, it is also possible that MepMs indirectly influence the expression of the *mexEF-oprN* cluster and thus affecting the amount of translated proteins. This possibility is supported by other researchers, who demonstrated an interaction between the activity of the multi-transcriptional regulator AmpR and the expression level of *mexEF-oprN* (Balasubramanian et al., 2012; Dhar et al., 2018) (see Figure 4). Statements about the influence of AmpR activity intertwined with MepM activity and expression of *mexEF-oprN* operon however lie beyond the scope of the present study. However in brief, AmpR inhibits MexT, while MexT controls *mexEF-oprN* expression (Balasubramanian et al., 2012; Dhar et al., 2018) (Figure 4). The expression of *mexEF-oprN* is again subject to the activity of MepMs. Multiple mechanisms apart from AmpR‘s regulation, contributes to the expression of the *mexEF-oprN* cluster. This explains the slight reduction in ß- lactam resistance observed in *mepM2* mutants despite increased *ampC* expression (Kemper, 2020; Sonnabend et al., 2020) and the elevated abundance of MexEF-OprN.

In line with this, the transcription factor of the *mexEF-oprN* operon MexT has been reported to possess a subsidiary function as a repressor of the *oprD* gene. OprD is an outer membrane pore that under normal conditions enables the uptake of carbapenems such as imipenem or meropenem into the cell (Köhler et al., 1999). As a consequence, it can be expected of ∆*mepM123* mutants which show elevated abundance of MexEF-OprN to display also carbapenem resistance resulting from increased MexT activity. In contrast to this scenario, ∆*mepM123* mutants show the greatest susceptibility to all tested ß-lactams, including imipenem (Kemper, 2020). This outcome is supported by other findings which described *nfxC*-type mutants displaying a *mexEF-oprN* overexpression without increased transcription of MexT (Köhler et al., 1999). In accordance, we suggest that increased abundance of MexEF-OprN reported in our study is facilitated by a MexT-independent and probably AmpR-independent manner. This would

explain the co-occurrence of increased abundance of MexEF-OprN alongside increased imipenem sensitivity.

Bringing our findings together with preliminary findings about the effects of *mepM* deletion, one can conclude that while deletion of MepM1 profoundly affects ß-lactam resistance by causing a reduction in *ampC* expression, deficiency of MepM2 shows its slight effect on ß-lactam resistance by increasing the MexEF-OprN levels. *mepM3* deletion shows neither reduced *ampC* expression nor elevated MexEF-OprN abundance, explaining its minor influence on reducing ß-lactam resistance. Of all the tested *mepM* deletion mutants, Δ*mepM3* exhibited the highest ß-lactam resistance, indicating that elevated *ampC* expression coupled with reduced MexEF-OprN abundance seems to be associated with ß-lactam resistance. Simultaneous deficiency of MepM1, MepM2 and MepM3 (Δ*mepM123)* displays both beneficial effects, thus combating ß-lactam resistance effectively (Kemper, 2020; Sonnabend et al., 2020).

The abundance of MexEF-OprN is hence another contributor of the many mechanisms orchestrating ß-lactam resistance in *P. aeruginosa*. Precise understanding on how the actions of MepMs influence ß-lactam resistance besides their regulation via *ampC* expression is still far from satisfactory and raises subjects for future research. More clarity on this behalf could be obtained by subsequent analysis of the mRNA expression of the *mexEF-oprN* cluster. This could be done with semi-quantitative RT-PCR of *mexE*. Alternatively, measuring of the transcriptional activity of the *mexEF-oprN* promoter for example with a luciferase reporter in different deletion mutants would be feasible. We thereby speculate that such investigations would indicate that the increased abundance of MexEF-OprN in a triple deletion mutant does not result from altered *mexE* expression but is more likely due to posttranscriptional regulation.

Additionally, it should be noted that quinolones are substrates of the MexEF-OprN pump. An increased abundance of MexEF-OprN resulting from *mepM123* deficiency possesses the potential to increase the bacterium's resistance to (fluoro)quinolones besides reducing ß-lactam resistance. In addition to these mechanisms, which determine *P. aeruginosa's* susceptibility to antibiotic

treatment, MepM's activity has also been found to affect the production of certain virulence factors.

## 4.2 MepMs affect AmpR associated genes involved in production of virulence factors

Virulence factors account for a large portion of the pathogenic phenotype of *P. aeruginosa*. It is therefore of great benefit to find ways to suppress the expression of these phenotypes. Hence, we investigated the role of MepMs in the secretion of virulence factors such as protease, elastase or pyocyanin. We hypothesised that inhibition or deletion of *mepM* would affect the rate of secreted virulent factors resulting in reduced detection of elastase, protease or pyocyanin.

Studies on *ampR* have shown that the transcriptional regulator AmpR does not only regulate the transcriptional activity of the *ampR* and the *ampC* genes but also has a global influence on many genes as shown in Figure 4. The control of AmpR is tightly linked to cell wall synthesis and recycling. Upon degradation of the cell wall, peptidoglycan fragments are transported into the cytoplasm and catabolized. Early catabolites (anhydroMurNAc-peptides) binds to the effector binding domain of AmpR and cause for derepression of AmpR. Meaning, AmpR is then able to bind to promoters to transactivate or inhibit genes. During PG catabolism, UDP-MurNAc-pentapeptide is generated as the basic building block of cell wall synthesis. UDP-MurNAc-pentapeptide however can bind to AmpR and cause for the repression of AmpR (Dhar et al., 2018; Sonnabend et al., 2020). Prevailing of this AmpR suppressor locks AmpR in a predominantly inactive state (Dik et al., 2017). This implies that the presence of ß-lactam antibiotics, which leads to damaging of the cell wall, also results in a higher concentration of anhydroMurNAc-peptides in the cytoplasm. Thus, inducing a stronger derepression or activity of AmpR. Consequently, increased *ampC* expression is expected to result besides reduced expression of efflux pumps such as MexEF- OprN and MexAB-OprM as well as altered quorum sensing which in turn mediates increased secretion of proteases, elastases and pyocyanin (Balasubramanian et al., 2012) (Figure 4). Preliminary studies by Kemper and Sonnabend et al. have shown that MepM1 deficiency or simultaneous defect of

all three MepMs (Δ*mepM123*) is associated with reduced *ampC* expression, consequently also reduced AmpR activity (Kemper, 2020; Sonnabend et al., 2020). This implies that as a result of *mepM* deletion, the production of AmpR-associated virulence factors such as virulent exoproteins might be decreased.

The manner by which AmpR exerts its influence on the production of virulence factors can be explained in the following way. It has previously repeatedly been reported that overexpression of the *mexEF-oprN* cluster seems to affect quorum sensing (QS) leading to altered production of rhamnolipids, pyocyanin and swarming motility (Köhler et al., 2001; Lamarche & Déziel, 2011). Köhler et al. proposed 3-oxo-C12-HSL (product of the *las* system) or PQS or perhaps precursors thereof (required for the *rhl* system) as putative substrates of this efflux pump (Köhler et al., 2001). This means that MexEF-OprN enable the transportation of these autoinducers out of the cell. As a consequence, the required concentration of these autoinducers in the cytoplasm, needed to communicate the presence of the critical cell-cell density to the organism might be delayed or entirely not reached. As a result, the respective QS-mediated effector genes may remain inactivated resulting in lesser production rate of effectors such as elastase, protease, rhamnolipids and pyocyanin. This hypothesis is supported by Köhler et al., who described that *nfxC*-type mutants of *P. aeruginosa* which are characterized by their overexpression of *mexEF-oprN* produces 20-fold less pyocyanin and show reduced production or activity of rhamnolipids and elastase. They attributed this effect of reduced production of exoproteins solely to the impact of *mexEF-oprN* overexpression (Köhler et al., 2001). Furthermore, Lamarche et al. demonstrated that overproduction of the MexEF-OprN efflux pump led to reduced swarming motility, pyocyanin production and biofilm formation via a signalling molecule of the QS family (Lamarche & Déziel, 2011). In line with this, it can be concluded that overexpression of *mexEF-oprN* mediates attenuation of virulence presented in the form of reduced pyocyanin, elastase or protease production.

Moreover, the fact that MexAB-OprM pumps ß-lactam out of the cell logically raises the question as to why its overexpression, facilitated by reduced AmpR activity (low *ampC* expression), does not lead to increased ß-lactam resistance

(Figure 4). According to Dhar et al., the influence of MexAB-OprM on the development of ß-lactam resistance is marginal. The major resistance driving force lies with the *ampC* expression rate and the *dacB* mutation (Dhar et al., 2018; Torrens et al., 2019).

Based on the findings of Köhler et al., we hypothesized that due to changes in MexEF-OprN levels upon *mepM123* deletion, changes in pyocyanin, elastase and protease levels could be detectable but this was not the case. Preceding, the question now arises as to why we were unable to discern any significant differences in the secretion of pyocyanin, elastase and protease in our study when comparing mutants with verifiably increased MexEF-OprN production (Δ*mepM123*) and those without (ID40 WT).

Regarding elastase and protease secretion of ID40 wildtype, it could be observed that this strain secretes very low levels of both elastase and proteases. Therefore, it cannot be expected to observe differences in the *mepM* deletion mutants. In contrast, PA14 produces detectable levels of elastase and proteases, but also in this strain MepMs seem to have no impact on elastase secretion. The hardly detectable levels of elastase in ID40 might be associated with the retrospective findings of the working group that, transcriptomics data as well as mRNA expression analyses by RT-qPCR reveal high mRNA expression levels of the *mexEF-oprN* operon of ID40 compared to PA14 (approximately 20-fold higher), indicating that ID40 per se overexpresses this efflux pump. In consequence one would expect in line with the data of Köhler et al. low levels of elastase (lasB) expression. This correlates with the observations found in the transcriptome data and elastase assay data as presented here (Figure 16). One possible reason why no differences for elastase were found in PA14 *mepM* deletion mutants could be derived from the fact that our protease and elastase experiment always had $OD_{600}$ values of below 3.5, or even around $OD_{600}$ = 2. According to Köhler et al., who measured *P. aeruginosa*'s elastase production, the presence of elastase was only detectable from $OD_{600}$ values above 2. Distinctive differences however between MexEF overproducers and control strains examined were not evident until the $OD_{600}$ values exceeded 3 (Köhler et al., 2001). Given that the quorum sensing-dependent induction of the production of exoprotein requires a particular

cell-cell density, it is considerable to deduce that our measurements at $OD_{600}$ values between 2 and 3.5 may have only measured the basal expression of elastase or protease in PA14 strains, which does not differ between WT and *mepM* mutants at this low cell density. The influence of MepM deficiency and MexEF-OprN production might therefore only come into play during the induction and increased secretion of exoproteins. Future studies should aim at measuring at higher $OD_{600}$ values (≥ 3) in order to crystallize potentially detectable and distinguishing differences. The same may apply to our experiments investigating pyocyanin production upon *mepM* deletion. They showed a cell-cell density ranging from $OD_{600}$ 0.9 to 2.

### 4.3 Deficiency of *mepM* results in reduced biofilm formation

Another virulence factor addressed in this study was biofilm production and how these are influenced by MepM activity. Biofilm formation provides multiple advantages for those bacteria embedded in it. Such advantages involve protection against attacks from the immune system, better survival in adverse environments, or reduced susceptibility to antimicrobial agents (Donlan, 2001; Kostakioti et al., 2013). Identifying methods or agents that may prevent or impede the formation of such protective biofilm aggregations provides potential solutions with which persistence of bacterial infections can be controlled. For this purpose, we investigated the role of murein endopeptidases (MepM) in biofilm formation. In order to accomplish this, the WT and *mepM* deletion mutants of *P. aeruginosa* strain ID40 were incubated under static conditions for 43 - 48 hours at 37°C. The biofilm formed was then evaluated by staining with crystal violet (CV) followed by photometric measurement.

Our results indeed show that the PG recycling enzymes of the murein endopeptidase group (MepMs) are able to modulate biofilm formation (Figure 15). Generally, deficiency of any of the tested MepMs causes for a reduction in the strain's virulence by reducing its ability to form biofilms. MepM1 carries hereby the dominant role. Upon its loss biofilm production is massively hampered. Additional deletion of further *mepM* genes leads to counteraction of this effect leading to a slight increasement in the productivity of biofilms. Nevertheless, the

triple mutant is still less avid in biofilm formation in comparison to the WT despite the additional deletion of *mepM2* and *mepM3* (Figure 15).

The formation of biofilm requires the expulsion of biofilm building blocks from the cytoplasm to the extracellular space. Efflux pumps play hereby an important role in biofilm formation. In agreement with this, Lorusso et al. reported that increased biofilm formation correlated positively with increased efflux pump activity (Lorusso et al., 2022). This suggests that the observed increase in biofilm formation upon *mepM123* deletion might be due to an increased abundance of an efflux pump perhaps of MexEF-OprN.

Summing things up, we conclude that the ability of biofilm formation as a virulent factor is subject to the activity of MepM1, MepM2 and MepM3 via a yet unknown mechanism. An involvement of efflux pumps in the formation of biofilm can be hypothesized. Suggesting that increased abundance of efflux pumps facilitated by certain MepM deletion combinations may favour easier biofilm formation. Moreover, biofilm formation often occurs in environments where shear forces are involved, such as in the case of blood flow or ventilation devices. Such forces may have influence on the expression rate of genes and activity of specific pathways, differing such conditions from static biofilm formation conditions. Our experiments were conducted in static conditions. Hence, statements about biofilm formation in non-static environments lie beyond the scope of this study. Moreover, when comparing the graphs of pyocyanin concentration to those of the biofilm production, one can observe a similarity in pattern (Figure 27).

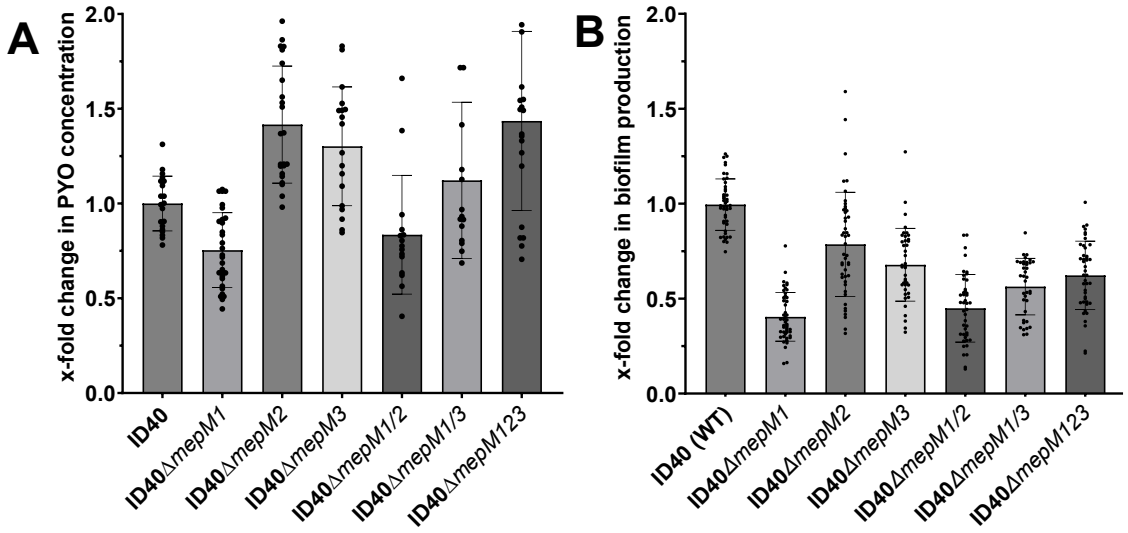


**Figure 27: Comparison of pattern between the graphs of pyocyanin concentration and biofilm production**
*Depicted are the graphs of pyocyanin concentration in x-fold change (A) compared to that of biofilm production also in x-fold change (B). Careful observation of these graphs beginning at ID40 ΔmepM1 towards ID40 ΔmepM123, display changes in similar patterns and magnitude. But while the effect upon biofilm production causes for a decline in all deletion mutants, the results for pyocyanin (PYO) secretion vary strongly above and below that of the WT.*

Scrutinization of these graphs starting at ID40 Δ*mepM1* towards ID40 Δ*mepM123*, display changes in similar patterns. With great caution, it could be argued that there might exist a common mechanism or perhaps a linkage between biofilm production and pyocyanin secretion, which by giving *mepM* deletion influences these virulence factors to a similar extent. But while upon biofilm production the effect causes for an invariable decline in all deletion mutants, the results for pyocyanin (PYO) secretion vary strongly. The results vary between an incline over the PYO concentration level of the WT or a decline beneath it. Interestingly, some literature describes a possible relationship between signalling molecules involved in QS, biofilm production and the virulence factor pyocyanin (Alayande et al., 2018). Hence indicating a linkage of mechanisms between biofilm and pyocyanin production as revealed in our results (Figure 27). Whether a relationship exists though, cannot be conclusively confirmed by our study. Although the outcome of our PYO experiments showed very similar tendencies as in biofilm assays, the results of the PYO assays failed to reach overall significance. This can be attributed to the fact that the biofilm assay yielded a high number of replicates (both biological and technical) thereby

facilitating highly significant differences, whereas the PYO assay was conducted with fewer biological and technical replicates.

Besides PYO, other small molecules such as pyoverdine are also associated with virulence in *P. aeruginosa* and seem to be influenced by biofilm production, leading us to further investigate the secretion of such siderophores.

### 4.4 Dependence between pyoverdine production and the ability of biofilm formation can be assumed

Bacteria living in environments with limited iron supply are in vital danger. Secreted pyoverdine (PVD) enables survival of such bacteria by acquiring iron and transporting it into the cell. PVD is yet another virulence factor that ensures the survival of bacteria, also in human hosts (Meyer et al., 1996). Hence, we investigated whether MepMs have any influence on the secretion of PVD and whether their deletion is reflected in the PVD secretion rates. For this purpose, we generated an iron-free condition by cultivating ID40 WT and its *mepM* mutants in iron-free succinate medium. Most studies in this area report a relationship between PVD production and biofilm formation. They established that reduced or attenuation of biofilm production favours lower PVD production. They further demonstrate that in conditions where iron limitation is present, biofilm deficient mutants surprisingly do show increased levels of PVD production. Thereby, abolishing differences between biofilm deficient mutants and the WT concerning PVD production (Kang & Kirienko, 2017). It appears that under normal conditions, PVD production is to some degree dependent on biofilm formation. Under conditions where iron is limited, rendering a sufficient acquisition of iron as a vital need for the survival of the bacterium, PVD production becomes uncoupled from biofilm formation. Thus, in the presence of iron starvation, the effect of biofilm-independent pathways upon PVD production may prevail.

Consequently, it could be expected of our *mepM* mutants, which uniformly show significantly reduced biofilm production compared to the ID40 WT to also show reduced PVD production. However, our PVD secretion assays present a condition of iron starvation. Implying that PVD production is independent from the biofilm formation in our assay condition. Possibly, under such condition of vital

threat to survival, mechanisms overruling the impact of biofilm formation which is subject to MepM activity may be present and prevail. Hence, despite previously proven influence of *mepM* deletion on biofilm production, our assay showed high fluctuations and no significant differences between PVD production rate and *mepM* deletion. Subsequent studies under non-iron limitation conditions would be beneficial in evaluating the relationship between MepM activity and PVD production.

After addressing *P. aeruginosa* strain ID40's antibiotic susceptibility, its virulence factors and the mechanisms involved therein, we proceeded to address the general lethality of this strain by giving MepM-deficiency.

### 4.5 Deletion of all three MepMs reduces lethality in *G. mellonella*.

Infection model with *G. mellonella* larvae was conducted to assess the effect various *mepM* deficiencies have upon the general lethality of the *P. aeruginosa* strains ID40 and PA14. For this purpose, *G. mellonella* larvae were infected with 10 µL of bacteria suspension with varying bacterial cell numbers and held at 37°C for 5 days. Deceased larvae were disposed of during the process. Our observations reveal that PA14 strains are more lethal than ID40 strains. Irrespective of the applied infection dosage or *mepM* mutation, none of the infected larvae could survive past day one upon PA14 infection. This stood in contrast to ID40, where the infected larvae on average survived past day 3. This outcome is supported by other findings, which show that MDR *P. aeruginosa* strains although resistant to treatment, exhibit a less virulent character (Köhler et al., 2001). This furthermore, supports our observation (data partly shown Figure 16) demonstrating ID40 WT to be less virulent in terms of protease, elastase or pyocyanin secretion compared to other sensitive *P. aeruginosa* laboratory strains.

To get an estimate whether *mepM1/2* or *mepM123* deletion mutants are less virulent than ID40 WT, many infection experiments were performed. Each single data point in Figure 26 represents 8-10 infected animals to determine the survival rate. The infection dose (CFU) for each experiment was determined. As can be seen in Figure 26, even a similar infection dose revealed a high variation of

survival rates after five days. Therefore, all data points were used to perform data analysis to determine the $LD_{50}$ five days post infection to approximate the virulence of the strains. To get a better idea about the virulence of *mepM* deletion mutants, other infection models (e.g mouse infection) might be of better value, but this was out of the scope of this study. Nevertheless, our findings suggest that deletion of all three tested *mepMs* (Δ*mepM123)* results in a slight but significant reduction of lethality in comparison to ID40 WT (Figure 26). Deletion of Δ*mepM1/2* showed a marginal reduction in lethality indicating a tendency. These experiments give at least some indications that MepMs contribute to virulence.

### 4.6 Behaviour of ID40 is contrary to predictions drawn from literature

Moreover, it is noteworthy to emphasize that the conclusions presented here are based mainly on data acquired with the MDR *P. aeruginosa* clinical strain ID40. This strain harbours multiple mutations differing it from other *P. aeruginosa* (clinical) strains. ID40 behaved in many aspects contrary to the expectations drawn from various literature. As a clinical MDR strain characterized by hyperproduction of AmpC (Moya et al., 2009; Sonnabend et al., 2020; Torrens et al., 2019), ID40 WT was consequently expected to exhibit higher activity of AmpR, which in turn should result in increased production of exoproteins such as protease, elastase and pyocyanin compared to the laboratory strains PA14 WT or PAO1 WT (Balasubramanian et al., 2012) (Figure 4). However, our preliminary experiments (data not shown) indicated that ID40 WT possesses the lowest secretion of pyocyanin compared to PA14 WT and PAO1 WT. ID40 furthermore was found to be less virulent and showed lower secretion of protease as well as undetectable levels of elastase compared to PA14 (data partly shown, Figure 16). In addition, ID40 WT and its *mepM* mutants displayed distinctive colour variations in static biofilm cultures, which were not observed in the PA14 equivalents (Figure 19). Furthermore, a link between the rate of biofilm production and that of PVD has been discussed in various literature, suggesting that increased biofilm production does favour higher PVD production (Kang & Kirienko, 2017). Consequently, leading to the reversed expectation that MepM-deficient strains, which display significantly reduced biofilm production might also show reduced

PVD production. This case however, could not be observed in our studies, whereas ID40's tendency to act differently than expected certainly plays a role, too, in addition to the reasons discussed in section 4.4. These contrasting behaviour of the MDR strain ID40 derives most likely from its multiple intrinsic and acquired mutations. Thus, emphasizing the need of caution when applying findings and observations reported here to other *P. aeruginosa* strains.

### 4.7 MepMs pose potential targets for antimicrobial agents

In summary, the overall goal of this present study was to assist in the identification and development of new antimicrobial compounds that can enhance the susceptibility of MDR *P. aeruginosa* strains to ß-lactam antibiotics by the inhibition of MepM proteins. In this context, it is relevant to evaluate whether inhibition of MepMs also influences, perhaps even inhibits, or reduces virulence, as this would enhance the attractiveness of MepM targeting.

We have demonstrated that deficiency of MepM proteins indeed can modulate the concentration of MexEF-OprN been incorporated into the cell envelope. With all due caution, which must be considered due to the partially varying results of the individual experiments, we proceed to propose that the interplay of MexEF- OprN abundance together with the *ampC* expression rate play a great role in conferring ß-lactam resistance to the MDR *P. aeruginosa* strain ID40. Hereby emphasizing the fact that reduced *ampC* expression levels signify decreased ß-lactamase activity. Hence, simultaneous inhibition of multiple MepMs, precisely MepM1, MepM2 and MepM3, promises to modulate activities in the cell towards increased ß-lactam sensitivity. However, with regard to MepM's effect on virulence, the question remains unanswered. Most studies in this area are in accordance with our elaboration suggesting that *mepM* deficiency might result in reduced virulence and lethality. Subsequent studies can provide further clarity on MepM's influence on virulence in general. It has been shown that the active sites of the murein endopeptidases MepM1, MepM2 and MepM3 all possess a LytM domain (Yakhnina et al., 2015). According to in-silico structure analysis (by Dr. Thales Kronenberger), both MepM1 and MepM2 have congruent catalytic centres, posing a rather promising possibility of combinatory inhibition

with a single drug (Kemper, 2020). Hence, obtaining multi-MepM inhibition with a single compound could be feasible.

It is furthermore important to bear in mind that in the event of similarities between the catalytic centres of MepMs and that of other bacteria, such as commensal gut bacteria or during mixed infections, an additional unintended perhaps adverse effect can be achieved (Kemper, 2020). On this behalf, more investigation is required to discern where similarities exist and determine the nature of effects awaiting non-pseudomonal bacteria upon combinatory MepM inhibition.

To conclude, this work has confirmed previous findings in this area while emphasizing murein endopeptidases (MepMs) besides other enzymes involved in PG turnover as promising targets of antimicrobial agents able to modulate the production rate of virulent exoproteins, biofilm formation and ß-lactam resistance. Thereby opening new fields for further investigations.

# 5 Summary

## 5.1 Summary in English

*Pseudomonas aeruginosa* is a Gram-negative rod-shaped bacterium found ubiquitously. This pathogen has multiple intrinsic resistance mechanisms and a high prevalence of MDR strains, making *Pa*. a concern in healthcare centres. On the quest of discovering novel antimicrobial methods against MDR *P. aeruginosa* infections, previous research findings have thrown light on enzymes involved in the turnover of the bacterial cell wall such as murein endopeptidases (MepM). MepMs seem to contribute to ß-lactam resistance of the MDR *P. aeruginosa* strain ID40.

The aim of the presented study is to investigate whether and which of the MepMs affect the abundance of the efflux pump MexEF-OprN and virulence phenotypes such as biofilm production, pyocyanin and elastase secretion as well as affecting virulence in a *Galleria mellonella* infection model. The findings of the current study reveal that MepMs indeed influence the abundance of the MexEF-OprN efflux pump found in the cell envelope. MepM1, MepM2 and MepM3 seem to act in concert to modulate the abundance of MexEF-OprN, which as recently proposed might be another contributor of ß-lactam resistance in *P. aeruginosa* strain ID40, together with the expression level of *ampC.* We furthermore report that the ability of biofilm formation as a virulent factor is subject to the activity of MepM1, MepM2 and MepM3 via a yet unknown mechanism. The involvement of efflux pumps in the formation of biofilm can be assumed. In contrast to various studies indicating an interaction between increased MexEF-OprN abundance and the secretion of virulence factors such as elastase or pyocyanin, our current study could not validate such a correlation.

To conclude, this work has confirmed previous findings in this area and furthermore spotlighted murein endopeptidases (MepM) as avid contributors to *P. aeruginosa's* ß-lactam resistance and virulence. Thereby suggesting a promising potential upon targeting of MepMs with antimicrobial agents to enable a novel way of controlling MDR *P. aeruginosa* strains.

## 5.2 Deutsche Zusammenfassung

*Pseudomonas aeruginosa* ist ein Gram-negatives, stäbchenförmiges Bakterium, das ubiquitär vorkommt. Dieser Erreger verfügt über verschiedene Resistenzmechanismen und hat eine hohe Prävalenz von klinischen multiresistenten Isolaten. Bei der Suche nach potenziellen Mediatoren von Multiresistenz haben vorangegangene Forschungsergebnisse auf Enzyme, welche am Umsatz der bakteriellen Zellwand beteiligt sind, hingewiesen. Zu solchen Enzymen zählen u.a. die Murein Endopeptidasen (MepM). MepMs scheinen zur ß-Lactam-Resistenz bei dem multiresistenten *P. aeruginosa* Stamm ID40 beizutragen.

Ziel dieser Arbeit war es zu untersuchen, ob und welche MepMs die Abundanz der Effluxpumpe MexEF-OprN und Virulenzphänotypen wie Biofilmproduktion, Elastase- und Pyocyaninsekretion sowie Virulenz im Galleriainfektionsmodell beeinflussen. Aus der aktuellen Arbeit geht hervor, dass MepMs tatsächlich Einfluss nehmen auf die Konzentration der in der Zellhülle vorkommenden MexEF-OprN Effluxpumpen. MepM1, MepM2 und MepM3 scheinen gemeinsam die Konzentration von MexEF-OprN zu beeinflussen, welche wie kürzlich vorgeschlagen neben der Expressionsrate von *ampC* zur ß-Laktamresistenz beiträgt. Außerdem berichten wir, dass die Fähigkeit zur Ausprägung des virulenten Faktors Biofilmbildung von der Aktivität von MepM1, MepM2 und MepM3 abhängig ist, wobei der Mechanismus noch unklar ist. Eine Beteiligung von Effluxpumpen an der Biofilmbildung kann angenommen werden. Im Kontrast zu den Ergebnissen vieler Studien, welche über einen Zusammenhang zwischen einer erhöhten MexEF-OprN-Konzentration und der Sekretion von Virulenzfaktoren wie Elastase und Pyocyanin berichten, konnte unsere Arbeit eine solche Korrelation nicht nachweisen.

Abschließend lässt sich zusammenfassen, dass diese Arbeit vorangegangene Erkenntnisse bestätigt hat und darüber hinaus Murein-Endopeptidasen als Modulatoren von ß-Lactam-Resistenz und Virulenz von *P. aeruginosa* identifiziert hat. Daraus ergibt sich ein vielversprechendes Potenzial der gezielten Inhibition von MepMs mit antimikrobiellen Wirkstoffen, um neue Methoden zur Bekämpfung von multiresistenter *P. aeruginosa* Stämmen zu generieren.

# 6 References


Abraham, E. P., & Chain, E. (1940). An Enzyme from Bacteria able to Destroy Penicillin. *Nature*, *146*(3713), 837-837. https://doi.org/10.1038/146837a0

Alayande, A. B., Aung, M. M., & Kim, I. S. (2018). Correlation Between Quorum Sensing Signal Molecules and Pseudomonas aeruginosa's Biofilm Development and Virulency. *Curr Microbiol*, *75*(7), 787-793. https://doi.org/10.1007/s00284-018-1449-5

Ambler, R. P. (1980). The structure of beta-lactamases. *Philos Trans R Soc Lond B Biol Sci*, *289*(1036), 321-331. https://doi.org/10.1098/rstb.1980.0049

Azghani, A. O. (1996). Pseudomonas aeruginosa and epithelial permeability: role of virulence factors elastase and exotoxin A. *Am J Respir Cell Mol Biol*, *15*(1), 132-140. https://doi.org/10.1165/ajrcmb.15.1.8679217

Bagge, N., Ciofu, O., Hentzer, M., Campbell, J. I., Givskov, M., & Hoiby, N. (2002). Constitutive high expression of chromosomal beta-lactamase in Pseudomonas aeruginosa caused by a new insertion sequence (IS1669) located in ampD. *Antimicrob Agents Chemother*, *46*(11), 3406-3411. https://doi.org/10.1128/AAC.46.11.3406-3411.2002

Balasubramanian, D., Schneper, L., Merighi, M., Smith, R., Narasimhan, G., Lory, S., & Mathee, K. (2012). The regulatory repertoire of Pseudomonas aeruginosa AmpC ss-lactamase regulator AmpR includes virulence genes. *PLoS One*, *7*(3), e34067. https://doi.org/10.1371/journal.pone.0034067

Barreteau, H., Kovac, A., Boniface, A., Sova, M., Gobec, S., & Blanot, D. (2008). Cytoplasmic steps of peptidoglycan biosynthesis. *FEMS Microbiol Rev*, *32*(2), 168-207. https://doi.org/10.1111/j.1574-6976.2008.00104.x

Berube, B. J., Rangel, S. M., & Hauser, A. R. (2016). Pseudomonas aeruginosa: breaking down barriers. *Curr Genet*, *62*(1), 109-113. https://doi.org/10.1007/s00294-015-0522-x

Bonten, M. J., Bergmans, D. C., Speijer, H., & Stobberingh, E. E. (1999). Characteristics of polyclonal endemicity of Pseudomonas aeruginosa colonization in intensive care units. Implications for infection control. *Am J Respir Crit Care Med*, *160*(4), 1212-1219. https://doi.org/10.1164/ajrccm.160.4.9809031

Bouhss, A., Crouvoisier, M., Blanot, D., & Mengin-Lecreulx, D. (2004). Purification and characterization of the bacterial MraY translocase catalyzing the first membrane step of peptidoglycan biosynthesis. *J Biol Chem*, *279*(29), 29974-29980. https://doi.org/10.1074/jbc.M314165200

Brown, K., Vial, S. C., Dedi, N., Westcott, J., Scally, S., Bugg, T. D., Charlton, P. A., & Cheetham, G. M. (2013). Crystal structure of the Pseudomonas aeruginosa MurG: UDP-GlcNAc substrate complex. *Protein Pept Lett*, *20*(9), 1002-1008. https://doi.org/10.2174/0929866511320090006

Bush, K. (2012). Antimicrobial agents targeting bacterial cell walls and cell membranes. *Rev Sci Tech*, *31*(1), 43-56. https://doi.org/10.20506/rst.31.1.2096

Bush, K., & Bradford, P. A. (2016). beta-Lactams and beta-Lactamase Inhibitors: An Overview. *Cold Spring Harb Perspect Med*, *6*(8). https://doi.org/10.1101/cshperspect.a025247

Chatterjee, M., Anju, C. P., Biswas, L., Anil Kumar, V., Gopi Mohan, C., & Biswas, R. (2016). Antibiotic resistance in Pseudomonas aeruginosa and alternative therapeutic options. *Int J Med Microbiol*, *306*(1), 48-58. https://doi.org/10.1016/j.ijmm.2015.11.004

De Duve, C., & Wattiaux, R. (1966). Functions of lysosomes. *Annu Rev Physiol*, *28*(1), 435-492. https://doi.org/10.1146/annurev.ph.28.030166.002251

Dhar, S., Kumari, H., Balasubramanian, D., & Mathee, K. (2018). Cell-wall recycling and synthesis in Escherichia coli and Pseudomonas aeruginosa - their role in the development of resistance. *J Med Microbiol*, *67*(1), 1-21. https://doi.org/10.1099/jmm.0.000636

Dik, D. A., Dominguez-Gil, T., Lee, M., Hesek, D., Byun, B., Fishovitz, J., Boggess, B., Hellman, L. M., Fisher, J. F., Hermoso, J. A., & Mobashery, S. (2017). Muropeptide Binding and the X-ray Structure of the Effector Domain of the Transcriptional Regulator AmpR of Pseudomonas aeruginosa. *J Am Chem Soc*, *139*(4), 1448-1451. https://doi.org/10.1021/jacs.6b12819

Dik, D. A., Madukoma, C. S., Tomoshige, S., Kim, C., Lastochkin, E., Boggess, W. C., Fisher, J. F., Shrout, J. D., & Mobashery, S. (2019). Slt, MltD, and MltG of Pseudomonas aeruginosa as Targets of Bulgecin A in Potentiation of beta-Lactam Antibiotics. *ACS Chem Biol*, *14*(2), 296-303. https://doi.org/10.1021/acschembio.8b01025

Donlan, R. M. (2001). Biofilm formation: a clinically relevant microbiological process. *Clin Infect Dis*, *33*(8), 1387-1392. https://doi.org/10.1086/322972

Doyle, R. J., Chaloupka, J., & Vinter, V. (1988). Turnover of cell walls in microorganisms. *Microbiol Rev*, *52*(4), 554-567. https://doi.org/10.1128/mr.52.4.554-567.1988

Driscoll, J. A., Brody, S. L., & Kollef, M. H. (2007). The epidemiology, pathogenesis and treatment of Pseudomonas aeruginosa infections. *Drugs*, *67*(3), 351-368. https://doi.org/10.2165/00003495-200767030-00003

Eggers, O., Renschler, F. A., Michalek, L. A., Wackler, N., Walter, E., Smollich, F., Klein, K., Sonnabend, M. S., Egle, V., Angelov, A., Engesser, C., Borisova, M., Mayer, C., Schütz, M., & Bohn, E. (2023). YgfB increases β-lactam resistance in Pseudomonas aeruginosa by counteracting AlpA-mediated ampDh3 expression. *Commun Biol*, *6*(1), 254. https://doi.org/10.1038/s42003-023-04609-4

El-Fouly, M. Z., Sharaf, A. M., Shahin, A. A. M., El-Bialy, H. A., & Omara, A. M. A. (2015). Biosynthesis of pyocyanin pigment by Pseudomonas aeruginosa. *Journal of Radiation Research and Applied Sciences*, *8*(1), 36-48. https://doi.org/10.1016/j.jrras.2014.10.007

Essar, D. W., Eberly, L., Hadero, A., & Crawford, I. P. (1990). Identification and characterization of genes for a second anthranilate synthase in Pseudomonas aeruginosa: interchangeability of the two anthranilate

synthases and evolutionary implications. *J Bacteriol*, *172*(2), 884-900. https://doi.org/10.1128/jb.172.2.884-900.1990

Filloux, A., & Ramos, J. L. (2014). Preface. Pseudomonas methods and protocols. *Methods Mol Biol*, *1149*, v. https://doi.org/10.1007/978-1-4939-0473-0

Frank, L. H., & Demoss, R. D. (1959). On the biosynthesis of pyocyanine. *J Bacteriol*, *77*(6), 776-782. https://doi.org/10.1128/jb.77.6.776-782.1959

Gisin, J., Schneider, A., Nagele, B., Borisova, M., & Mayer, C. (2013). A cell wall recycling shortcut that bypasses peptidoglycan de novo biosynthesis. *Nat Chem Biol*, *9*(8), 491-493. https://doi.org/10.1038/nchembio.1289

Glauner, B., Holtje, J. V., & Schwarz, U. (1988). The composition of the murein of Escherichia coli. *J Biol Chem*, *263*(21), 10088-10095. https://www.ncbi.nlm.nih.gov/pubmed/3292521

Hanson, N. D., & Sanders, C. C. (1999). Regulation of inducible AmpC beta-lactamase expression among Enterobacteriaceae. *Curr Pharm Des*, *5*(11), 881-894. https://www.ncbi.nlm.nih.gov/pubmed/10539994

Hauser, A. R. (2009). The type III secretion system of Pseudomonas aeruginosa: infection by injection. *Nat Rev Microbiol*, *7*(9), 654-665. https://doi.org/10.1038/nrmicro2199

Hmelo, L. R., Borlee, B. R., Almblad, H., Love, M. E., Randall, T. E., Tseng, B. S., Lin, C., Irie, Y., Storek, K. M., Yang, J. J., Siehnel, R. J., Howell, P. L., Singh, P. K., Tolker-Nielsen, T., Parsek, M. R., Schweizer, H. P., & Harrison, J. J. (2015). Precision-engineering the Pseudomonas aeruginosa genome with two-step allelic exchange. *Nat Protoc*, *10*(11), 1820-1841. https://doi.org/10.1038/nprot.2015.115

Hof, H., Schlüter, D., & Dörries, R. (2019). *Medizinische Mikrobiologie* (7th ed.). Thieme. https://doi.org/10.1055/b-006-163249

Ibrahim, E. H., Ward, S., Sherman, G., & Kollef, M. H. (2000). A comparative analysis of patients with early-onset vs late-onset nosocomial pneumonia in the ICU setting. *Chest*, *117*(5), 1434-1442. https://doi.org/10.1378/chest.117.5.1434

Ikeda, M., Wachi, M., Jung, H. K., Ishino, F., & Matsuhashi, M. (1991). The Escherichia coli mraY gene encoding UDP-N-acetylmuramoyl-pentapeptide: undecaprenyl-phosphate phospho-N-acetylmuramoyl-pentapeptide transferase. *J Bacteriol*, *173*(3), 1021-1026. https://doi.org/10.1128/jb.173.3.1021-1026.1991

Jacobs, C., Huang, L. J., Bartowsky, E., Normark, S., & Park, J. T. (1994). Bacterial cell wall recycling provides cytosolic muropeptides as effectors for beta-lactamase induction. *EMBO J*, *13*(19), 4684-4694. https://doi.org/10.1002/j.1460-2075.1994.tb06792.x

Jacobs, C., Joris, B., Jamin, M., Klarsov, K., Van Beeumen, J., Mengin-Lecreulx, D., van Heijenoort, J., Park, J. T., Normark, S., & Frere, J. M. (1995). AmpD, essential for both beta-lactamase regulation and cell wall recycling, is a novel cytosolic N-acetylmuramyl-L-alanine amidase. *Mol Microbiol*, *15*(3), 553-559. https://doi.org/10.1111/j.1365-2958.1995.tb02268.x

Jana, B., Cain, A. K., Doerrler, W. T., Boinett, C. J., Fookes, M. C., Parkhill, J., & Guardabassi, L. (2017). The secondary resistome of multidrug-resistant Klebsiella pneumoniae. *Sci Rep*, *7*, 42483. https://doi.org/10.1038/srep42483

Jurado-Martin, I., Sainz-Mejias, M., & McClean, S. (2021). Pseudomonas aeruginosa: An Audacious Pathogen with an Adaptable Arsenal of Virulence Factors. *Int J Mol Sci*, *22*(6). https://doi.org/10.3390/ijms22063128

Kamio, Y., & Nikaido, H. (1976). Outer membrane of Salmonella typhimurium: accessibility of phospholipid head groups to phospholipase c and cyanogen bromide activated dextran in the external medium. *Biochemistry*, *15*(12), 2561-2570. https://doi.org/10.1021/bi00657a012

Kang, D., & Kirienko, N. V. (2017). High-Throughput Genetic Screen Reveals that Early Attachment and Biofilm Formation Are Necessary for Full Pyoverdine Production by Pseudomonas aeruginosa. *Front Microbiol*, *8*, 1707. https://doi.org/10.3389/fmicb.2017.01707

Kemper, J. (2020). *Characterization of the murein endopeptidase MepM as a potential target for the development of adjuvants to overcome β-lactam resistance* [Dissertation, Medizinische Fakultät der Eberhard Karls Universität Tübingen].

Kida, Y., Higashimoto, Y., Inoue, H., Shimizu, T., & Kuwano, K. (2008). A novel secreted protease from Pseudomonas aeruginosa activates NF-kappaB through protease-activated receptors. *Cell Microbiol*, *10*(7), 1491-1504. https://doi.org/10.1111/j.1462-5822.2008.01142.x

Köhler, T., Epp, S. F., Curty, L. K., & Pechere, J. C. (1999). Characterization of MexT, the regulator of the MexE-MexF-OprN multidrug efflux system of Pseudomonas aeruginosa. *J Bacteriol*, *181*(20), 6300-6305. https://doi.org/10.1128/JB.181.20.6300-6305.1999

Köhler, T., van Delden, C., Curty, L. K., Hamzehpour, M. M., & Pechere, J. C. (2001). Overexpression of the MexEF-OprN multidrug efflux system affects cell-to-cell signaling in Pseudomonas aeruginosa. *J Bacteriol*, *183*(18), 5213-5222. https://doi.org/10.1128/JB.183.18.5213-5222.2001

Kong, K. F., Aguila, A., Schneper, L., & Mathee, K. (2010). Pseudomonas aeruginosa beta-lactamase induction requires two permeases, AmpG and AmpP. *BMC Microbiol*, *10*, 328. https://doi.org/10.1186/1471-2180-10-328

Korfmann, G., & Sanders, C. C. (1989). ampG is essential for high-level expression of AmpC beta-lactamase in Enterobacter cloacae. *Antimicrob Agents Chemother*, *33*(11), 1946-1951. https://doi.org/10.1128/AAC.33.11.1946

Kostakioti, M., Hadjifrangiskou, M., & Hultgren, S. J. (2013). Bacterial biofilms: development, dispersal, and therapeutic strategies in the dawn of the postantibiotic era. *Cold Spring Harb Perspect Med*, *3*(4), a010306. https://doi.org/10.1101/cshperspect.a010306

Lamarche, M. G., & Déziel, E. (2011). MexEF-OprN efflux pump exports the Pseudomonas quinolone signal (PQS) precursor HHQ (4-hydroxy-2-heptylquinoline). *PLoS One*, *6*(9), e24310. https://doi.org/10.1371/journal.pone.0024310

Langaee, T. Y., Gagnon, L., & Huletsky, A. (2000). Inactivation of the ampD gene in Pseudomonas aeruginosa leads to moderate-basal-level and hyperinducible AmpC beta-lactamase expression. *Antimicrob Agents Chemother*, *44*(3), 583-589. https://doi.org/10.1128/AAC.44.3.583-589.2000

Lee, M., Hesek, D., Dik, D. A., Fishovitz, J., Lastochkin, E., Boggess, B., Fisher, J. F., & Mobashery, S. (2017). From Genome to Proteome to Elucidation of Reactions for All Eleven Known Lytic Transglycosylases from Pseudomonas aeruginosa. *Angew Chem Int Ed Engl*, *56*(10), 2735-2739. https://doi.org/10.1002/anie.201611279

Legaree, B. A., Daniels, K., Weadge, J. T., Cockburn, D., & Clarke, A. J. (2007). Function of penicillin-binding protein 2 in viability and morphology of Pseudomonas aeruginosa. *J Antimicrob Chemother*, *59*(3), 411-424. https://doi.org/10.1093/jac/dkl536

Livermore, D. M. (1984). Penicillin-binding proteins, porins and outer-membrane permeability of carbenicillin-resistant and -susceptible strains of Pseudomonas aeruginosa. *J Med Microbiol*, *18*(2), 261-270. https://doi.org/10.1099/00222615-18-2-261

Livermore, D. M. (2001). Of Pseudomonas, porins, pumps and carbapenems. *J Antimicrob Chemother*, *47*(3), 247-250. https://doi.org/10.1093/jac/47.3.247

Livermore, D. M. (2002). Multiple mechanisms of antimicrobial resistance in Pseudomonas aeruginosa: our worst nightmare? *Clin Infect Dis*, *34*(5), 634-640. https://doi.org/10.1086/338782

Lorusso, A. B., Carrara, J. A., Barroso, C. D. N., Tuon, F. F., & Faoro, H. (2022). Role of Efflux Pumps on Antimicrobial Resistance in Pseudomonas aeruginosa. *Int J Mol Sci*, *23*(24). https://doi.org/10.3390/ijms232415779

Lyczak, J. B., Cannon, C. L., & Pier, G. B. (2000). Establishment of Pseudomonas aeruginosa infection: lessons from a versatile opportunist. *Microbes Infect*, *2*(9), 1051-1060. https://doi.org/10.1016/s1286-4579(00)01259-4

Mayer, C. (2019). Peptidoglycan Recycling, a Promising Target for Antibiotic Adjuvants in Antipseudomonal Therapy. *J Infect Dis*, *220*(11), 1713-1715. https://doi.org/10.1093/infdis/jiz378

Mesaros, N., Nordmann, P., Plesiat, P., Roussel-Delvallez, M., Van Eldere, J., Glupczynski, Y., Van Laethem, Y., Jacobs, F., Lebecque, P., Malfroot, A., Tulkens, P. M., & Van Bambeke, F. (2007). Pseudomonas aeruginosa: resistance and therapeutic options at the turn of the new millennium. *Clin Microbiol Infect*, *13*(6), 560-578. https://doi.org/10.1111/j.1469-0691.2007.01681.x

Meyer, J. M., Neely, A., Stintzi, A., Georges, C., & Holder, I. A. (1996). Pyoverdin is essential for virulence of Pseudomonas aeruginosa. *Infect Immun*, *64*(2), 518-523. https://doi.org/10.1128/iai.64.2.518-523.1996

Mohammadi, T., van Dam, V., Sijbrandi, R., Vernet, T., Zapun, A., Bouhss, A., Diepeveen-de Bruin, M., Nguyen-Disteche, M., de Kruijff, B., & Breukink, E. (2011). Identification of FtsW as a transporter of lipid-linked cell wall

precursors across the membrane. *EMBO J*, *30*(8), 1425-1432. https://doi.org/10.1038/emboj.2011.61

Moya, B., Dotsch, A., Juan, C., Blazquez, J., Zamorano, L., Haussler, S., & Oliver, A. (2009). Beta-lactam resistance response triggered by inactivation of a nonessential penicillin-binding protein. *PLoS Pathog*, *5*(3), e1000353. https://doi.org/10.1371/journal.ppat.1000353

Mulani, M. S., Kamble, E. E., Kumkar, S. N., Tawre, M. S., & Pardesi, K. R. (2019). Emerging Strategies to Combat ESKAPE Pathogens in the Era of Antimicrobial Resistance: A Review. *Front Microbiol*, *10*, 539. https://doi.org/10.3389/fmicb.2019.00539

Nordmann, P., & Guibert, M. (1998). Extended-spectrum beta-lactamases in Pseudomonas aeruginosa. *J Antimicrob Chemother*, *42*(2), 128-131. https://doi.org/10.1093/jac/42.2.128

O'Malley, Y. Q., Reszka, K. J., Spitz, D. R., Denning, G. M., & Britigan, B. E. (2004). Pseudomonas aeruginosa pyocyanin directly oxidizes glutathione and decreases its levels in airway epithelial cells. *Am J Physiol Lung Cell Mol Physiol*, *287*(1), L94-103. https://doi.org/10.1152/ajplung.00025.2004

Ohfuji, K., Sato, N., Hamada-Sato, N., Kobayashi, T., Imada, C., Okuma, H., & Watanabe, E. (2004). Construction of a glucose sensor based on a screen-printed electrode and a novel mediator pyocyanin from Pseudomonas aeruginosa. *Biosens Bioelectron*, *19*(10), 1237-1244. https://doi.org/10.1016/j.bios.2003.11.010

Osmon, S., Ward, S., Fraser, V. J., & Kollef, M. H. (2004). Hospital mortality for patients with bacteremia due to Staphylococcus aureus or Pseudomonas aeruginosa. *Chest*, *125*(2), 607-616. https://doi.org/10.1378/chest.125.2.607

Perley-Robertson, G. E., Yadav, A. K., Winogrodzki, J. L., Stubbs, K. A., Mark, B. L., & Vocadlo, D. J. (2016). A Fluorescent Transport Assay Enables Studying AmpG Permeases Involved in Peptidoglycan Recycling and Antibiotic Resistance. *ACS Chem Biol*, *11*(9), 2626-2635. https://doi.org/10.1021/acschembio.6b00552

Raetz, C. R., & Whitfield, C. (2002). Lipopolysaccharide endotoxins. *Annu Rev Biochem*, *71*, 635-700. https://doi.org/10.1146/annurev.biochem.71.110601.135414

Ramos-Aires, J., Plesiat, P., Kocjancic-Curty, L., & Köhler, T. (2004). Selection of an antibiotic-hypersusceptible mutant of Pseudomonas aeruginosa: identification of the GlmR transcriptional regulator. *Antimicrob Agents Chemother*, *48*(3), 843-851. https://doi.org/10.1128/AAC.48.3.843-851.2004

Rice, L. B. (2008). Federal funding for the study of antimicrobial resistance in nosocomial pathogens: no ESKAPE. *J Infect Dis*, *197*(8), 1079-1081. https://doi.org/10.1086/533452

Sabuda, D. M., Laupland, K., Pitout, J., Dalton, B., Rabin, H., Louie, T., & Conly, J. (2008). Utilization of colistin for treatment of multidrug-resistant Pseudomonas aeruginosa. *Can J Infect Dis Med Microbiol*, *19*(6), 413-418. https://doi.org/10.1155/2008/743197

Schaefer, P., & Baugh, R. F. (2012). Acute otitis externa: an update. *Am Fam Physician*, *86*(11), 1055-1061. https://www.ncbi.nlm.nih.gov/pubmed/23198673

Schleifer, K. H., & Kandler, O. (1972). Peptidoglycan types of bacterial cell walls and their taxonomic implications. *Bacteriol Rev*, *36*(4), 407-477. https://doi.org/10.1128/br.36.4.407-477.1972

Schwinn, M. K., Machleidt, T., Zimmerman, K., Eggers, C. T., Dixon, A. S., Hurst, R., Hall, M. P., Encell, L. P., Binkowski, B. F., & Wood, K. V. (2018). CRISPR-Mediated Tagging of Endogenous Proteins with a Luminescent Peptide. *ACS Chemical Biology*, *13*(2), 467-474. https://doi.org/10.1021/acschembio.7b00549

Sham, L. T., Butler, E. K., Lebar, M. D., Kahne, D., Bernhardt, T. G., & Ruiz, N. (2014). Bacterial cell wall. MurJ is the flippase of lipid-linked precursors for peptidoglycan biogenesis. *Science*, *345*(6193), 220-222. https://doi.org/10.1126/science.1254522

Silhavy, T. J., Kahne, D., & Walker, S. (2010). The bacterial cell envelope. *Cold Spring Harb Perspect Biol*, *2*(5), a000414. https://doi.org/10.1101/cshperspect.a000414

Sonnabend, M. S., Klein, K., Beier, S., Angelov, A., Kluj, R., Mayer, C., Gross, C., Hofmeister, K., Beuttner, A., Willmann, M., Peter, S., Oberhettinger, P., Schmidt, A., Autenrieth, I. B., Schutz, M., & Bohn, E. (2020). Identification of Drug Resistance Determinants in a Clinical Isolate of Pseudomonas aeruginosa by High-Density Transposon Mutagenesis. *Antimicrob Agents Chemother*, *64*(3). https://doi.org/10.1128/AAC.01771-19

Srivastava, D., Seo, J., Rimal, B., Kim, S. J., Zhen, S., & Darwin, A. J. (2018). A Proteolytic Complex Targets Multiple Cell Wall Hydrolases in Pseudomonas aeruginosa. *mBio*, *9*(4). https://doi.org/10.1128/mBio.00972-18

Strateva, T., & Yordanov, D. (2009). Pseudomonas aeruginosa - a phenomenon of bacterial resistance. *J Med Microbiol*, *58*(Pt 9), 1133-1148. https://doi.org/10.1099/jmm.0.009142-0

Strominger, J. L., & Tipper, D. J. (1965). Bacterial cell wall synthesis and structure in relation to the mechanism of action of penicillins and other antibacterial agents. *Am J Med*, *39*(5), 708-721. https://doi.org/10.1016/0002-9343(65)90093-8

Stubbs, K. A., Balcewich, M., Mark, B. L., & Vocadlo, D. J. (2007). Small molecule inhibitors of a glycoside hydrolase attenuate inducible AmpC-mediated beta-lactam resistance. *J Biol Chem*, *282*(29), 21382-21391. https://doi.org/10.1074/jbc.M700084200

Suarez-Cuartin, G., Smith, A., Abo-Leyah, H., Rodrigo-Troyano, A., Perea, L., Vidal, S., Plaza, V., Fardon, T. C., Sibila, O., & Chalmers, J. D. (2017). Anti-Pseudomonas aeruginosa IgG antibodies and chronic airway infection in bronchiectasis. *Respir Med*, *128*, 1-6. https://doi.org/10.1016/j.rmed.2017.05.001

Sykes, R. B., & Matthew, M. (1976). The beta-lactamases of gram-negative bacteria and their role in resistance to beta-lactam antibiotics. *J Antimicrob Chemother*, *2*(2), 115-157. https://doi.org/10.1093/jac/2.2.115

Tacconelli, E., Carrara, E., Savoldi, A., Harbarth, S., Mendelson, M., Monnet, D. L., Pulcini, C., Kahlmeter, G., Kluytmans, J., Carmeli, Y., Ouellette, M., Outterson, K., Patel, J., Cavaleri, M., Cox, E. M., Houchens, C. R., Grayson, M. L., Hansen, P., Singh, N., . . . Group, W. H. O. P. P. L. W. (2018). Discovery, research, and development of new antibiotics: the WHO priority list of antibiotic-resistant bacteria and tuberculosis. *Lancet Infect Dis*, *18*(3), 318-327. https://doi.org/10.1016/S1473-3099(17)30753-3

Templin, M. F., Ursinus, A., & Holtje, J. V. (1999). A defect in cell wall recycling triggers autolysis during the stationary growth phase of Escherichia coli. *EMBO J*, *18*(15), 4108-4117. https://doi.org/10.1093/emboj/18.15.4108

Torrens, G., Sanchez-Diener, I., Jordana-Lluch, E., Barcelo, I. M., Zamorano, L., Juan, C., & Oliver, A. (2019). In Vivo Validation of Peptidoglycan Recycling as a Target to Disable AmpC-Mediated Resistance and Reduce Virulence Enhancing the Cell-Wall-Targeting Immunity. *J Infect Dis*, *220*(11), 1729-1737. https://doi.org/10.1093/infdis/jiz377

Vanderlinde, E. M., Strozen, T. G., Hernandez, S. B., Cava, F., & Howard, S. P. (2017). Alterations in Peptidoglycan Cross-Linking Suppress the Secretin Assembly Defect Caused by Mutation of GspA in the Type II Secretion System. *J Bacteriol*, *199*(8). https://doi.org/10.1128/JB.00617-16

Vazirani, J., Wurity, S., & Ali, M. H. (2015). Multidrug-Resistant Pseudomonas aeruginosa Keratitis: Risk Factors, Clinical Characteristics, and Outcomes. *Ophthalmology*, *122*(10), 2110-2114. https://doi.org/10.1016/j.ophtha.2015.06.007

Vöhringer, K. (unpublished). *Advanced target validation and development of an activity assay for inhibitor evaluation of MepM murein endopeptidases as anti-virulence and resistance-breaking targets.* Medizinische Fakultät der Eberhard Karls Universität Tübingen].

Vollmer, W., & Bertsche, U. (2008). Murein (peptidoglycan) structure, architecture and biosynthesis in Escherichia coli. *Biochim Biophys Acta*, *1778*(9), 1714-1734. https://doi.org/10.1016/j.bbamem.2007.06.007

Vollmer, W., Joris, B., Charlier, P., & Foster, S. (2008). Bacterial peptidoglycan (murein) hydrolases. *FEMS Microbiol Rev*, *32*(2), 259-286. https://doi.org/10.1111/j.1574-6976.2007.00099.x

Watson, D., MacDermot, J., Wilson, R., Cole, P. J., & Taylor, G. W. (1986). Purification and structural analysis of pyocyanin and 1-hydroxyphenazine. *European Journal of Biochemistry*, *159*(2), 309-313. https://doi.org/10.1111/j.1432-1033.1986.tb09869.x

Weiner-Lastinger, L. M., Abner, S., Edwards, J. R., Kallen, A. J., Karlsson, M., Magill, S. S., Pollock, D., See, I., Soe, M. M., Walters, M. S., & Dudeck, M. A. (2020). Antimicrobial-resistant pathogens associated with adult healthcare-associated infections: Summary of data reported to the National Healthcare Safety Network, 2015-2017. *Infect Control Hosp Epidemiol*, *41*(1), 1-18. https://doi.org/10.1017/ice.2019.296

Weissman, B. A., Mondino, B. J., Pettit, T. H., & Hofbauer, J. D. (1984). Corneal ulcers associated with extended-wear soft contact lenses. *Am J Ophthalmol*, *97*(4), 476-481. https://doi.org/10.1016/s0002-9394(14)76131-8

***References***


Willmann, M., Götting, S., Bezdan, D., Maček, B., Velic, A., Marschal, M., Vogel, W., Flesch, I., Markert, U., Schmidt, A., Kübler, P., Haug, M., Javed, M., Jentzsch, B., Oberhettinger, P., Schütz, M., Bohn, E., Sonnabend, M., Klein, K., . . . Peter, S. (2018). Multi-omics approach identifies novel pathogen-derived prognostic biomarkers in patients with Pseudomonas aeruginosa bloodstream infection. *bioRxiv*, 309898. https://doi.org/10.1101/309898

Yakhnina, A. A., McManus, H. R., & Bernhardt, T. G. (2015). The cell wall amidase AmiB is essential for Pseudomonas aeruginosa cell division, drug resistance and viability. *Mol Microbiol*, *97*(5), 957-973. https://doi.org/10.1111/mmi.13077

Yang, J., Zhao, H. L., Ran, L. Y., Li, C. Y., Zhang, X. Y., Su, H. N., Shi, M., Zhou, B. C., Chen, X. L., & Zhang, Y. Z. (2015). Mechanistic insights into elastin degradation by pseudolysin, the major virulence factor of the opportunistic pathogen Pseudomonas aeruginosa. *Sci Rep*, *5*, 9936. https://doi.org/10.1038/srep09936

Yoshimura, F., & Nikaido, H. (1982). Permeability of Pseudomonas aeruginosa outer membrane to hydrophilic solutes. *J Bacteriol*, *152*(2), 636-642. https://doi.org/10.1128/jb.152.2.636-642.1982

Zamorano, L., Reeve, T. M., Deng, L., Juan, C., Moya, B., Cabot, G., Vocadlo, D. J., Mark, B. L., & Oliver, A. (2010). NagZ inactivation prevents and reverts beta-lactam resistance, driven by AmpD and PBP 4 mutations, in Pseudomonas aeruginosa. *Antimicrob Agents Chemother*, *54*(9), 3557-3563. https://doi.org/10.1128/AAC.00385-10

Zamorano, L., Reeve, T. M., Juan, C., Moya, B., Cabot, G., Vocadlo, D. J., Mark, B. L., & Oliver, A. (2011). AmpG inactivation restores susceptibility of pan-beta-lactam-resistant Pseudomonas aeruginosa clinical strains. *Antimicrob Agents Chemother*, *55*(5), 1990-1996. https://doi.org/10.1128/AAC.01688-10

Zhang, W., Lee, M., Hesek, D., Lastochkin, E., Boggess, B., & Mobashery, S. (2013). Reactions of the three AmpD enzymes of Pseudomonas aeruginosa. *J Am Chem Soc*, *135*(13), 4950-4953. https://doi.org/10.1021/ja400970n

# 7 Erklärung zum Eigenanteil

Die Arbeit wurde im Institut für Medizinische Mikrobiologie und Hygiene des Universitätsklinikum Tübingen unter Betreuung von PD Dr. rer. nat. Erwin Bohn durchgeführt. PD Dr. Erwin Bohn in Zusammenarbeit mit PD Dr. Monika Schütz und Dr. Fabian Renschler haben dieses Projekt konzipiert.

Die Versuchsdurchführungen erfolgten nach einer Einarbeitung durch die Labormitglieder der AG-Schütz/Bohn, namentlich PD Dr. Erwin Bohn, Dr. Fabian Renschler, Fabian Smollich, Sarah Akinci, Ole Eggers, Valentin Egle und Andrea Schäfer. Sämtliche Versuche wurden selbstständig von mir mit technischer Unterstützung durch Noémie Teyssandier und Andrea Schäfer durchgeführt. Vereinzelte Schritte der Metagenese wurden von PD Dr. Erwin Bohn übernommen.

Die statistische Auswertung erfolgte nach Anleitung durch PD Dr. Erwin Bohn, Dr. Fabian Renschler und Ole Eggers durch mich. Eine Prüfung auf Rechtschreib- und Grammatikfehler erfolgte simultan zum Schreibprozess mit Grammarly nach der Standardbearbeitungsoption der kostenlosen Version.

Ich versichere das Manuskript selbstständig nach Anleitung durch PD Dr. Erwin Bohn verfasst zu haben und keine weiteren als die von mir angegebenen Quellen verwendet zu haben.

Tübingen, den

_____

Unterschrift

# 8 Danksagung

An dieser Stelle möchte ich mich ganz herzlich bei allen bedanken, die durch ihre Unterstützung und ihr Mitwirken zur Vollendung dieses Promotionsprojekts beigetragen haben. Ein besonderer Dank gilt meinem Doktorvater PD Dr. Erwin Bohn für die Konzeption dieses Projekts sowie für seine unermüdliche, motivierende, humorvolle und stets kompetente Unterstützung während dieser prägenden Zeit. Seinem Wohlwollen und seinem Glauben an mich verdanke ich die Vollendung dieses Promotionsprojekts.

Des Weiteren gebührt mein Dank allen weiteren Mitgliedern der AG Schütz/Bohn, namentlich Dr. Fabian Renschler, PD Dr. Monika Schütz, Valentin Egle, Ole Eggers, Laura Luib, Lea Friedrich, Sarah Akinci, Tanja Späth, Andrea Schäfer, Lara Breuer, Fabian Smollich und Kathrin Vöhringer sowie allen Mitgliedern des NCCT-Teams, die meine zahlreichen Fragen stets freundlich beantwortet haben und immer zur Hilfe bereitstanden. Darüber hinaus habt ihr mir nicht nur die Grundlagen wissenschaftlichen Arbeitens vermittelt, sondern auch ein Vorzeigebeispiel für Teamwork und ein positives Arbeitsklima geboten, in dem ich mich wohlfühlte und Raum für persönliches Wachstum hatte.

Mein großer Dank gilt zudem Noémie Teyssandier, deren Zusammenarbeit mir in der Anfangsphase dieser neuen und herausfordernden Zeit die Sorgen genommen habt.

Weiterhin möchte ich den Verantwortlichen des IZKF-Promotionskollegs für die großzügige Förderung meiner Promotion danken.

Zu guter Letzt danke ich meiner Familie und meinen Freunden, insbesondere Francisca Farkas, für ihre beständige mentale Unterstützung und ihren Glauben an mich, die mir stets ein stabiles Fundament zum Wachsen bietet.